EXPERIMENTAL AND NUMERICAL STUDY ON PERFORMANCE OF UNDOWELLED JOINTS IN CONCRETE PAVEMENTS

Thesis

Submitted in partial fulfilment of the requirements for the degree of

DOCTOR OF PHILOSOPHY

by

ASHIK BELLARY

(Registration Number: 177068CV002)

DEPARTMENT OF CIVIL ENGINEERING
NATIONAL INSTITUTE OF TECHNOLOGY KARNATAKA,
SURATHKAL, MANGALORE – 575 025
JUNE 2022

EXPERIMENTAL AND NUMERICAL STUDY ON PERFORMANCE OF UNDOWELED JOINTS IN CONCRETE PAVEMENTS

Thesis

Submitted in partial fulfilment of the requirements for the degree of

DOCTOR OF PHILOSOPHY

by

ASHIK BELLARY

Under the Guidance of

Dr. SURESHA S N

Associate Professor

DEPARTMENT OF CIVIL ENGINEERING
NATIONAL INSTITUTE OF TECHNOLOGY KARNATAKA,
SURATHKAL, MANGALORE – 575 025

JUNE 2022

D E C L A R A T I O N

by the Ph.D. Research Scholar

I hereby *declare* that the Research Thesis entitled **"Experimental and Numerical Study on Performance of Undowelled Joints in Concrete Pavements"** which is being submitted to the National Institute of Technology Karnataka, Surathkal in partial fulfillment of the requirements for the award of the Degree of Doctor of Philosophy in **Civil Engineering**, is a *bonafide report of the research work carried out by me*. The material contained in this Research Thesis has not been submitted to any University or Institution for the award of any degree.

.....

177068CV002, ASHIK BELLARY

Department of Civil Engineering

Place: NITK-Surathkal

Date:

C E R T I F I C A T E

This is to *certify* that the Research Thesis entitled **"Experimental and Numerical Study on Performance of Undowelled Joints in Concrete Pavements"** submitted by **Mr. ASHIK BELLARY (Register Number: 177068CV002)** as the record of the research work carried out by him, is *accepted as the Research Thesis submission* in partial fulfillment of the requirements for the award of degree of Doctor of Philosophy.

Research Guide
Dr. SURESHA S N
Associate Professor

Chairperson-DRPC
Prof. B R Jayalekshmi
Professor and HOD

DEDICATED
TO MY
MOTHER,
TO MY
LATE.FATHER
AND TO MY
TEACHERS

ACKNOWLEDGEMENTS

I would like to express my sincere gratitude of thanks to my research supervisor Dr. Suresha S N, Associate Professor, Department of Civil Engineering, NITK, for his encouragement, motivation and invaluable guidance throughout my research work. I am grateful to him for his wholehearted interest and passion in every phase of this research work. His moral support, guidance, interactions, discussions and precious suggestions have greatly helped me to complete this research work. It has been my greatest opportunity and pleasure to work under him.

I acknowledge my sincere thanks to Prof. A.U Ravi Shankar, Department of Civil Engineering, NITK and Dr. Ramesh H, Associate Professor, Department of Water Resources & Ocean Engg (Formerly Applied Mechanics and Hydraulics), NITK, for being the members of Research Progress Assessment Committee and giving valuable suggestions and the encouragement provided at various stages of this research work.

I would like to thank Prof. B R Jayalekshmi, Head of the Department of Civil Engineering and the former Heads, Prof. K. Swaminathan and Prof. Varghese George, for all the support throughout my stay. I sincerely express thanks to the Director of the Institute (NITK) for the financial support provided and for extending the facilities for the research.

I would like to thank the examiners, Dr. A.K. Swamy, Associate Professor. Department of Civil Engineering. Indian Institute of Technology Delhi and Prof. G. D. Ransinchung R. N., Professor, Indian Institute of Technology Roorkee for their valuable and beneficial comments, which helped me to improve the quality of this thesis.

I am also thankful to the suppliers of fibers, M/S Concrete Solutions, Mangalore, India and Kalyani Polymers Pvt. Ltd., Bangalore, for my research work. I thank Infra Support Engineering Consultants Pvt Ltd. (Engineering consultant in Bengaluru -18 Karnataka, India) for providing the FWD device to conduct the field studies.

I wish to thank my mother, Smt. Ratna C Bellary who has always motivated me and provided me with the best education, and encouraged me to do PhD. I also thank my relative Prof. Gangadhar V Kurli and former principal Prof. V V Katti, KLS VDIT, Haliyal, for encouraging me to pursue PhD. I thank all my Aunties and Uncles for their encouragement and support from childhood to this point of time.

I appreciate the co-operation and help rendered by the office staff of the Civil Engineering Department. My heartfelt thanks to the Department of Civil Engineering laboratory staff, NITK, Mr. Ramesh Pal, Mr. Pavankumar, Mr. Shashikant Devadiga, Mr. Geetesh Shetty, Mr. Ranjit and Mr. Ramanath who helped me to complete my laboratory studies safely and smoothly. I thank Machine shop laboratory staff Mr. Varghese, Mr. Nishanth, Mr. Sudhakar and Mr. Pavan for their support in fabrication work.

I affectionately acknowledge the moral support and help extended by my best friends and colleagues during this journey. Their informal support and encouragement have been very vital. I am grateful to everybody who helped and encouraged me during this research work.

Place: NITK, Surathkal **(ASHIK BELLARY)**

Date:

ABSTRACT

Joints are the major structural feature of concrete pavements, which play a major role in the effective and efficient performance of pavements. The load transfer across the transverse joints occurs mainly through dowel bars in jointed plain cement concrete pavements (JPCPs). However, in whitetopping and short-panelled concrete pavements, the joints are undowelled, and load transfer mainly occurs through aggregate interlocking. In India, there are no specific guidelines available for the design of short-panelled concrete pavements. In some of the projects, IRC SP:76-2015, which is the guidelines for the design and construction of whitetopping, was followed to design and construct short-panelled concrete pavements. The guideline IRC SP:76-2015 does not account for the load transfer across the joint as a critical factor for the design. It is assumed that the underlying pavement provides considerable support to the joints, which improves the load transfer across the joint. However, it was reported that the poor load transfer across the aggregate interlocked joints results in debonding with the underlying bituminous layers in the case of whitetopping. The poor performance of aggregate interlocking results in faulting, spalling and corner breaks in short-panelled concrete pavements. Since, the performance of the whitetopping and short-panelled concrete pavement depends on the performance of aggregate interlocked joints, the parameters influencing the performance of aggregate interlocked joints have to be evaluated at the design stage and at the time of service.

In the present study, a new test methodology is proposed to characterise the shear transfer ability of aggregate interlocking in plain, micro and macro-fiber reinforced pavement quality concrete (PQC) cylindrical specimens by conducting the direct shear test in the laboratory. The influence of the nominal maximum aggregate size (NMAS), fiber dosages and groove depth (GD) on shear strength (τ), joint shear stiffness (K), and fracture energy in mode - II (G_{IIF}) of aggregate interlocking in pavement quality concrete (PQC) mixes are studied under the static loading. A relationship between G_{IIF} and K is determined for each of the PQC mixes. Also, a shear fatigue test is conducted at higher stress levels to evaluate the effect of NMAS, fiber dosages and GD on the performance of aggregate interlocking in PQC specimens at the grooved cross-section. Statistical analysis was carried out to understand the influence

of GD and stress levels on the fatigue performance of plain, micro, and macro-fiber reinforced PQC mixes.

A small-scale test setup was developed to simulate the aggregate interlocking of concrete pavements. The simulated test setup was used to evaluate the performance of aggregate interlocking in terms of load transfer efficiency (LTE). The beam specimens were utilised to carry out this test. The relationship between the relative movement of the beam (difference in deflection of loaded and unloaded side) and LTE is developed for each PQC mix and is compared with the field FWD results for validation. The 3D FE models are also developed in ANSYS for the two tests proposed in this study. The 3-D finite element model results are in good agreement with the experimental results for both proposed tests.

In the present study, an improvement to the existing analytical model is also presented that can be used to compute the joint stiffness of white-topping pavements directly from the FWD deflection data. Further, ANN models have been developed and compared for the proposed and previously available analytical models in the literature. The joint stiffness calculated from the ANN model developed from the proposed analytical model is used as an input parameter in the FE model, and LTE is compared with the field studies. The proposed ANN model is simple, efficient and accurate enough to estimate the joint stiffness directly from FWD deflection data.

From the experimental tests carried out in this research work, it is concluded that the proposed test methods can be used to evaluate undowelled joints in concrete pavements. Also, from the laboratory studies, it is concluded that larger NMAS (31.5 mm) and dosage of macro-fiber (0.75%) can substantially improve the aggregate interlocking in short panelled concrete pavements, and the use of fiber dosage up to 2.1 kg/m^3 micro-fibers can substantially improve the undowelled/aggregate interlocked joint performance of whitetopping when compared to other dosages under study.

KEYWORDS: Aggregate Interlocking, ANN, Finite Element Model, Fracture Energy, Groove Depth (GD), Joint Shear Stiffness, Macro-fiber, Micro-fiber, NMAS, PQC, shear fatigue tests

TABLE OF CONTENTS

LIST OF FIGURES

LIST OF TABLES

CHAPTER 1

INTRODUCTION

1.1 BACKGROUND

Joints are the major structural feature of cement concrete pavements, which play a vital role in the effective and efficient performance of pavements. Joints are decisively introduced discontinuities to control random cracking and facilitate the construction of rigid pavements. The joints are considered to be a critical factor in the design of rigid pavements. The main function of joints is to provide freedom of movement of the slab relative to concrete volume changes due to drying shrinkage, temperature changes and moisture differences (Tabatabaie et al. 1979). The load transfer across these joints occurs either by aggregate interlocking, dowels, underlying base or through all of these. The effective transferring of the load across the joints would result in lower deflections, reduced faulting, spalling, corner breaks and improved riding quality (Maitra et al. 2009).

The three major types of joints in transverse directions of the concrete pavements are contraction joints, construction joints and expansion joints. Contraction joints are generally used to control the random cracking in the concrete pavement. They are formed by introducing a weakened plane into the concrete and allowing the crack to form at the weakened plane, whereas construction joints are required between lanes of paving and where it is necessary to stop construction within a paving lane. Expansion joints are used at the intersections of pavements with structures, and in some cases, within pavements (Westall 1965; Yoder and Witczak 1991).

The longitudinal joints are provided in the longitudinal direction of the concrete pavement to relieve the warping stresses and to divide the pavement into convenient lanes (Yoder and Witczak 1991). Typical joint details of various joints in concrete pavements are shown in Figure 1.1. The performance of the joints is assessed in terms of load transfer efficiency (LTE), which is the percentage ratio of deflection of the unloaded slab to the deflection of the loaded slab. The LTE value of zero indicates the

poor performance of the joint, and the LTE value of a hundred indicates an excellent performance of the joint.

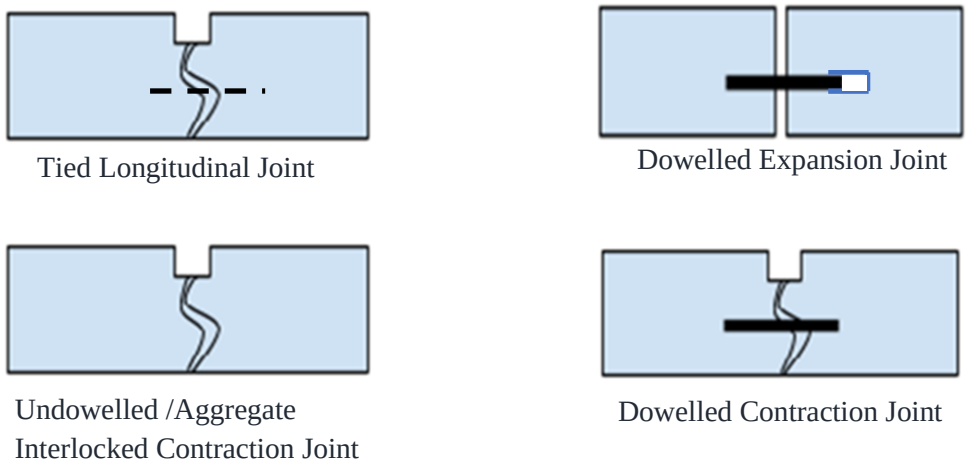

Figure 1.1 Details of various joints in concrete pavements (Huang 2004)

In jointed plain cement concrete pavements (JPCPs), load transfer across the transverse joints occurs mainly through dowel bars (Huang 2004). Whereas in case of the concrete overlays and short panelled concrete pavements, the joints are undowelled, and load transfer mainly occurs through aggregate interlocking. Thus, these joints are often termed as aggregate interlocked joints (Maitra et al. 2010). Concrete overlays are the plain cement concrete (PCC) layer constructed over an existing distressed bituminous pavement. These are one of the popular, feasible and economic rehabilitation techniques to address the distresses in bituminous pavements (Rasmussen and Rozycki 2004; Barman et al. 2017; Jayakesh and Suresha 2018). Short panelled concrete pavements are similar to JPCPs, in which the joints are saw-cut in both transverse and longitudinal directions to form panels of smaller sizes. These types of pavements have become a popular choice over the conventional JPCPs as the construction costs reduce up to 25% (Covarrubias 2012).

In aggregate interlocked joints, the load is transferred by pure shear action (Ioannides and Korovesis 1990). The aggregate interlocking is quantified in terms of shear strength (τ), joint shear stiffness (K), and fracture energy in mode I (G_{IF}) and mode II (G_{IIF}) of concrete at the joint under static loading. The poor performance of aggregate interlocked joints may result in faulting, spalling, and corner breaks in the case of short panelled concrete pavements. Also, the poor performance of aggregate

interlocked joints increases the chances of debonding with the underlying bituminous layer in whitetopping pavements (Barman 2014).

The performance of aggregate interlocked joints depends mainly on the crack width and nominal maximum aggregate size (NMAS) used in the concrete mix (Maitra et al. 2010). In addition, it also depends on the addition of fibers to the concrete mix. In the past, researchers have studied the performance of aggregate interlocking in concrete pavement joints by casting the full-depth pavement structures in a test box and applying repetitive loads alternatively on each slab (Brink 2003; Colley and Humphrey 1968; Jensen and Hansen 2001). Jensen and Hansen (2006) conducted an experimental study using a large-scale slab tester in which truckload was applied, and deflections were measured continuously. However, to perform these tests, high-end equipment and a large quantity of materials are required. It is required to develop a test method to quantify the aggregate interlocking of concrete mixes in the laboratory.

1.2 OBJECTIVES AND SCOPE

The main objective of the present research is to evaluate the performance of aggregate interlocked joints by conducting laboratory tests. The specific research objectives are listed below:

1. To propose a new shear test methodology to evaluate the influence of nominal maximum aggregate size (NMAS) at two different groove depths (GD) on the aggregate interlocked joint by conducting the static and cyclic shear load tests on the pavement quality concrete (PQC) specimens.
2. To investigate the influence of micro and macro polypropylene fibers on the aggregate interlocked joint by conducting the static and fatigue shear load tests on the pavement quality concrete (PQC) specimens.
3. To simulate the aggregate interlocked joint load transfer mechanism of concrete pavements experimentally in the laboratory by using a small-scale test setup.
4. To simulate the experimental results of load transfer efficiency of aggregate interlocked joints using the finite element method (FEM) under static conditions.

5. To study the performance of aggregate interlocked joints in the field using a falling weight deflectometer (FWD).

The aggregate interlocking not only depends on the crack width and NMAS but also on the contact area of aggregates at the joint, which in turn depends on the groove depth (GD). Since the crack width changes over time with variation in the temperature (Nam et al. 2014), it is the responsibility of the designer to meticulously select the NMAS, and the onus is on the site engineer to monitor the groove depth in the field. Considering this, a new simple laboratory test methodology is proposed in the present study in which a pure shear load in mode II is applied to PQC cylindrical specimens. The three different modes of loading are shown in Figure 1.2. The mode I loading accounts for the energy required for the propagation of the crack. But mode II is an in-plane shear which accounts for the resistance offered across the plane. Thus, mode II loading is applied on PQC cylindrical specimens as it accounts for the resistance offered by the aggregates and fibers across the grooved cross-section.

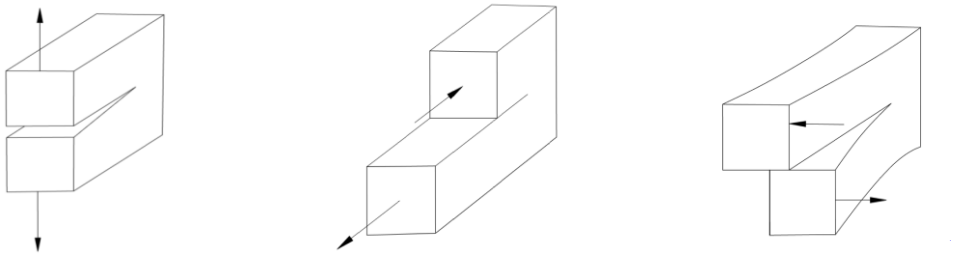

(a) Mode I: Opening (b) Mode II: Shearing (c) Mode III: Tearing

Figure 1.2 Three different modes of loading in fracture (Broek 1986)

The three different NMAS 19, 26.5 and 31.5 mm were selected based on the IRC 44-2017 guidelines, and two groove depths 1/3rd of thickness and 1/4th of the thickness were selected as per MoRT&H guidelines. The proposed test methodology was also used to study the influence of the addition of fibers on the performance of aggregate interlocking of the PQC mix. All the concrete mixtures were tested for fresh and hardened properties such as workability, compressive strength, split tensile strength, flexural strength, and modulus of elasticity as per standard test procedures.

The static direct shear test was conducted to evaluate the shear parameter of aggregate interlocked joints in pavement quality concrete (PQC) mixes using the

cylindrical specimens with a preformed groove. The relationship is developed between joint shear stiffness and fracture energy. The fatigue shear test was conducted on the cylindrical PQC specimens, and statistical analysis was carried out for the obtained shear fatigue data. The S-N curves for different concrete mixtures, along with their relationships for individual mixes, are presented. The survival curves are plotted, and a log-rank test is used to understand the influence of groove depth and stress ratio on the performance of aggregate interlocked joints under shear fatigue loading. The probabilistic analysis and distribution fitting techniques are used to understand the distribution of shear fatigue life of concrete mixes. The goodness of fit of two distributions (three-parameter Weibull and lognormal) for the obtained shear fatigue data is studied using the Anderson-Darling test, which is popularly known as the AD test.

A small-scale test setup was developed in the laboratory to simulate the load transfer of aggregate interlocked joint in concrete pavements. This test setup was used to measure the LTE of the concrete beam specimens at different crack widths. The influence of groove depth, NMAS, and addition of fibers on the crack width and LTE was studied and is presented.

The field FWD test was conducted on the selected whitetopping stretches, and the ANN model to predict the joint stiffness directly from the field FWD studies was developed. The whitetopping pavement is modelled in ANSYS software. The comparison of results from the experiment and the model are presented.

1.3 RESEARCH PLAN

The research plan for the performance evaluation of aggregate interlocked joints in concrete pavements is shown in Figure 1.3. The performance of aggregate interlocked joint was evaluated in terms of joint stiffness by conducting the static direct shear test and in terms of LTE by using the proposed small-scale test setup in this research work. The performance of aggregate interlocked joint of PQC mix with different NMAS, micro and macro fiber dosages were evaluated. The experimental test results were used to develop the 3D FE model. Field evaluation of aggregate interlocked joints was carried out to validate the proposed small-scale test setup results. The field

evaluation data was also utilised to develop an ANN model to directly predict joint stiffness from FWD data. As loads coming on pavements are repetitive loads, the fatigue shear test was carried out on cylindrical specimens, and statistical analysis was also carried out.

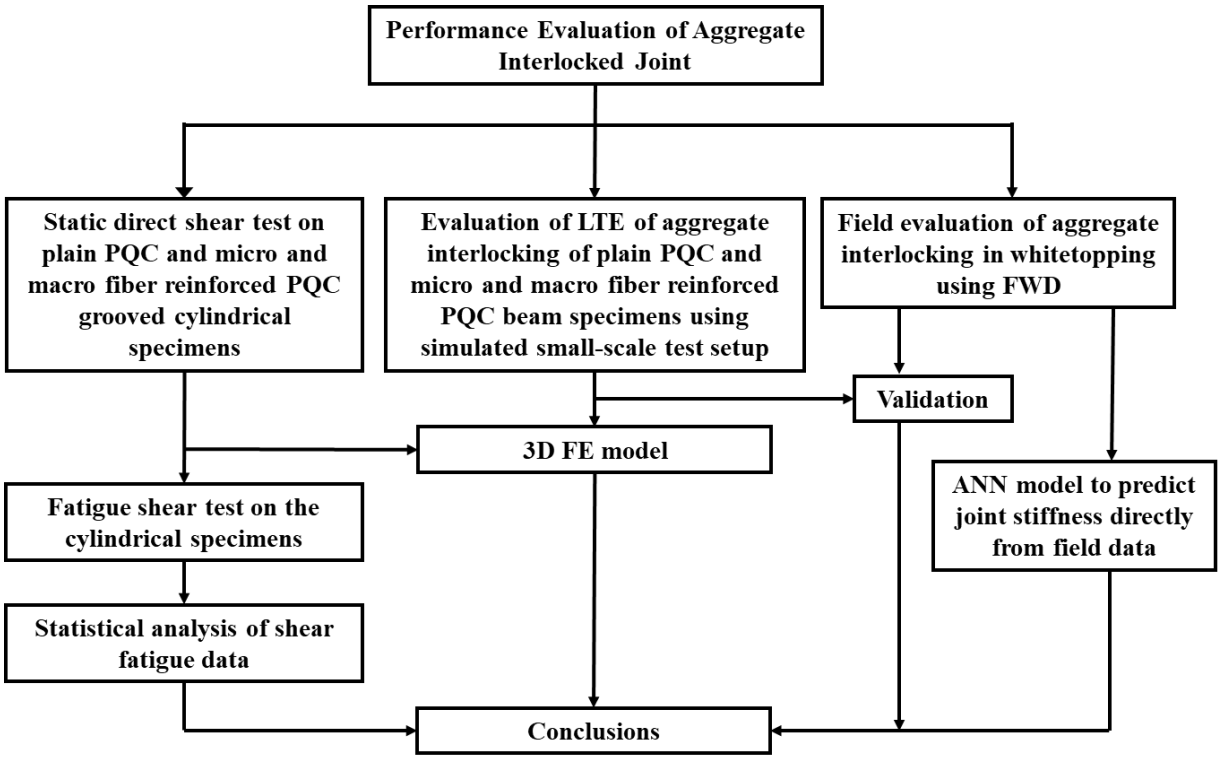

Figure 1.3 Flowchart for performance evaluation of aggregate interlocked joints in concrete pavements

1.4 THESIS ORGANIZATION

The thesis is divided into eight chapters. Chapter one provides a brief description of joints in concrete pavements, types of joints, the importance of aggregate interlocked joints in short panelled concrete pavements and concrete overlays, research objectives and the scope of the research work.

The second chapter presents a comprehensive review of relevant literature on the factors influencing the performance of aggregate interlocking, various test methods to evaluate the performance of aggregate interlocking, field FWD studies and FE simulations.

The third chapter provides a brief description of the materials used for the preparation of pavement quality concrete (PQC) mix. Also, the basic test results of materials used and the mechanical properties of concrete mixtures are presented. The proposed test methodology for evaluating the shear parameters and the test setup to simulate the load transfer in whitetopping is explained. In addition, the evaluation of whitetopping pavement in the field is described in this chapter.

Chapter four presents a detailed discussion on the results of static shear tests performed using the proposed methodology. The various statistical methods and distributions used to analyze the shear fatigue performance of PQC mix prepared using different NMAS and with the addition of micro and macro-fibers under shear fatigue loading are presented in detail.

Chapter five presents the repeated flexural loading test results of concrete beam specimens prepared using three different NMAS and with the addition of micro and macro-fibers conducted using the small-scale test setup developed in the laboratory. The relationship between crack width and LTE was developed for different PQC mixes.

Chapter six presents the modeling of the proposed tests in FE based software, ANSYS, and compares the obtained experimental and simulation results.

Chapter seven presents the development of the ANN model to predict the joint stiffness of aggregate interlocked joints of whitetopping directly from the field FWD data.

Along with summarizing the detailed work, Chapter eight provides conclusions, limitations of the present research work and scope for future research work.

CHAPTER 2

LITERATURE REVIEW

2.1 GENERAL

In recent years, concrete pavements are being constructed in many road projects, as these pavements warrant for less maintenance and have longer service lives compared to bituminous pavements. In urban areas, concrete pavements are being preferred by the municipal authorities over bituminous pavements as concrete pavements can easily tackle drainage problems. The jointed plain cement concrete pavements of dimensions 4.5 m × 4.5 m with thicker slabs are generally provided for the rural highways. Short panelled concrete pavements are similar to JPCPs with lower joint spacing (Chattaraj and B.B.Pandey 2014). The joints are saw-cut in both transverse and longitudinal directions to form panels of smaller sizes. These pavements are laid on top of the base and subbase courses as a new construction. The joints in these pavements are undowelled, and the load transfer across the joints occurs through aggregate interlocking. These pavements can be advantageous in regions with moderate to light traffic, especially in urban, semi-urban and built-up areas.

The whitetopping/ concrete overlays have become a popular alternative for the rehabilitation of distressed bituminous pavements in urban areas. The concrete overlays have several advantages, such as extended service life, improved structural and functional capacity and lower life cycle costs when compared to bituminous overlays. In whitetopping pavements also, the load transfer occurs by aggregate interlocking. In India, IRC SP: 76 2015 is the guideline being followed for the design of whitetopping. There are no specific guidelines for the design of short panelled concrete pavements. However, in some of the projects, IRC SP:76 2015 was used for the construction of short panelled concrete pavements (Chattaraj and B.B.Pandey 2014). The guidelines IRC SP:76 2015 does not consider the load transfer across the joint as a critical factor for whitetopping. It is assumed that the underlying pavement provides considerable support to the joints, which improves the load transfer across the joint. However, it was reported that the poor load transfer across the aggregate interlocked joints results in

debonding with the underlying bituminous layers in the case of whitetopping (Barman 2014). The poor performance of aggregate interlocking results in faulting, spalling and corner breaks in the case of short panelled concrete pavements.

The aggregate interlocking is the natural mechanism of load transfer across the joints. The aggregate interlocking is not only important for short panelled concrete pavement and whitetopping joints but also for other concrete structural applications such as dams, repair of buildings and bridges. In the following section of this chapter, a brief review of the literature has been presented on the aggregate interlocked joint performance terms, various experimental studies conducted to evaluate the performance of aggregate interlocking, factors influencing the performance of aggregate interlocking and finite element modelling of aggregate interlocking.

2.2 AGGREGATE INTERLOCKED JOINT PERFORMANCE TERMS

The performance of the pavements depends on the performance of their joints, as these are the critical locations in the pavement structure. Thus, it is necessary to quantify the performance of these joints. The various terms used in the past to quantify the aggregate interlocked joint is explained below.

2.2.1 Load transfer efficiency (LTE)

The performance of any joint, whether it is a doweled or aggregate interlocked, is measured in terms of deflection load transfer efficiency or simply load transfer efficiency is given as follows:

$$LTE = \left(\frac{\Delta_U}{\Delta_L}\right) \times 100 \tag{2.1}$$

where Δ_U, Δ_L are the deflections of the unloaded and the loaded side of a joint, respectively. LTE value of hundred indicates the excellent performance of the joint. LTE value of zero indicates the poor performance of the joint.

2.2.2 Non-dimensional joint stiffness (AGG*)

Ioannides and Korovesis (1990) developed a sigmoidal relationship between a non-dimension joint stiffness (AGG*) and LTE based on the finite element investigation

carried out using the ILLISLAB software. The AGG* is calculated using following equation

$$AGG^* = \left(\frac{AGG}{kl}\right) \tag{2.2}$$

where AGG is the shear spring stiffness, k is the modulus of subgrade reaction, and *l* is the radius of relative stiffness, which can be obtained by using the following equation

$$l = \left[\frac{Eh^3}{12\,k\,(1-\mu^2)}\right]^{0.25} \tag{2.3}$$

where h is the thickness of concrete pavement and E is the modulus of elasticity of concrete. The relationship is shown in Figure 2.1.

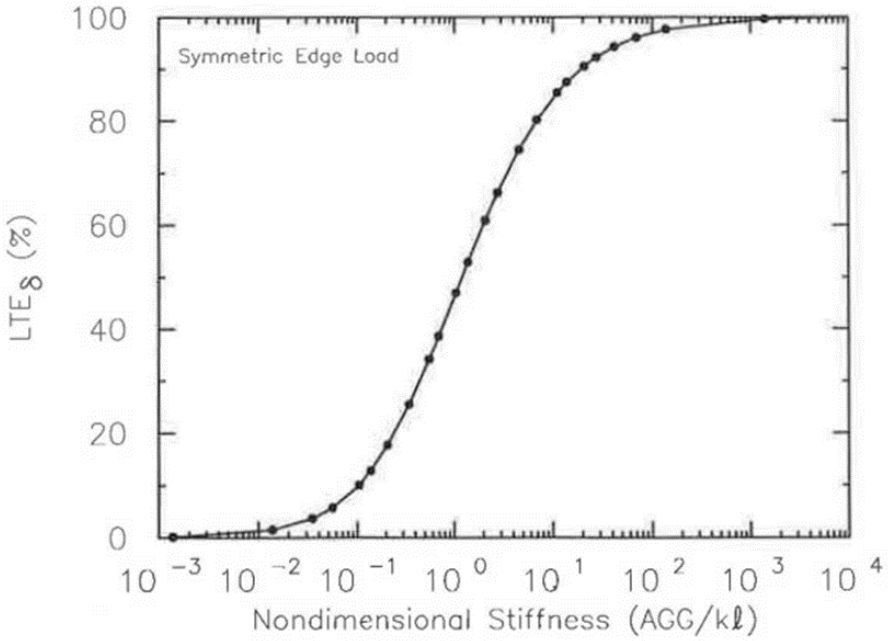

Figure 2.1 Relation between non-dimensional joint stiffness (AGG*) and LTE (Ioannides and Korovesis, 1990)

2.2.3 Static direct shear strength (τ), joint shear stiffness (K), fracture energy and number of repetitions

Aggregate interlocking is also quantified in terms of shear strength (τ), joint shear stiffness (K), and fracture energy either in mode I (G_{IF}) or in mode II (G_{IIF}) of concrete at the joint under static loading. The aggregate interlocked joint performance is measured in terms of its number of repetitions to failure under repeated loading. Wattar (2001) quantified the aggregate interlocked joint performance in the laboratory in terms

of shear strength (τ) and joint shear stiffness (K) under static loading. The authors measured the aggregate interlocked joint performance under repeated loading is in terms of the number of repetitions to failure. Chupanit and Roesler (2008) conducted wedge split tests to quantify the aggregate interlocking in terms of fracture energy.

2.3 PREVIOUS STUDIES ON AGGREGATE INTERLOCKED JOINT PERFORMANCE EVALUATION

The performance of joints in the field is evaluated by using the falling weight deflectometer (FWD) device. The FWD devices are more useful for the evaluation of in-service pavements. The FWD is the most reliable and accurate device to measure the deflection values in the field (Han et al. 2021; Marecos et al. 2017). The LTE can be determined using the following equation.

$$LTE = \beta \times \frac{D_{-150}}{D_{150}} \times 100 \tag{2.4}$$

where β is the correction factor when deflection sensors are at a distance of 300 mm apart, and its value lies between 1.05 and 1.15. D_{150} is the measured deflection of the unloaded slab at a distance of 150 mm away from the joint. D_{-150} is the measured deflection of the loaded slab at a distance of 150 mm away from the joint.

The information about the joint performance would help in the design of concrete pavements. Thus, various researchers have proposed laboratory methodologies to quantify the aggregate interlocked joint performance. The various experimental studies conducted in the past to evaluate the performance of aggregate interlocking are tabulated in Table 2.1 and are discussed in this section.

In the past, researchers have studied the performance of aggregate interlocking in concrete pavement joints by casting the full-depth pavement structures in a test box and applying repetitive loads alternatively on each slab (Brink 2003; Colley and Humphrey 1967; Jensen and Hansen 2001). Jensen and Hansen (2006) conducted an experimental study using a large-scale slab tester in which truckload was applied, and deflections were measured continuously. However, in order to conduct these tests, high-end equipment and a large quantity of materials are required.

Table 2.1 Summary of experiments carried out by previous researchers on aggregate interlocked joint performance

Sl. No.	Authors	Compressive strength of concrete used (MPa)	Slab/Beam dimensions L X B X T (mm)	Type and size of coarse aggregate used	Joint opening (mm)	Type and amount of loading	Type of base	Method of crack induction	Major conclusion
1.	Fenwick (1966)	33 (Days)	100 X 100 X 350 (Beam specimen)	-	0.06 to 0.38	pure shear load to assess aggregate interlock	-	A 6.35 mm saw cut was made around the centre-line of the block prior to testing and tensile load to create cracks at mid-section	Aggregate interlock contributed up to 60% of shear strength in beams
2.	Colley and Humphrey (1967)	38.5 (28 days)	i) 1219.20 X 5486.40 X 177.80 ii) 1219.20 X 5486.40 X 228.60 (Slab specimens)	Natural Siliceous gravel - 38 mm and Dolomitic crushed Stone – 38 mm	0.1 to 2.54	40 kN load applied to sides of the crack with two actuators at a simulated speed of 48.3 km/h on circular loading plates	Silty clay subgrade, with two types of sub-base: sand-gravel and cement-treated base material	A groove of 25 mm in depth was formed on the surface of the slab directly over the metal strip when concrete was in a plastic state	Joint effectiveness increased with increased angularity of the aggregates.
3.	Nowlen (1968)	38.5 (28 days)	i) 1219.20 X 5486.40 X 177.80 ii) 1219.20 X 5486.40 X 228.60 (Slab specimens)	Natural Siliceous gravel - 38 mm and Dolomitic crushed Stone – 38 mm	0.1 to 2.54	40 kN load applied to sides of the crack with two actuators at a simulated speed of 48.3 km/h on circular loading plates	Silty clay subgrade, with two types of sub-base: sand-gravel and cement-treated base material	A groove of 25 mm in depth was formed on the surface of the slab directly over the metal strip when concrete was in a plastic state	Joint effectiveness improved with use of cement-treated base.
4.	Paulay and Loeber (1974)	34.96 to 38.82	470 X 300 X 152 (Beam specimens)	Crushed and rounded aggregates	0.13, 0.25 and 0.51	Monotonic and cyclic shear loading	-	Tension cracks are created across a crack plane	The NMAS have no significant effect on aggregate interlock

Table 2.1 Contd.

Sl. No.	Authors	Compressive strength of concrete used (MPa)	Slab/Beam dimensions L X B X T (mm)	Type and size of coarse aggregate used	Joint opening (mm)	Type and amount of loading	Type of base	Method of crack induction	Major conclusion
5.	Ball and Childs (1975)	28.96 ± 2.76 (14 days)	750 X 150 X 150 (Beam specimens)	Crushed aggregates	0 to 3.175	Monotonic and cyclic loading	Subgrade and Cement Treated Base	By placing different shapes	Cement-treated subbase improved the joint performance.
6.	Mattock et al. (1976)	17.24 to 41.37	305 X 559 X 127 (Beam specimens)	Lightweight aggregates (coated and crushed)	0.254	Static loading	-	By applying direct shear load	The shear transfer strength is not significantly affected by the type of aggregate.
7.	Walraven (1981)	13, 33, 37 and 59	600 X 400 X 120 (Beam specimens)	Gravel 16 mm and 32 mm	0, 0.2 and 0.4	The vertical load applied on top via a knife hinge	The specimens were supported on roller bearings	Cracked along the shear plane by pulling steel rods in V-shaped grooves at the front and rear faces of the specimen	The aggregates having a size less than half of the crack widths have no contribution to load transfer.
8.	Millard and Johnson (1984)	30.4 to 45.4	476 X 300 X 100	-	0.125 to 0.35	Static loading	-	Direct tensile force applied	The aggregate mechanism results from a combination of crushing and overriding of the crack faces.
9	Pruijssers and Lung (1985)	50 to 70	600 X 500 X 150	16mm aggregates	0.01 to 0.08	Cyclic and static loading	-	By splitting	The whole crack plane of a specimen contributes to the shear transfer.
10.	Tassios and Vintzēleou (1987)	16, 30 and 40	900 X 300 X 150	Limestone crushed aggregates	15	Static and cyclic loading	-	By splitting	There is no significant deterioration of the smooth interface during loading
11.	Frénaij (1989)	51 and 70	600 X 500 X 150	16 mm glacial river gravel aggregate	0.1	Static loading	-	Using a knife-edge	The method of shear load application is insignificant

Table 2.1 Contd.

Sl. No.	Authors	Compressive strength of concrete used (MPa)	Slab/Beam dimensions L X B X T (mm)	Type and size of coarse aggregate used	Joint opening (mm)	Type and amount of loading	Type of base	Method of crack induction	Major conclusion
12.	Madasamy et al. (1999)	31.17 (31 days)	914.4 X 304.8 X 254	-	6.35 to 9.5	Direct shear	-	Saw cut	The proposed test method was validated with FE analysis
13.	Buch and Frabizzio (2000)	38 (28 days)	1220 X 915 X 254 (Slab specimens)	Crushed Limestone - 19 mm and 25 mm and River Gravel - 19 mm and 25 mm	0 to 1.4	40 kN load applied on both the sides of the crack with two actuators at a simulated speed of 48.3 km/h on circular loading plates	FABCEL-Neoprene pads with a k-value of 27 MPa/mm	Metal strip inserted in fresh concrete	The increase in the pavement surface temperature results in an increase in LTE of joints
14.	Wattar (2001)	39 (28days)	610 X 305 X 305 (Beam specimens)	Gravel - 25 mm	2	Horizontal Shear force applied statically and at constant amplitude	-	Tensile forces after few hours of casting	The use of gap gradation would improve the performance of aggregate interlocking
15.	Jensen and Hansen (2001)	30.6 to 34.8 (28 days)	3000 X 1800 X 250 (Slab specimens)	25 mm limestone and 25 mm and 50 mm glacial gravel	0.1 to 2.5	Cyclic wheel load of 40 kN at one side of crack at 3 Hz.	Michigan Highway foundation: 102 mm open-graded drainage course on 400 mm thick sub-base	Slab subjected to horizontal displacement at surface slot, 7 to 10 days after curing	Tough and large-size aggregates improve the load transfer across the joint

Table 2.1 Contd.

Sl. No.	Authors	Compressive strength of concrete used (MPa)	Slab/Beam dimensions L X B X T (mm)	Type and size of coarse aggregate used	Joint opening (mm)	Type and amount of loading	Type of base	Method of crack induction	Major conclusion
16.	Brink (2003)	35 (28 days)	1800 X 600 X 230 (Slab specimens)	Dolomite - 19 mm and 37.5 mm and Granite - 19 mm and 37.5 mm	0 to 2.5	Dynamic load using actuators 20 kN on each side of joint	Rubber pads used to simulate different base conditions.	Angle iron was used as crack inducer.	The increase in NMAS increased the LTE of the joint.
17.	Arnold et al. (2005)	-	100 X 100 X 400 mm long beam specimens	10mm and 20mm	0.7	Cyclic loading	-	By applying three points bending load	The proposed test procedure provides a valuable insight into joint and crack degradation
18.	Yi et al. (2017)	39.3 to 43.2 (28 days)	200 X 400 X 2000 and 200 X 400 X 2600 (Reinforced beams)	Gravel – 10,20,31.5 and 40mm	Uncracked	Flexural loading	-	-	The maximum aggregate size improved the shear capacity of beams without shear reinforcement.
19.	Barman and Hansen (2018)	50.5 to 64.25 (28 days)	6009 X 152 X 152 (Fiber reinforced beams)	River gravel	0.01	Flexural loading	Neoprene pads	By applying three points bending load	LTE is 20% higher for fiber reinforced beams when crack width is less than 2 mm.

The most common methods used to measure the shear strength of aggregate interlocking in concrete include the push-off method, the International Federation for Structural Concrete (FIP) method and JSCE_G 553 method. Many researchers have conducted push-off tests to study the shear strength of both plain and reinforced concrete mixes (Mansur et al. 2008; Mattock et al. 1976; Walraven 1980; Yang et al. 2012; Yi et al. 2017). The shear stress field is complex in the push-off test method, and the test setup is complicated in the FIP method (Abdi Moghadam and Izadifard 2019). In JSCE_G 553 method, the failure may not be due to pure shear as there is a possibility of rotation of unloaded external blocks.

Roesler and Chupanit (2008) conducted wedge split tests on concrete specimens and found that higher fracture energy resulted in higher joint shear stiffness. Also, aggregate type influences the aggregate interlocking in terms of fracture energy in mode I for the same crack width (Jensen and Hansen 2000). Cracks in mode I propagate sideways from the notch tip and absorb lower fracture energy. However, in mode II, the crack propagates vertically from the notch and thus absorbs higher fracture energy. The fracture energy in mode I account only for the energy required to create inclined tensile microcracks in the fracture process zone (FPZ). While the fracture energy in mode II accounts for both the energy required to create a crack in FPZ as well as the energy required to break the resistance offered by the aggregate interlocking at the joint (Bazant and Pfeiffer 1986). Hence, mode II shear fracture energy has to be used to quantify the aggregate interlocking in the concrete mix. However, very few studies have been reported on the influence of NMAS on the fracture energy in mode II (Reinhardt and Xu 2000, Kumar and Rao 2010, Rao et al. 2011). Most of these studies have been conducted by following the test method proposed by Reinhardt et al. (1997) using double-edge notched concrete specimens. However, in this test method, the unloaded part of the specimen may rotate once the crack starts propagating, and failure occurs due to the combination of shear and bending. Thus, there is a scope to develop a new test method to study the aggregate interlocking in the concrete mix in terms of fracture energy in mode II.

2.4 FACTORS INFLUENCING THE PERFORMANCE OF AGGREGATE INTERLOCKED JOINT

Several parameters influence the performance of aggregate interlocked joint such as the type of coarse aggregate, nominal maximum aggregate size (NMAS) of coarse aggregates, the strength of concrete, addition of fibers, joint opening and the type of foundation. These factors are discussed in detail below.

2.4.1 Type of coarse aggregate

Different types of aggregates are available in different regions of the world. Based on the availability, different aggregates are used in the construction of pavement. The aggregates from different sources have different hardness. The hardness of aggregate is determined from Los Angeles Abrasion Test. The harder aggregates create a longer crack path, thus increase the LTE significantly. Pradena et al. (2017) reported that LTE mainly depends on the type of aggregate in short panelled concrete pavements.

Nowlen (1968) found that stronger aggregates have higher LTE, and coarse aggregates with Los Angeles abrasion value (LAAV) equal to 17% showed no deterioration in the performance over the number of load repetitions. Abdel-Maksoud (1999) conducted a laboratory investigation on concrete specimens made with limestone, trap rock and gravel. The specimens were subjected to cyclic loading. Authors found that increasing the cyclic load, the carbonate aggregate (limestone) exhibited higher displacement as limestone has the lowest abrasion value among all the other aggregates. Buch and Frabizzio (2000) investigated in-service pavements in Michigan State, constructed using four different coarse aggregates, limestone, natural gravel, recycled aggregates and slag. The LTE of pavements made with different aggregates is tabulated in Table 2.2.

Table 2.2 Effect of type of aggregate on LTE (Buch and Frabizzio 2000)

Type of coarse aggregate	LTE (%)
Recycled	77.44
Carbonate	83.81
Natural Gravel	86.91
Slag	90.83

The authors also conducted the volumetric surface texture (VST) test and found that recycled and slag aggregates had smooth textures, whereas the natural gravels and carbonates were found to have rough textures.

Snyder and Raja (1991) found that LTE is higher for gravel and limestone when compared to slag and recycled aggregates in Jointed Reinforced Concrete Pavements (JRCPs). Authors reported that not only the crack width but the surface texture of the joint also plays an important role. The concrete fracture properties highly influence the surface texture of joint crack. It is assumed to be a function of a number of twists and turns formed at the joint interface, which is difficult to measure accurately. It is a known fact that the LTE of the aggregate interlocked joint depends on the surface texture of aggregates. Brink (2003) conducted tests on concrete slabs made from dolomite and granite aggregates. The author found that though dolomite has a greater elastic modulus than granite, the LTE of granite is greater than that of dolomite for all crack widths. Giaccio and Zerbino (1998) studied the change in fracture energy on concrete mix prepared using four different types of aggregates having different compressive strengths. Authors concluded that granitic crushed stone (GCS) was found to have higher compressive strengths and higher fracture energy.

Many researchers have concluded that aggregates with lower abrasion values have rougher crack surface texture than aggregates with higher value (Wattar 2001; Rao et al. 2002; Roesler and Chupanit 2005). The strong coarse aggregates would produce a higher surface roughness as cracks propagate around the harder aggregate particles and never pass through them. Thus, coarse aggregate type is considered to be the influencing parameter for the LTE. Ramirez (2010) conducted a volumetric surface texture ratio (VSTR) test on coarse aggregates having three different ranges of abrasion values LAAV≤19, 20≤LAAV≤30 and LAAV≥31 and concluded that the coarse aggregates with 20≤LAAV≤30 had the largest VSTR whereas LAAV≥31 had lowest VSTR. Jensen and Hansen (2000) conducted a wedge split fracture test on concrete prepared using two different types of aggregates and concluded that the fracture energy of concrete specimens prepared using hard aggregates was found to be higher when compared to the fracture energy of concrete prepared using soft aggregates. Thus, the

authors concluded that the LTE of aggregate interlocking is higher for the stronger aggregates.

2.4.2 Nominal maximum aggregate size (NMAS) of coarse aggregates

The nominal maximum aggregate size (NMAS) has a great influence on the performance of the joint. Many researchers have studied the effect of NMAS on the LTE of joint. Nowlen (1968) tested the concrete slabs and found that change in NMAS from 19.1 mm up to 38.1 mm has no noticeable effect on joint effectiveness. But authors reported that larger NMAS (above 38.1 mm) improved joint effectiveness, especially for larger joint openings. Paulay and Loeber (1974) reported that for the NMAS ranging between 8.5 mm to 19.1 mm, the NMAS has no significant effect on the performance of joints.

Walraven (1980) conducted direct shear (push-off) tests on the plain and reinforced beams with two different NMAS, 16 mm and 32 mm. No significant conclusions were made on the influence of the NMAS on the performance of the aggregate interlocked joint. However, the author stated that the aggregates having a size less than half of the crack widths have no contribution to load transfer, and these aggregates can be considered to be inactive. Bruinsma et al. (1995) used 25 mm and 40 mm NMAS to test the large slabs, which almost simulated the field condition. The authors concluded that the LTE increases with the increase in NMAS. Wattar (2001) used 25 mm, and 37.5 mm sized aggregates for the preparation of concrete beam specimens. The author found that there is no significant effect of NMAS on joint performance. Brink (2003) tested the concrete slabs made with dolomite and granite aggregates of top sizes 19 mm and 37.5 mm for the preparation of concrete slab specimens. The author concluded that the increase in NMAS increased the LTE of the joint. Vandenbossche (1999) made an attempt to relate joint roughness to NMAS by using the Volumetric Surface Texture (VST) Test. The author reported that as NMAS increases, the roughness of the joint face increases. The author found a relationship between LTE of aggregate interlocked joint and Volumetric Surface Texture Ratio (VSTR). VSTR is defined as the volume of texture per unit surface area obtained by

conducting VST test and expressed in cm^3/cm^2. The relationships between LTE and VSTR are given below:

For laboratory data,

$$LTE = 40\, log\left(\frac{VSTR}{w}\right) + 6 \tag{2.5}$$

For field data,

$$LTE = 120\, log\left(\frac{VSTR}{w}\right) + 101 \tag{2.6}$$

where w is joint opening/ crack width in cm.

Chupanit and Roesler (2005) found that using larger sized aggregates results in more zigzag crack patterns in the joint, creating a rougher surface and improving joint performance. The authors concluded that as the NMAS increases, the fracture energy of concrete increases. It should be noted that in high strength concrete mix, it is essential to use aggregates with smaller NMAS (Al-Oraimi et al. 2006). As smaller sized aggregates have more surface area, it increases the bond strength between aggregate and mortar, thus increasing concrete's overall strength. It is necessary to balance this parameter in order to achieve sufficient strength for concrete slab and LTE across the joint.

2.4.3 Coarse aggregate angularity

In addition to the size of coarse aggregates, the shape of the aggregate particles has a significant role in deciding the roughness of the joint, which influences the load transfer mechanism. The coarse aggregate angularity is related to the number of fractured faces of an aggregate. The number of fractured faces of coarse aggregates increases the interlocking of aggregate at the joint increases, thus increasing the LTE of the joint. But as the angularity increases, the concrete workability reduces. Colley and Humphrey (1967) showed from their investigation that the load transfer at the joint gets improved when the angular aggregate particles are used in the concrete mix. The angularity of aggregate can be determined accurately using image analysis technology (Rao et al. 2002).

2.4.4 Aggregate gradation

The gradation of aggregates plays an important role in influencing the performance of the aggregate interlocked joint. Wattar (2001) studied the effect of gap and dense gradation on surface roughness and stiffness of joint. They concluded that the use of gap gradation would improve the crack/joint surface roughness that enhances the performance of the aggregate interlocking. Studies concluded that the use of gap graded aggregates in concrete results in significantly higher joint stiffness values when compared to the use of dense-graded aggregates in the concrete. Chupanit and Roesler (2008) studied the influence of dense and gap gradation on the joint surface texture (roughness) and fracture energy of concrete in order to relate the aggregate gradation with a joint performance. The authors found that the use of gap graded aggregates results in higher fracture energy and rougher surface. The use of gap graded aggregates results in a reduction in the strength of concrete.

2.4.5 Strength of concrete mix

Khazanovich and Gotlif (2003) studied the effect of concrete compressive strength on LTE of joints of CRCP, doweled and non-dowelled jointed concrete pavements. The authors concluded that no significant correlation exists between compressive strength and LTE for any of the pavement type.

2.4.6 Addition of fibers

Fibers are used mainly in the construction of ultra-thin whitetopping (UTW). There are two types of fibers being used in pavement construction. The fibers are classified as micro and macro-fibers based on their elasticity modulus values and lengths. The fibers with less than 30 mm in length and lower elastic modulus values are termed non-structural fibers or micro-fibers. The fibers with greater than 30 mm in length and higher elastic modulus values are structural fibers or macro-fibers (Blazy and Blazy 2021). The use of micro-fibers reduces the plastic shrinkage cracks in the fresh concrete (Leong et al. 2020; Yew et al. 2016; Zhang and Li 2013). The micro-fibers are used in many of the UTW projects. Researchers have studied the influence of synthetic micro-fibers on the flexural fatigue performance of concrete (Kasu et al. 2020) and the

durability of concrete (Xu et al. 2021). However, the contribution of micro-fibers on joint performance has not been investigated.

It is reported that the use of macro-fibers in concrete improves the joint stiffness, toughness and flexural strengths significantly (Belshe et al. 2011; Roesler et al. 2006). Roesler et al. (2012) conducted the accelerated pavement test and demonstrated that the performance of aggregate interlocked joints could be improved with the addition of structural fibers. Barman and Hansen (2018) conducted laboratory tests on fiber reinforced beams and plain concrete beams and found that LTE is about 20% higher for fiber reinforced beams when crack width is less than 2 mm. But when joint opening exceeds 2 mm, the LTE is comparatively higher for plain beams. Authors also reported from the field study that the contribution of the fibers was significant during winter when compared to summer.

2.4.7 Joint opening

The joint opening is considered to be the key parameter that influences the LTE of the aggregate interlocked joint. Colley and Humphrey (1967) studied the influence of joint opening on aggregate interlocking in the laboratory. They showed that the LTE and joint opening are inversely related. The authors concluded that an increase in the joint opening from 0.635 mm to 2.16 mm results in an 80% loss in joint effectiveness under a constant amplitude cyclic loading. Brink (2003) reported that narrower crack width results in lower relative movement at the aggregate interlocked joints.

Jensen and Hansen (2001) proposed that the LTE is solely related to the joint opening. In order to find a relationship, the authors plotted the LTE Vs Joint opening and obtained a curve. The curve was divided into three different stages. It was observed that in stage I, LTE was 100% when the joint opening was less than 0.5 mm. The LTE decreases with an increased joint opening in stage II and stage III; when the joint opening exceeds 2.5 mm, the load is transferred through the pavement base. Lee et al. (2010) reported that as the number of load repetitions increases, the joint opening increases leading to poor load transfer across the aggregate interlocked joint.

2.4.8 Thickness of concrete slab

Many researchers have studied the effect of thickness on LTE of joint. Colley and Humphrey (1967) studied the joint effectiveness of two slabs with different thicknesses 177.8 mm and 228.6 mm and found that slabs with higher thickness showed better performance in terms of load transfer across the joint. The effectiveness values of are converted into LTE values using a regression relationship. The test results are shown in Figure 2.2.

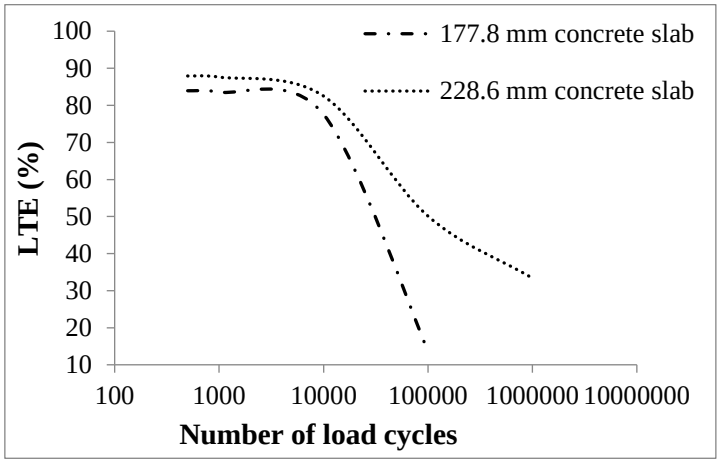

Figure 2.2 Influence of thickness of concrete slab on LTE (after Colley and Humphrey 1967)

Ball and Childs (1975) also demonstrated that thicker slabs effectively transfer load across the aggregate interlocked joint. It can be seen from Figure 2.2 that at any given number of load cycles, the LTE of the thicker slab is higher. Similar observations were reported by Maitra et al. (2010) and Sadeghi and Hesami (2018) after conducting the finite element analysis of aggregate interlocked joints.

2.4.9 Type of support

The type of foundation support provided below the concrete pavement has a greater influence on the performance of joints in whitetopping and short panelled concrete. The use of superior quality material as a base layer would improve the performance of joints (Taylor et al. 2007). The base provides continuity below the joint and transfers the part of the load. The total LTE of any joint is obtained by the following equation (Darter et al. 2001)

$$LTE_{joint} = 100 \times \left(1-\left(1-\frac{LTE_{AGG}}{100}\right)\times\left(1-\frac{LTE_{dowel}}{100}\right)\times\left(1-\frac{LTE_{base}}{100}\right)\right) \quad (2.7)$$

where LTE_{joint} is total joint LTE in percentage, LTE_{dowel} is joint LTE in percentage (if dowels are the only mechanism of load transfer), LTE_{base} is joint LTE in percentage (if the base is the only mechanism of load transfer) LTE_{AGG} is joint LTE in percentage (if aggregate interlock is the only mechanism of load transfer). There are no methods to evaluate the contribution of the underlying base to the load transfer across joints. Darter et al. (2001) provided the LTE values representing the load transfer contributed by the base course only. These values were recommended based on the field measurements and partly engineering judgement of the authors. The recommended values of LTE for different base support types are tabulated in Table 2.3.

Table 2.3 Recommended values of LTE for different base support types (Darter et al. 2001)

Type of base support	LTE of base, %
Aggregate base (WMM or WBM)	20
Asphalt treated or cement treated base	30-40
Lean concrete base	40-50

Colley and Humphrey (1967) found that joint effectiveness improved with an increase in the strength of the base below the pavement slab. The use of a cement-treated sub-base doubled the joint effectiveness. Nowlen (1968) also agreed that the use of cement-treated base improves joint efficiency. Ball and Childs (1975) conducted laboratory tests on concrete beams resting on stabilised (Cement treated base - CTB) and un-stabilised layers (granular layers). Authors found that beams resting on stabilised layers showed a better LTE. Taylor et al. (2005) and Wadkar et al. (2011) reported that stabilised base improved the load transfer across the joint. Even Mu et al. (2016) reported that the stabilised base improved LTE in aggregate interlocked joints, whereas it posed an adverse effect on LTE of doweled joints.

Interestingly, Khazanovich et al. (2003) concluded from the field study that LTE of non-doweled joints was slightly lower for pavements with a lean concrete base when compared to pavements with other base types. They made an interesting observation

that a stiff base may increase PCC slab curling and result in poor load transfer across the joints. The authors also concluded that LTE is higher for coarse-grained subgrade when compared to fine-grained subgrade. It is also interesting to note that the type of support and uniformity play an important role in the LTE of the aggregate interlocked joint. When the concrete slab is in full contact with the base, LTE of AI is equal to 100% (Owusu-antwi et al. 1990).

2.4.10 Environmental conditions

The environmental conditions are different across the globe, and these conditions vary with time. Pavement materials are highly susceptible to these variations in environmental conditions. As the performance of aggregate interlocked joints is highly dependent on the pavement material properties, it gets influenced by the variation in environmental conditions. Kapiri et al. (2000) collected temperature and falling weight deflectometer data at the Denver International Airport (DIA). Authors found it interesting that the LTE values for the same joint were as low as 13% during the winter and as high as 85% during the summer season. This is because in winter, the temperature will be low, leading to larger joint opening that results in lower LTE, and in summer, the joint is tight, which results in higher LTE.

Poblete et al. (1998) have measured differences in the bottom and surface temperature for slab thickness of 228.6 mm to 254 mm. The temperature differential ranged from 0 to 263.71K. The effects are attributed to the slab curling and warping; the rotation of the vertical edges of concrete slab curl or warp which compresses either top or bottom portions of the slab together, resulting in a significant improvement in the performance of the aggregate interlocked joint.

Owusu-Antwi et al. (1990) conducted tests in the Pavement Research Facility laboratory and have shown that the LTE increases in the order of 20% to 40% for any joint opening when the temperature differential varied from 249.82 K to 263.71 K. However, no significant change in LTEs was seen when the joint was kept closed (tight joint). Authors concluded that LTE increases with an increase in vertical temperature differential in pavements and found no change across the joints in rigid pavements. Frabizzio and Buch (1999) reported that the increase in the pavement surface

temperature results in an increase in LTE of joints. For a pavement surface temperature range of 278.15 - 288.15K (5 – 15°C), the LTE of the joint was less than 30%. But when the pavement surface temperature range was increased to 303.15 - 315.15K (30 - 42°C), the LTE of the joint was found to be increased to 40 -70%. Ongel and Harvey (2004) found a poor correlation between the LTE and the surface temperature of the slab. Rufino and Roesler (2004) conducted deflection studies using the heavyweight deflectometer test, and the authors found a regression relation between LTE and average pavement temperature by fitting a curve. The regression equation is given below

$$LTE = 0.0112 \times AT^2 + 0.0185 \times AT + 6.397 \quad (2.8)$$

$$R^2 = 0.9354$$

where LTE is load transfer efficiency of aggregate interlocked joint in percentage

AT is average pavement temperature in degree Fahrenheit

Perera et al. (2005) also reported that higher mean annual air temperatures of about 284K (10.85°C) resulted in better load transfer through the aggregate interlocked joint when compared to mean annual air temperatures of about 280.6 K. Conversely, Aure and Ioaninides (2015) reported that the increase in differential temperature did not affect LTE during the night. But, LTE is inversely proportional to temperature differential during daytime.

2.5 FINITE ELEMENT METHOD

The design procedures and analysis methods for concrete pavements used in India are based on closed-form solutions. The limitations of these procedures are that the available design equations are based on the single slab results and do not account for load transfer across the joints. The finite element method (FEM) overcomes these limitations. The method is capable of analysing multiple slabs with different load configurations.

2.5.1 Two-dimensional FE models

Using the classical plate theory, Huang and Wang (1973, 1974) developed a two-dimensional finite element model named KENSLABS. The model assumes that the slab is thin and is supported on a subgrade foundation, either elastic or layered or

Winkler type. Tabatabaie and Barenberg (1978) developed ILLISLAB (another 2-D FE model) to analyse concrete pavements. Tia et al. (1987) developed a 2-D FE computer program called FEACONS III, which can analyse the behaviour of concrete pavements effectively and realistically. Zaman and Alvappilai (1995) developed the FE model to study moving aircraft loads on concrete pavements. DYNASLAB code was proposed by Chatti and Kim (2001) for the dynamic analysis of concrete pavement. Authors assumed that the foundation was either Winkler or layered. King and Roesler (2014) analysed a bonded concrete overlay model in ILLISLAB to develop a back-calculation procedure for the FWD tests on these pavements. Most of these 2-D FE models were developed based on the thin plate theory, in which the main assumption is that the thickness of the slab is minimum. But the pavement slabs are moderately thick, and shear deformation is significant.

2.5.2 Three-dimensional FE models

Three-dimensional FE models can overcome the limitations of two-dimensional FE models. With advanced computers and processors, the 3-D FE models provide more realistic and accurate results. Many researchers have modelled concrete pavements using this method by considering its advantages. Software such as ANSYS, ABAQUS and EverFE provide a user-friendly platform to model the concrete pavements. Channakeshava et al. (1993) developed a 3-D FE model to assess the performance of dowels in concrete pavements. Wu and Shen (1996) developed a 3-D FE model to study the response of pavements by subjecting them to moving loads. Vepa and George (1997) developed a regression equation to predict the deflection response of FWD by performing the multilayer 3-D FE analysis of pavements in ABAQUS. Researchers have used 3-D FE models to study the temperature variation across the depth of the slab (Kuo 1998; Pane et al. 1998). For the structural analysis of concrete pavements, a more advanced and user-friendly program named EverFE was developed by (Davids 1998), which includes both aggregate interlock and dowel load transfer. Brink (2003) used EverFE software to model the concrete pavement and compared the experimental test results with 3-D FE model results.

Maitra et al. (2009) developed a 3-D FE model in ANSYS to analyse the performance of dowels in JPCPs. Authors also developed a generalized equation for the determination of LTE of doweled joints after conducting several simulations. In the subsequent year, Maitra et al. (2010) modelled the aggregate interlocked joint of JPCP and proposed a new term to quantify the aggregate interlocking called modulus of the interlocking joint (K_j). The 3-D FE results of the model were validated with the experimental results available in the literature. Barman (2014) developed a 3-D FE model of bonded concrete overlays in ABAQUS to study the influence of fibers on the performance of joints and developed a generalized equation to calculate LTE of joint bonded concrete overlays. Researches have also developed 3-D FE model for fracture analysis of concrete pavements (Aure and Ioannides 2015; Maitra et al. 2014; Ramsamooj 1999).

2.5.3 Modeling the structural components of concrete pavement

The major structural components of concrete pavements are a concrete slab on top, a foundation base at the bottom and a joint system. Most researchers have modelled concrete slab as medium thick plate element for the 2-D FE analysis (Huang and Deng 1983; Ioannides and Korovesis 1990; King and Roesler 2014; Tabatabaie and Barenberg 1978; Zaman and Alvappilai 1995). Kuo (1994) modelled using the shell elements. Authors assumed that the concrete slab is elastic, homogeneous and isotropic in nature. The modulus of elasticity of concrete and Poisson's ratio are the two input parameters used for representing the concrete slab in 2-D FE. As stated earlier, these models ignore the shear strength of plates. In the past, the concrete slab was represented by the linear elastic 3-D brick elements (Barman 2014; Davids et al. 1998; Maitra et al. 2009, 2010; Swarna et al. 2018). This provides a more accurate representation of the concrete slab in the 3-D FE model.

The foundation base for a concrete slab usually consists of a base layer (either DLC or CTB), sub-base (GSB) layer and subgrade for new construction. The foundation base for overlays consists of deteriorated bituminous layer on top of the layers mentioned above. The base layer is also modelled using the linear elastic 3-D brick elements (Davids et al. 1998; Maitra et al. 2009, 2010; Swarna et al. 2018).

Barman (2014) modelled deteriorated bituminous pavement layer using the linear elastic 3-D brick elements.

Theoretically, various subgrade models are available in the literature to represent subgrade. The Winkler foundation model, elastic solid foundation model, and two-parameter foundation model are popularly used to represent subgrade. Many researchers have modelled subgrade using the Winkler foundation model. It is simple and requires modulus of subgrade reaction (k) as single input (Kuo 1994; Maitra et al. 2009, 2010; Swarna et al. 2018; Uddin et al. 1995; Zaman and Alvappilai 1995).

The dowels are the major component of a joint system for load transfer across the joint for high volume roads. Many researchers have used beam elements to represent dowel bars in the 3-D FE model (Channakeshava et al. 1993; Davids et al. 1998; Kuo 1994; Maitra et al. 2009; Uddin et al. 1995; Zaman and Alvappilai 1995). The modulus of dowel support (K) is used as a parameter to define the strength of dowels. The higher the value indicates better load transfer across the doweled joint.

In whitetopping and short panelled concrete pavements, the load transfer across the joints take place through aggregate interlocked joints. In an aggregate interlocked joint, the load is transferred in the form of shear. The researchers have represented the aggregate interlocked joint using a series of springs connected from one side of the slab to another slab (Barman 2014; Ioannides and Korovesis 1990; King and Roesler 2014; Kuo 1994; Maitra et al. 2010; Tabatabaie and Barenberg 1978; Uddin et al. 1995; Zaman and Alvappilai 1995). The spring stiffness is used as an input parameter to model the aggregate interlocked joint. The spring stiffness is back-calculated using the field deflection measurements. Ioannides and Korovesis (1990) developed a relation between a non-dimensional joint stiffness (AGG/kl) and LTE. Also, Maitra et al. (2010) developed a model to estimate spring stiffness based on the joint opening and the nominal maximum aggregate size. This model was developed based on the experimental studies conducted by Brink (2003) in the laboratory. Byrum (2012) developed a model that can directly compute the joint stiffness from the field FWD data. However, there are no proper guidelines available for selecting spring stiffness for

whitetopping and short panelled concrete pavement joints neither at the stage of design nor at the time of service.

2.6 APPLICATION OF ARTIFICIAL NEURAL NETWORK (ANN)

In the recent past, artificial neural network (ANN) are being used in various civil engineering applications. The major advantage of ANN is that it can learn from past experiences to enhance their performance and adjust to the changes in the atmosphere. Once trained, these models will gain the ability to effectively predict the output even for noisy and incomplete input data (Heravi and Eslamdoost 2015). ANN models are suitable when the relationship between the input and output data is unknown and non-linear. These models are invariably used in different engineering fields due to their adaptive nature and savings in energy, cost and computation time (Kallannavar et al. 2021).

Many researchers have developed ANN models for predicting the performance of construction materials and structures. ANN models have been used in the performance prediction of various concrete types, such as self-compacting concrete (Asteris et al. 2016), plastic concrete (Ghanizadeh et al. 2019), and ultra-high-performance concrete (Abellán García et al. 2020). Asteris et al. (2016) used Back-Propagation Neural Network (BPNN) method to develop the ANN models to predict the compressive strength of self-compacting concrete and reported that the predicted values were very close to the experimental results, and the correlation coefficient further confirmed it. Ghanizadeh et al. (2019) developed an ANN model to predict the compressive strength of bentonite/sepiolite plastic concretes by using the Levenberg-Marquardt algorithm to train the network. Authors reported that the ANN model was efficient to predict the compressive strength values of plastic concrete. In another study, García et al. (2020) developed an ANN model for predicting the slump flow and compressive strengths of ultra-high-performance concrete (UHPC) and concluded that the developed ANN model was efficient enough to predict the slump flow and compressive strengths of UHPC. Jalal et al. (2020) developed an optimum ANN model to predict the behaviour of a rubberised cement composite interms of compressive strength by using experimental results as input data. In their study, the authors used

Levenberg–Marquardt back-propagation (LMBP) technique to train the network. It was reported that the developed ANN model was able to predict the behaviour of rubberised cement composite with an accuracy of 98%. Elshafey et al. (2013) developed the ANN prediction model using the feed-forward back-propagation (FFBP) method to predict crack width in reinforced concrete members. It was reported that the experimental crack width values were in agreement with the ANN predicted values. Heravi and Eslamdoost (2015) developed ANN models to predict the construction labour productivity in developing countries. Authors used the Bayesian regularisation method to train the dataset and concluded that the technique provides better performance than other training techniques. Rezaali et al. (2021) developed an ANN model to forecast urban water demand using the LMBP training algorithm and reported that the ANN models are efficient in forecasting the urban water demand.

In past few years, the ANN models have been developed to predict pavement materials testing and pavement performance evaluation in terms of both functional and structural aspects. Hussain et al. (2021) developed an ANN model to characterise the phase angle behaviour of bituminous concrete mixes in a gyratory compactor and concluded that the ANN model could be used as a surrogate to laboratory testing for assessing the performance of bituminous concrete mixes. Researchers used the feed-forward back-propagation ANN technique to evaluate and develop the relationship between deformation and stiffness modulus of FORTA-FI strengthened bituminous mixtures (Khasawneh et al. 2019). Fakhri and Shahni Dezfoulian (2019) developed a relationship between FWD deflection bowl parameters, and pavement surface distresses interms of International Roughness Index (IRI) and Pavement Surface Evaluation and Rating index (PASER) using ANN and other non-intelligent models and concluded that ANN models were accurate and outperformed the other non-intelligent models. Nivedya and Mallick (2020) developed an ANN model to predict the field permeability of flexible pavement layers and concluded that the model accurately predicted the field permeability of flexible pavement layers. Lekshmipathy et al. (2020) developed an ANN model to detect road bumps, potholes, cracks and patches based on the data collected from smartphone sensor-based technique. Authors used the LMBP algorithm to train the neural network.

Hossain et al. (2020) developed an ANN model to predict the international roughness index (IRI) of rigid pavements. Authors used only the climatic and traffic data for developing the ANN model, and it was concluded that the model was able to predict the IRI with an error of 1% for the rigid pavement constructed in the non-freezing and wet climatic conditions. The ANN model developed using the Long-Term Pavement Performance (LTPP) database predicted IRI of jointed plain concrete pavement (JPCP) sections in the USA with only a 7% prediction error (Kaloop et al. 2020). Alatoom and Al-Suleiman (2021) developed an ANN model to predict IRI based on smartphone measurements on the flexible pavement. It was concluded that the developed ANN models were more accurate in predicting IRI than the regression models. Wang et al. (2021) developed an ANN model for predicting maximum tensile and shear strains in the airfield bituminous pavement directly from the FWD surface deflections data. The ANN model was developed using the data generated from a validated FE model. It was concluded that the accuracy of the ANN model was better than the traditional prediction method when the strains of both the models were compared with field strain measurements conducted at the National Airport Pavement Testing Facility (NAPTF).

Bayrak and Ceylan (2008) developed ANN models to predict the layer moduli of rigid pavements from FWD data. Authors concluded that the ANN models not only predicted accurately but also reduced the computation time drastically. Considering the abilities and advantages of ANN, these models can be used to predict the performance of the aggregate interlocked joints.

2.7 LITERATURE SUMMARY

It is found from the literature that the researchers have made significant contributions to evaluate the aggregate interlocked joints in concrete pavement by conducting experimental, numerical and field studies. Most of the researchers conducted tests by casting large concrete slabs in the laboratory to evaluate the performance of the aggregate interlocked joint in terms of load transfer efficiency (LTE). However, these experimental methods are uneconomical as they require a huge quantity of materials and high-end equipment. A very limited studies available which

have developed a small-scale test setup. These small-scale test setups are complex and use costlier equipment. Thus, there is a scope for developing a simple, reliable and low-cost laboratory small scale test setup that can be used to assess the performance of aggregate interlocked joints in terms of LTE. The aggregate interlocking mechanism is also useful in concrete structures such as dams, repair of buildings and bridges. Researchers have used the push-off method, the International Federation for Structural Concrete (FIP) method and JSCE_G 553 method to evaluate the aggregate interlocking in concrete in terms of shear strength. These test methods were failed to apply the pure shear load at the joint. The efforts were also made to quantify the aggregate interlocking in terms of joint stiffness and fracture energy. Many of these studies measured fracture energy in mode I, which does not account for the aggregate interlocking at the joint.

Considering the advantages of the finite element method, many researchers have used the method to understand the behaviour of aggregate interlocked joints and the concrete pavement as a whole. The linear spring elements are generally used to represent the aggregate interlocked joints in concrete pavements. The load is transferred through the springs across the joint in the simulated concrete pavement model. Limited works of literature are available for selecting the spring stiffness values based on laboratory experiments. There is a need for a method that can quantify the aggregate interlocking of concrete pavement joints in the laboratory in terms of joint stiffness. The value can be used to numerically analyse the aggregate interlocked joints of concrete pavements at the design stage in FE based software.

In many of the studies, a falling weight deflectometer (FWD) was used to evaluate the performance of aggregate interlocked joints in concrete pavements. Researchers back-calculated the joint stiffness values by using them in the FE model to match the field deflection measurements using FWD. A relationship between LTE and joint stiffness is also available in the literature. In one of the studies, attempts were made to develop a model that can compute joint stiffness directly from the FWD deflection measurements. However, these models are applicable only to conventional concrete pavements. The ability of these models to predict the joint stiffness of whitetopping pavements has not been studied so far. There is a scope to improve the model available in the literature that can be used directly to predict the joint stiffness of

whitetopping pavement joints from the field FWD data. Also, the ANN model can be developed as it saves computational time and cost.

The aggregate interlocking is dependent on the nominal size of aggregate (NMAS) used in concrete, groove depth and addition of fibers to concrete. There is a need to evaluate the performance of aggregate interlocked joint considering these significant factors. The poor performance of aggregate interlocked joints results in poor performance of white-topping and short panelled concrete pavements. Thus, there is a need to evaluate the performance of the aggregate interlocked joints in the laboratory at the design stage. The ANN model has to be developed that can properly estimate the joint stiffness of whitetopping to assess the performance of aggregate interlocked joints during service life. The experimental and model results can be utilised to formulate the guidelines to design and maintain the white topping and short panelled concrete pavements for Indian conditions.

CHAPTER 3

MATERIALS AND METHODOLOGY

3.1 GENERAL

This chapter provides a brief description of the materials used to prepare pavement quality concrete (PQC) mix and the experimental procedures employed to achieve the objectives of the present research.

3.2 MATERIALS

3.2.1 Cementitious materials

The Ordinary Portland Cement (OPC-43 grade) conforming to IS 269-2015 and GGBS conforming to IS 12089-1987 were used to prepare PQC mixes. The percentage of GGBS was limited to 50% as per IRC 44-2017. The physical properties of binder materials, cement and GGBS, are tabulated in Table 3.1 and Table 3.2, respectively.

Table 3.1 Physical properties of cement (OPC-43 grade)

Sl. No.	Tests	Test results	Requirements as per code
1	Initial and final Setting time	52 minutes and 242 minutes, respectively	Minimum 30 minutes and Maximum 600 minutes, respectively
2	Specific surface of cement	3240 cm^2/gm	Minimum 2250 cm^2/gm
3	Specific gravity test	3.15	-

Table 3.2 Physical and chemical properties of GGBS

Physical Properties	
Loss of ignition	0.04%
Specific gravity	2.8
Insoluble residue	0.3
Bulk density (kg/m^3)	1200
Specific surface area (m^2/kg)	370
Chemical Properties	
CaO	41
SiO_2	35
Al_2O_3	11
Fe_2O_3	1

3.2.2 Coarse aggregates

The granitic aggregates are from igneous rock origin and the igneous rocks are generally hard, strong and durable. The aggregates from the igneous rock origin are suitable for road construction (Kazi and Al-Mansour 1980). Due to the availability of granitic aggregates and their influence on the fracture properties of concrete, the crushed granitic aggregates were used in the present study. The coarse aggregates were obtained from a local quarry. The aggregates used in this study conform to the requirements of MoRT&H (2013) fifth revision specifications. The physical requirements of the coarse aggregates are presented in Table 3.3.

Table 3.3 Physical properties of coarse aggregates

Properties	Crushed Granite aggregates Results	Requirement as per MoRT&H (5^{th} revision) Specifications
Aggregate Los Angeles abrasion value	24%	Maximum 35%
Water absorption	0.3 %	Maximum 2%
Combined flakiness and elongation index	25%	Maximum 35%
Specific gravity test	2.69	-
Aggregate crushing value	21%	-
Aggregate impact value	22%	-

3.2.3 Fine aggregates

In the present study, clean, dry river sand obtained from a local supplier conforming to IS: 383-2016 is adopted. The physical properties of the fine aggregates are presented in Table 3.4.

Table 3.4 Physical properties of fine aggregates

Tests	Test procedure as per IS-code	Results
Specific gravity test	IS: 2386-1963 (Part 3)	2.54
Water absorption	IS: 2386-1963 (Part 3)	1%
Sieve analysis	IS: 383-1970	Zone-II

Three gradations with different nominal sized aggregates were used in this research in order to study the effect of nominal maximum aggregate size (NMAS) on the shear

strength properties of PQC mixes. The aggregates of 19 mm NMAS were used in the preparation of micro and macro fiber reinforced PQC mixes. Table 3.5 presents the recommended combined grading of fine and coarse aggregates for different NMAS and Figure 3.1 shows the adopted combined aggregate gradation for each NMAS.

Table 3.5 Recommended combined grading of fine and coarse aggregates for different NMAS (IRC:44-2017)

Sieve Designation	Percentage weight by passing		
	NMAS		
	31.5 mm	26.5 mm	19 mm
37.5 mm	100	100	100
31.5 mm	90-100	100	100
26.5 mm	85-95	90-100	100
9.0 mm	68-88	75-95	90-100
9.5 mm	45-65	50-70	48-78
4.75 mm	30-55	30-55	30-58
600 µ	8-30	8-30	8-35
150 µ	0-10	0-10	0-12
75 µ (Wet Sieving)	0-2	0-2	0-2

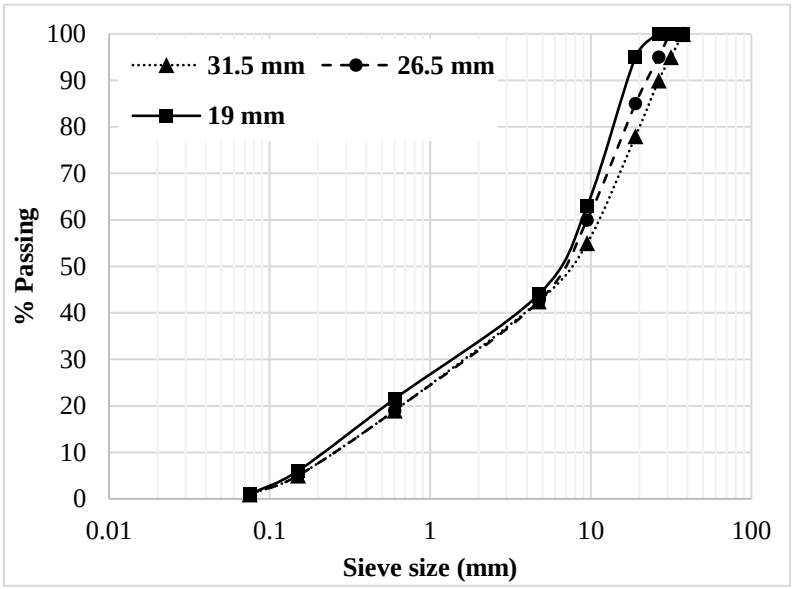

Figure 3.1 Adopted combined aggregate gradation for each NMAS 19, 26.5 and 31.5 mm

3.2.4 Chemical Admixture

A commercially available Chloride free Naphthalene Sulfonate admixture having a specific gravity of 1.05, conforming to IS 9103-1999, was added to improve the workability of the concrete mixture, ensuring that the other concrete parameters such as segregation, ultimate strength and concrete permeability are unaffected. An amount of 1% admixture by weight of the binder was added to achieve the desired slump of 0 to 25.

3.2.5 Water

Potable water conforming to IS: 456-2000 was used for mixing and curing of PQC mixes with or without the addition of fibers.

3.2.6 Fibers

In the present study, two types of polypropylene fibers, shown in Figure 3.2, were used to prepare the fiber-reinforced PQC mixes. One was polypropylene monofilament micro-fiber (Recron 3s) provided by M/S Concrete Solutions, Mangalore, India. The other was polypropylene waved macro-fiber provided by Kalyani Polymers Pvt. Ltd., Bangalore, India. The properties of both micro and macro-fibers are presented in Table 3.6.

Polypropylene micro-fiber (Recron 3s)

Polypropylene waved macro-fiber

Figure 3.2 Polypropylene fibers used in the present study

Table 3.6 Physical properties of fiber

Properties	Results	
	Micro-fiber (source: M/S Concrete Solutions, Mangalore, India	Macro-fiber (source: Kalyani Polymers Pvt. Ltd., Bangalore)
Cross-section	Triangular	Rectangular
Structure	Monofilament	Waved
Length (mm)	12	48
Diameter/Thickness (mm)	0.038	0.89
Aspect ratio (length/diameter)	320	54
Specific gravity	0.90	0.91
Tensile strength (MPa)	410	600
Modulus of elasticity (MPa)	5445	14240

3.3 MIX DESIGN OF PLAIN AND FIBER REINFORCED PQC MIXES

The mix design was carried out for the M40 grade of PQC as per IRC 44-2017. The water-binder ratio (w/c) of 0.36 was maintained constant for all the concrete mixes to achieve a slump of 25 mm. The concrete mixtures with NMAS 19 mm, 26.5 mm, and 31.5 mm were designated with A19, A26.5 and A31.5, respectively. The proportions of ingredients of concrete prepared using these three different NMAS for M40 grade of concrete are presented in Table 3.7.

Table 3.7 Proportions of plain PQC mix (kg/m^3)

Mix ID	Water	Cement	GGBS	Fine aggregates	Coarse aggregates	Superplasticizer
A19	144	200	200	666	1304	4
A26.5	135	188	188	631	1414	3.75
A31.5	130	181	181	624	1320	3.62

The fiber reinforced PQC mix design was also carried out as per IRC 44-2017. One set of fiber reinforced PQC mixtures were prepared using the 19 mm NMAS. The polypropylene micro-fiber (Recron 3s) was added by varying the dosages 0.9, 2.1 and 3.0 kg/m^3 by volume and designated with F0.9, F2.1 and F3.0. Another set of fiber reinforced PQC mixtures were prepared with three different dosages of 0.25%, 0.50% and 0.75% total volume of the concrete mix using the 19 mm NMAS and were designated with PF 0.25, PF 0.5 and PF 0.75.

3.4 PRELIMINARY TESTS ON PLAIN AND FIBER REINFORCED PQC

3.4.1 Workability of fresh plain and fiber reinforced PQC mixes

The slump test was conducted using the standard Abraham's slump cone on plain and fiber reinforced PQC fresh mixes. The workability and consistency of the plain PQC mix prepared using different NMAS, and fiber reinforced PQC mix with micro and macro-fibers were determined by conducting the slump cone test as per IS 1199-1959.

3.4.2 Hardened mechanical plain and fiber reinforced PQC mixes

The hardened mechanical properties of plain PQC mixtures prepared using different NMAS and fiber reinforced PQC mixes prepared using varying dosages of micro and macro-fibers were determined. The hardened properties of plain PQC and fiber reinforced PQC mixes such as compressive strength, flexural strength, split tensile strength, and modulus of elasticity (E) were determined after 28 days of curing in the water. The compressive strength test was conducted on a standard 150 ×150 × 150 mm cube specimen, and the flexural strength test was conducted on 100 × 100 × 500 mm beam specimens. A standard cylinder of size 150 mm in diameter and 300 mm in height was used for conducting the split tensile strength and elastic modulus tests. The compressive strength, flexural strength and modulus of elasticity tests were performed according to IS 516-1959, and the split tensile strength test was conducted according to IS 5816-1999.

3.5 PRELIMINARY TESTS RESULTS

3.5.1 Slump test

The workability of plain and fiber reinforced PQC mixtures measured in terms of slump values are tabulated in Table 3.8. It is seen from Table 3.8 that the slump value decreases with an increase in NMAS of plain PQC mixtures. This is due to the reduction in water content with an increase in NMAS. The slump values are lower for the fiber reinforced PQC mix when compared to the PQC mix. The slump value decreases with an increase in the dosages of micro-fibers. A similar trend can be seen in the literature (Karimipour 2022; Karimipour and de Brito 2021). Also, the slump value decreases with an increase in fiber dosages for the fiber reinforced PQC mix prepared using macro

polypropylene fibers. The reduction in slump value is due to the increase in cohesive forces and bonding between fibers and concrete matrix (Fallah and Nematzadeh 2017).

Table 3.8 Slump values of concrete mixes

Type of concrete mix	Mix ID	Slump Value (mm)
Plain PQC	A19	22
	A26.5	20
	A31.5	18
Micro-fiber reinforced PQC	F0.9	19
	F2.1	17
	F3.0	15
Macro-fiber reinforced PQC	PF0.25	20
	PF0.50	19
	PF0.75	17

3.5.2 Compressive strength

The 28 days compressive strengths (with 95% confidence interval) of plain pavement quality concrete mixtures prepared using three different NMAS 19, 26.5 and 31.5 mm and micro and macro-fiber reinforced PQC mixtures are presented in Figure 3.3.

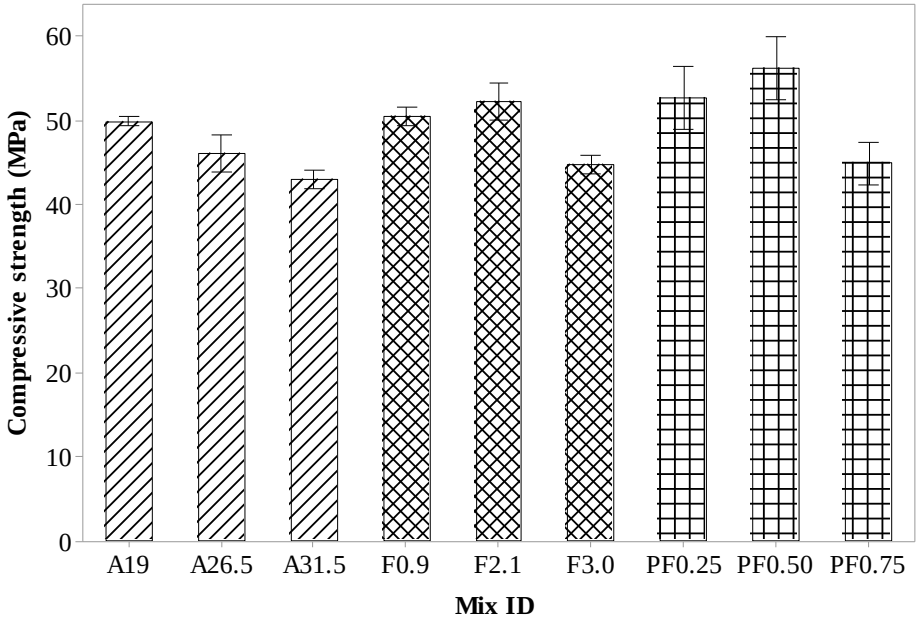

Figure 3.3 Compressive strength test results for different PQC mixes

It can be seen that the compressive strength decreases with an increase in NMAS of PQC mix specimens. This is due to the formation of the weaker interfacial transition

zone (ITZ) in the concrete mix (Mehta and Monteiro 2014). The compressive strength is higher for fiber reinforced PQC. However, the compressive strength increases with increased fiber content up to a certain value, beyond which decreases with increased fiber dosages for both micro and macro-fiber reinforced PQC mix specimens. The lower volume fractions of fiber improve the bridging of microcracks and reduce the formation of the pores in the concrete mix, but the high volume of fiber fractions results in fiber clumping and increase the chances of pore formation in the concrete mix, which results in lower compressive strengths. Similar observations can be seen in the literature for both micro-fiber reinforced concrete (Fallah and Nematzadeh 2017; Yazici et al. 2015) and macro-fiber reinforced concrete(Alberti et al. 2014; Yazdanbakhsh et al. 2015).

3.5.3 Flexural strength

The flexural strength tests were conducted after 28 days of curing in water. The flexural strengths (with 95% confidence interval) of plain pavement quality concrete mixtures prepared using three different NMAS and micro and macro-fiber reinforced PQC mixtures are presented in Figure 3.4.

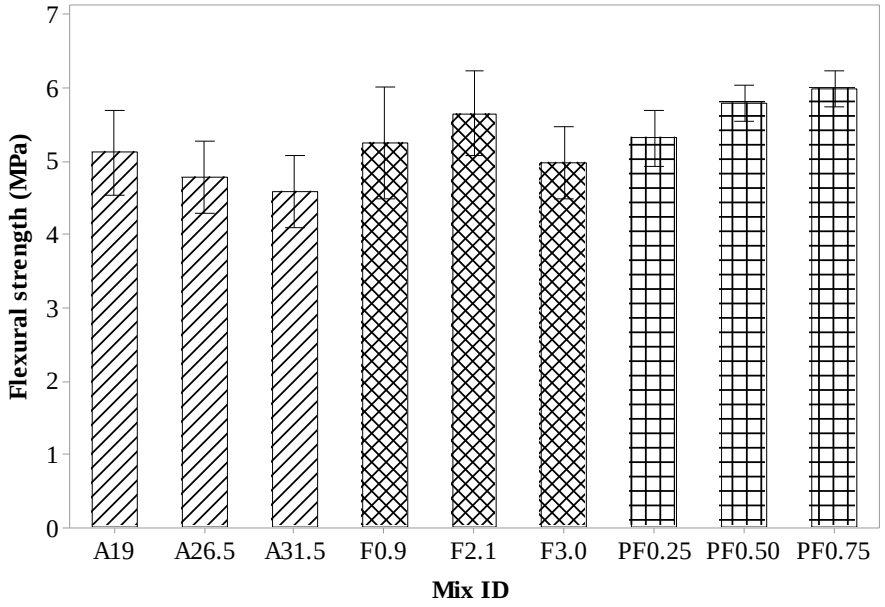

Figure 3.4 Flexural strength test results for different PQC mixes

It can be observed from Figure 3.4 that with the increase in NMAS, the flexural strength decreases. The results are similar to the tests results reported by Kasu et al. (2019). The use of micro-fibers and macro-fiber increases the flexural strength of concrete as these

fibers bridge the matrix and aggregate, increasing the bond strength. However, in the case of micro-fiber reinforced PQC, the flexural strength increases up to an optimum dosage and decreases with a further increase in the fiber dosage. This is due to the agglomeration of micro-fibers in the concrete with an increase in fiber dosage (Kasu et al. 2020). In the case of macro-fiber reinforced PQC with an increase in fiber dosages, the flexural strength increases as the chances of fiber cluster are reduced due to even distribution of fibers in the concrete mix (Fallah and Nematzadeh 2017).

3.5.4 Split tensile strength

The split tensile strength tests were conducted on the plain PQC mixtures prepared using three different NMAS and micro, and macro-fiber reinforced PQC mix specimens after curing them in water for 28 days. The test results are presented in Figure 3.5.

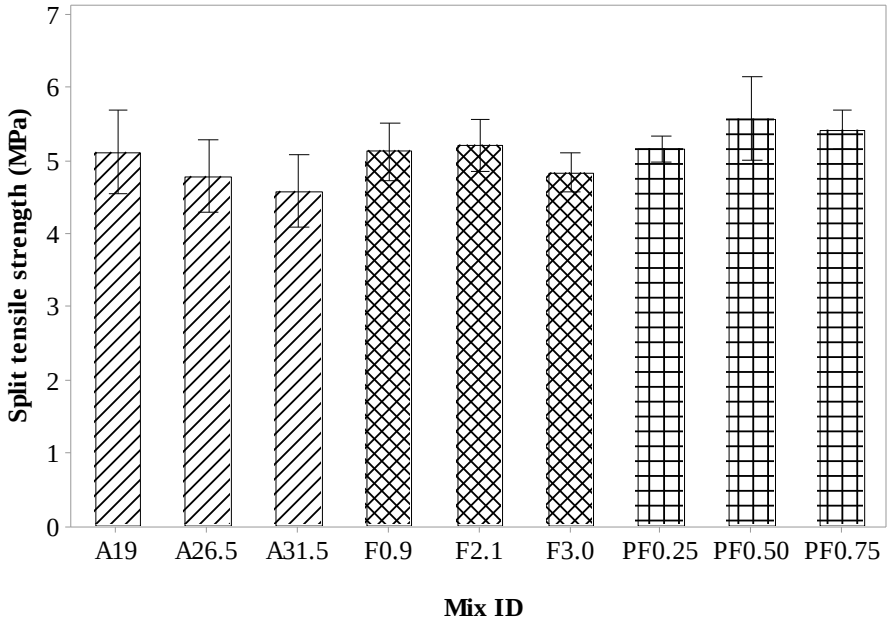

Figure 3.5 Split tensile strength test results for different PQC mixes

It is observed that with an increase in the NMAS, the split tensile strength decreases. In micro-fiber reinforced PQC with increased fiber dosage, split tensile strength increases initially up to an optimum value beyond which the split tensile strength reduces. The increase in split tensile strength up to the optimum value is due to the increase in stress transfer by the random orientation of fibers in the concrete mix. The reduction in strength value beyond optimum is due to increased pores in the concrete mix (Noushini et al. 2013, 2014). The increase in fiber dosages increases the

chances of water absorption, resulting in stiff cement paste due to inappropriate hydration (Siamardi and Shabani 2021). For macro-fiber reinforced PQC, the split tensile strength increased with increased fiber dosages up to 0.5% of volume, beyond which it reduces marginally. This may be attributed to the orientation and distribution of fibers in the concrete mix.

3.5.5 Modulus of elasticity

The 28 days elastic modulus (with 95% confidence interval) of plain pavement quality concrete mixtures prepared using three different NMAS 19, 26.5 and 31.5 mm and micro and macro-fiber reinforced PQC mixtures are presented in Figure 3.6.

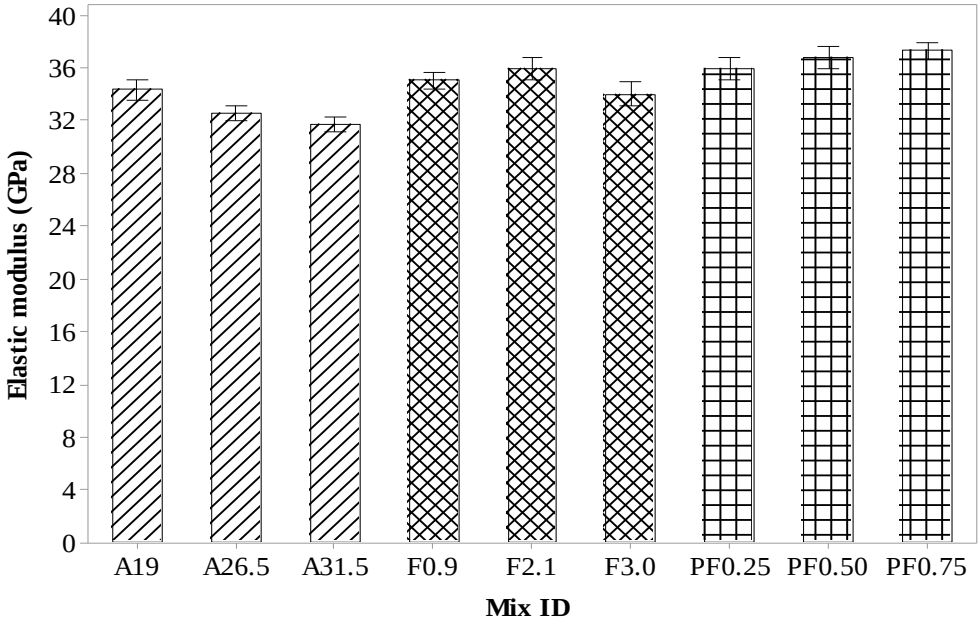

Figure 3.6 Modulus of elasticity test results for different PQC mixes

In plain concrete specimens, with an increase in the NMAS, the modulus of elasticity of concrete decreases. The higher NMAS in the concrete mix increases the air content resulting in a lower modulus of elasticity. The test results are in line with the findings reported by Saouma *et al.* (1991) for the concrete used for dams. In micro-fiber reinforced PQC mix specimens, with the increase in fiber dosage, elastic modulus increases initially and reduces thereafter due to the clumping of micro-fibers in the concrete mix (Noushini et al. 2013, 2014). The modulus of elasticity increases with increased fiber dosages in macro-fiber reinforced PQC due to the increased potential of crack bridging of fibers in the concrete.

3.6 SHEAR TEST METHODOLOGY

3.6.1 Specimen preparation for direct shear test

In the present research work, the cylindrical specimens of size 150 mm in diameter and 170 mm in height with preformed grooves of depths 50 mm (1/3rd of diameter) and 37.5 mm (1/4th of diameter) were prepared to conduct the shear test. The width of the groove was kept constant (5 mm) for all the specimens. To prepare the cylindrical specimens with preformed grooves, the usual cylindrical moulds which are used for preparing concrete specimens for split tensile strength tests of size 150 mm diameter and 300 mm height were modified. Circular rings of two different inner diameters, 100 mm and 112.5 mm, and outer diameter 150 mm, are welded at the height of 100 mm from the base of the cylindrical mould. The concrete mix proportions were mixed, weighed and poured into the properly lubricated modified cylindrical moulds and the next day, specimens were carefully unmoulded. Utmost, care was taken while unmoulding the samples. The samples are cured in a water tank for 28 days. Figure 3.7 shows the contact area at groove regions for two different GD considered for the study.

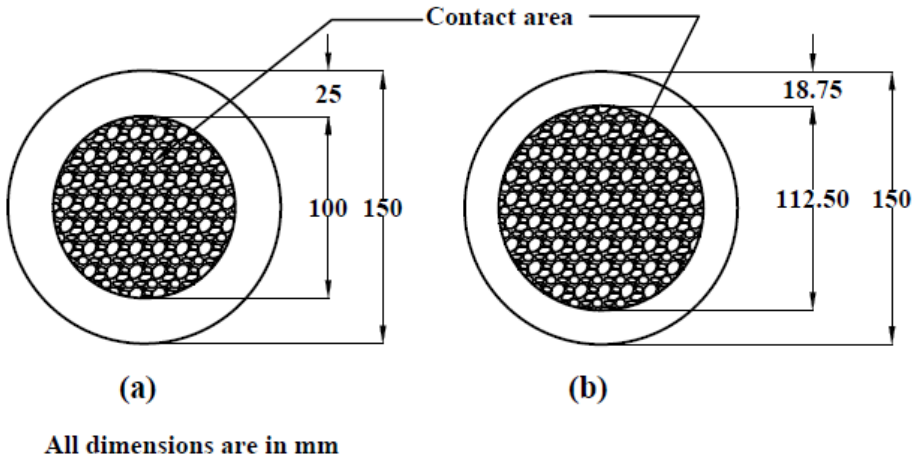

Figure 3.7 Contact area at grooved regions for different GDs (a) 1/3rd of diameter and (b) 1/4th of diameter

3.6.2 Static direct shear strength test

The direct shear strength test methodology proposed and used in this study consists of a compression testing machine of five tonnes capacity and a direct shear test apparatus. The schematic diagram of the shear test apparatus is shown in Figure 3.8. As

shown in Figure 3.8, the test apparatus has three sections which include an upper and lower cylindrical section and a semi-circular shearing head section. The lower section is fixed to the bottom plate, and the upper section is placed on the specimen. The upper and lower cylindrical sections act as a stationary sample holder, whereas the shearing head segment moves down during shear force application. A 5 mm gap is maintained between the static sample holder and shearing head sections to allow the direct shear load at the grooved cross-section. The horizontal locking plate is fastened at the top to eliminate the effect of bending moment. The direct shear test apparatus used for the present study is developed by the authors Jayakesh and Suresha (2018) for determining the interfacial bond strength of bituminous and concrete layer in the ultrathin white topping (UTW). The compression testing machine is fitted with a loading frame and dial gauges with a least count of 0.01 mm.

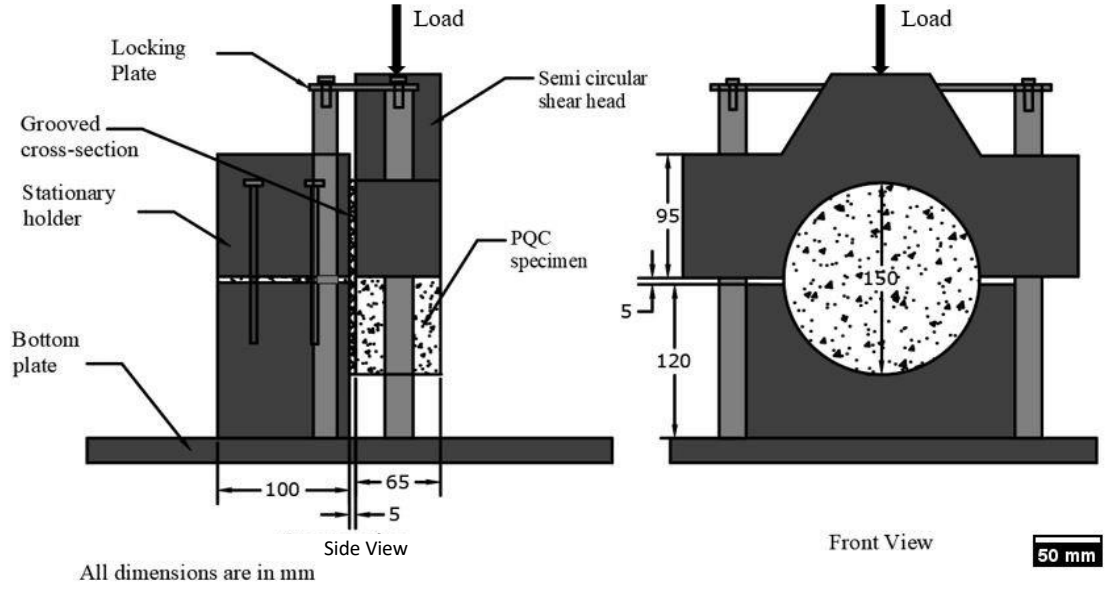

Figure 3.8 Schematic diagram of the shear test apparatus

The cylindrical specimens, test apparatus and failed specimens after the test are shown in Figure 3.9 (a) – (d).

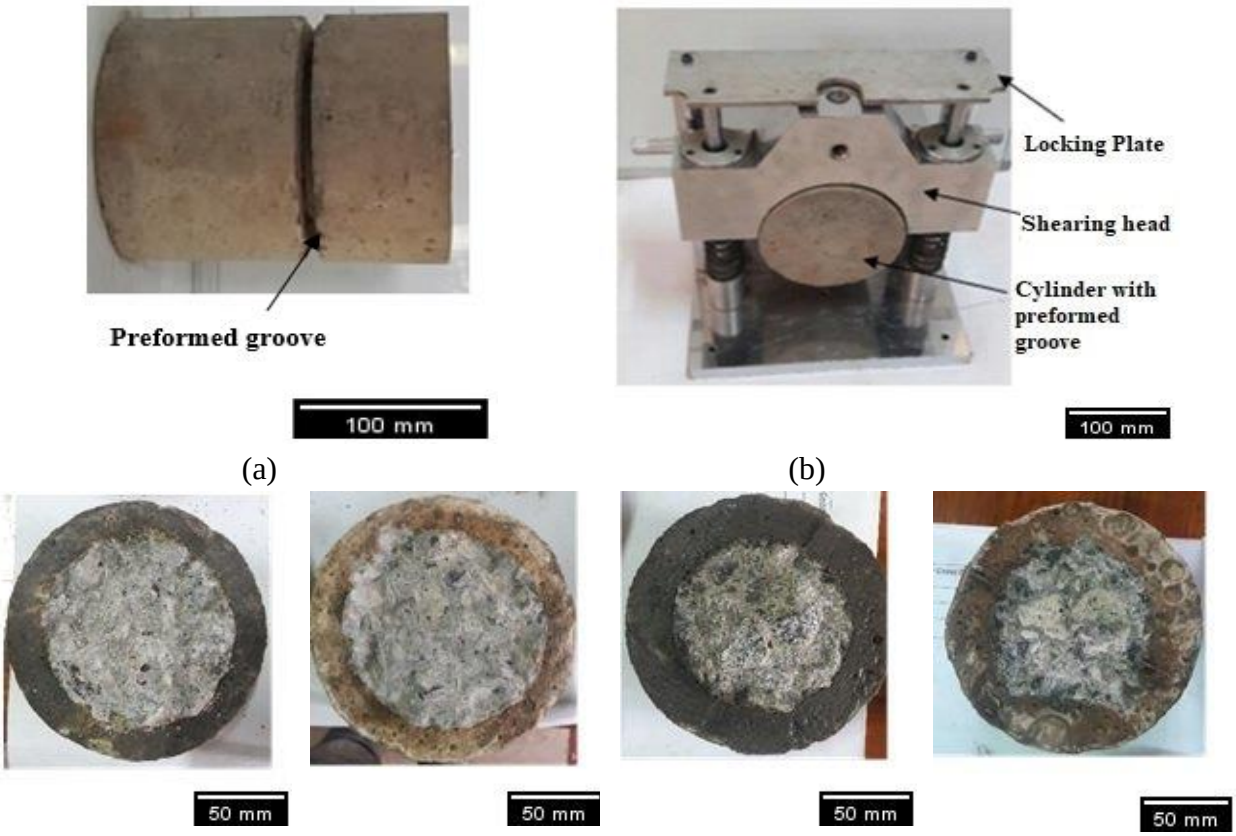

Figure 3.9 (a) Cylindrical concrete specimen, (b) Shear loading test setup, (c) and (d) failed plain PQC specimens

The load dial gauge readings are taken at different deformations. The ultimate shear load is noted for maximum deformation. The shear strength (τ) is calculated using the following formula for two different GDs.

For a GD of 1/3rd of diameter, $\tau = \left(\frac{4P}{\Pi(d - 0.33d)^2}\right)$ (3.1)

For a GD of 1/4th of diameter, $\tau = \left(\frac{4P}{\Pi(d - 0.25d)^2}\right)$ (3.2)

Where τ is shear strength in N/mm^2, P is shear load in N and d is the diameter of cylindrical specimen in mm.

The joint shear stiffness (K) is determined by taking the slope of the linear portion of the shear stress against the shear displacement curve, as shown in Figure 3.10. Stage I is a region of free slip, where a displacement occurs under a very low shear stress. The amount of free slip that occurs is primarily dependent on the surface

characteristics of the joint. Stage II is a region of linear stiffness with displacements increasing in proportion to the applied load. Stage III starts on the onset of heavy crushing and/or fracturing of the aggregate and the concrete matrix. This action results in degradation of joint stiffness with the rate of displacements increasing continuously as the applied load is increased, until a peak shear stress is reached (Wattar 2001).

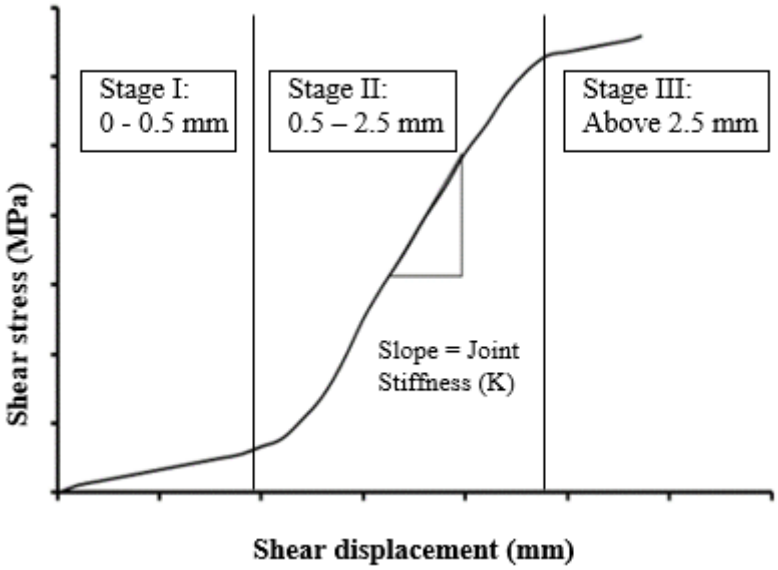

Figure 3.10 Shear stress Vs shear displacement curve for PQC mix (Wattar 2001)

The fracture energy in mode II (G_{IIF}) is obtained by dividing the area under the shear load-displacement curve by the shear resisting area. The area under the shear load-displacement curve (Figure 3.11) is obtained by integrating the best-fit equation for the experimentally obtained curve (Rao et al. 2011).

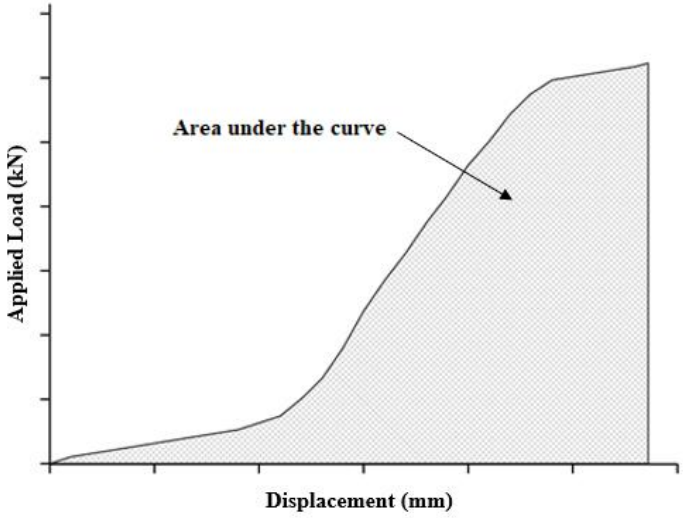

Figure 3.11 Shear load Vs shear displacement curve for PQC mix (Rao et al. 2011)

3.6.3 Shear fatigue test

The repeated loading system of five tonnes capacity was utilised for running the fatigue shear tests. The fatigue loading machine (along with the shear test apparatus) used in the present study is shown in Figure 3.12.

Figure 3.12 Repeated load system of five tonnes capacity used for shear fatigue loading

The repeated load testing instrument used in the present study is capable of applying a maximum loading frequency of 2 Hz. Also, it was observed from the literature that most of the researchers had selected loading frequency as 2 Hz for conducting flexural fatigue tests on concrete slabs (Roesler et al. 2005; Roesler and Barenberg 1999) and repeated shear tests on joints (Wattar 2001). Thus, a loading frequency of 2 Hz was used in the present study to save the testing time.

A frequency of 2 Hz with three stress levels of 80, 85 and 90% was applied on the grooved concrete cylindrical specimens after 28 days of curing. The stress level is the percentage load value applied in a repeated load test to the ultimate failure load value obtained from the static direct shear strength test. A minimum seating load of 40 kg was applied to all the specimens. The loading waveform is a haver-sine wave in

which loads were applied from minimum (seating load) to maximum load (applied load corresponding to stress level). This waveform is almost similar to the traffic loads applied on the pavement. The applied load is measured for each cycle, and the test is stopped once the specimen fails.

3.6.4 Statistical analysis of shear fatigue test data

The statistical analysis was conducted on the obtained shear fatigue data using MINITAB (Release 17, trial version). To understand the effect of GD and stress levels on the shear fatigue performance of various PQC mixtures and to represent the same graphically, the Kaplan-Meir (K-M) Survival analysis was used in the present study. The Kaplan-Meir (K-M) analysis is a widely utilized method for analyzing fatigue data without the assumption of any distribution. Further, the survival plots obtained from K-M analysis would pictorially represent the effect of different parameters on fatigue lives. The K-M plots provide the graphical representation of the probability of an event at any given time interval. The theory is being used in the medical field mainly to study the survival probability of cancer patients (Usman et al. 2014). In recent years this theory is being used to assess the performance of fatigue data of concrete specimens (Chandrappa and Biligiri 2017; Kasu et al. 2019). Also, the K-M plots were used to compare the survival probabilities of PQC specimens at three different stress levels and two GDs. The log-rank test was used to compare the survival curves. The obtained shear fatigue data were fitted to 3- parameter Weibull and lognormal distribution. To assess the goodness of fit of the distribution, the Anderson-Darling test was performed (Chandrappa and Biligiri 2016; Zimmermann et al. 2012).

3.7 LABORATORY EVALUATION METHODOLOGY FOR LOAD TRANSFER IN AGGREGATE INTERLOCKED JOINTS

3.7.1 Specimen preparation for load transfer evaluation

The standard beam specimens of size 100 × 100 × 500 mm that are generally used for flexural strength tests were used to evaluate load transfer through aggregate interlocking. The beam specimens were prepared as per IS 516: 1959. After curing the concrete beam specimens in water for 28 days, the concrete specimens were grooved at

the centre for two groove depths (1/3rd and 1/4th of depth). The beam specimens were placed inverted under a flexural testing machine and loaded exactly at the centre to create an artificial crack to the full depth of the beams.

3.7.2 Joint load transfer evaluation test

A small-scale laboratory test set-up has been fabricated to simulate the load transfer in aggregate interlocked joints. The test setup consists of a 20 mm thick plate having a width of 240 mm and a length of 700 mm. Two L sections of dimension 70 mm × 150 mm × 20 mm are provided to restrain the moment at the end of the beams. This also restrains the cantilever action that may take place due to loading near the joint. Another two rectangular sections of dimension 200 mm × 58 mm × 10 mm are bolted at a distance of 1/4th of length from the ends of the beam to resist any moments that act on the beam. A rubber pad having modulus equivalent to the base condition was placed below the beam. The schematic representation of the test setup is shown in Figure 3.13.

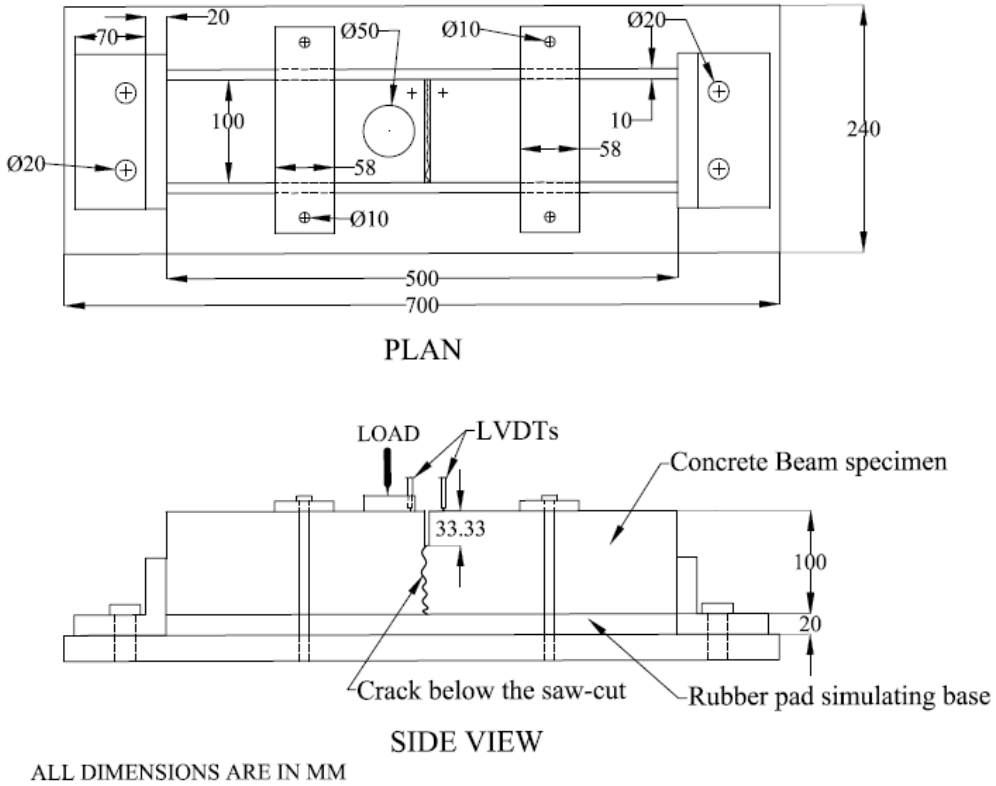

Figure 3.13 Test setup used to simulate the load transfer in aggregate interlocked joints

The repeated load testing instrument capable of applying a maximum loading frequency of 2 Hz was used to apply the repeated load. The test setup and the specimen resting on the rubber pad were placed under the repeated load testing instrument, as shown in Figure 3.14.

Figure 3.14 Small-scale test setup along with specimen

The load was applied at a distance of 10 mm away from the joint. The load amplitude was kept as 2000 kg for all the specimens. The part of the beam which is loaded simulates the loaded slab, and the other part of the beam represents the unloaded slab. Two LVDTs were placed on these two parts of the beam at the corners that automatically record the deflections at each cycle. The crack width was measured using the ruler shown in Figure 3.15. The crack widths were noted manually at different repetition cycles.

Figure 3.15 Crack width ruler used in the present study

3.8 3-D FE MODEL

A 3-D finite element (FE) model was developed in ANSYS for the two proposed test methodologies to evaluate the aggregate interlocking in terms of shear parameters and LTE. The concrete cylindrical and beam specimens were modelled using the eight noded SOLID185 brick elements with three degrees of freedom. The aggregate interlocking was modelled using the COMBIN14 spring elements. The same elements were also used to model the fibers contributing to aggregate interlocking in fiber reinforced PQC mixtures. The test results are compared with simulation results.

3.9 FIELD EVALUATION OF AGGREGATE INTERLOCKED JOINTS OF WHITETOPPING USING FALLING WEIGHT DEFLECTOMETER

3.9.1 Description of falling weight deflectometer (FWD)

The field study was carried out using the KUAB 70 vehicle-mounted falling weight deflectometer shown in Figure 3.16. The device can apply loads in the range of 10-70 kN. The device consists of an impact loading arrangement in which a load cell is used to measure the load and seven geophones to record the deflections. The deflection sensors can measure the pavement surface deflection with an accuracy of 1μm.

Figure 3.16 KUAB 70 vehicle-mounted falling weight deflectometer (FWD)

3.9.2 Field FWD experimental plan

The whitetopping pavement stretch selected for evaluation was the seventh main road, Dodda Banaswadi, Bangalore. The selected stretch for evaluation is shown in Figure 3.17.

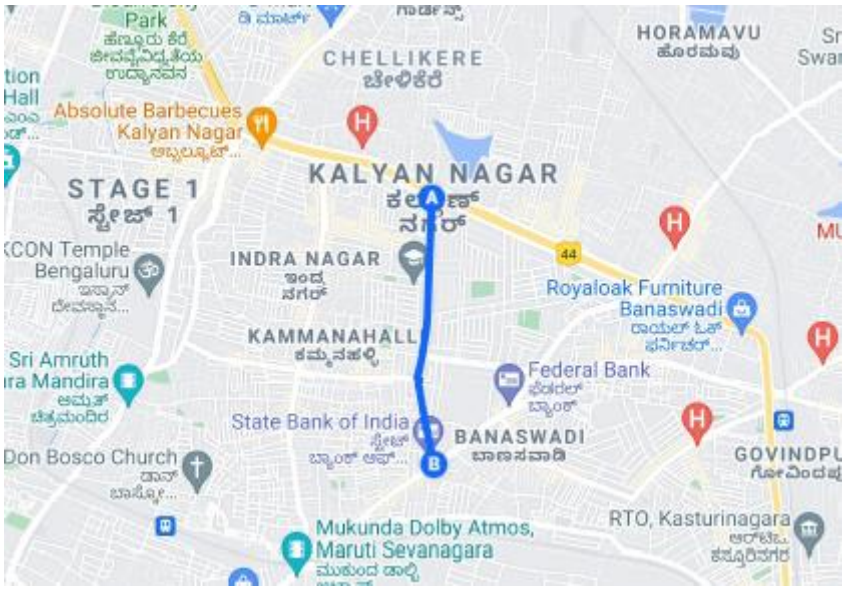

Figure 3.17 Selected stretch for joint performance evaluation (Source: Google Maps)

The whitetopping stretch selected for evaluation has a length of 1.17 km, the panels are of size 1.5 m × 1.5 m, and the thickness of whitetopping is 200 mm. The selected stretch was designed and constructed as per IRC: SP:76-2015.

3.9.3 Field evaluation procedure

As of now, there are no fixed guidelines available to conduct the FWD tests on whitetopping pavements. In the present study, IRC:117-2014 is followed to perform the FWD tests on whitetopping. The loading plate was placed on the edge of the slab panel so that the center of the loading plate was at a location at a distance of -150 mm away from the joint, as shown in Figure 3.18.

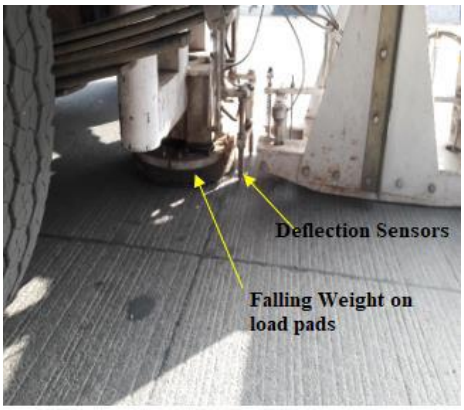

Figure 3.18 Falling weight load applied at the joint

The schematic representation of load and deflection measurement arrangement is shown in Figure 3.19.

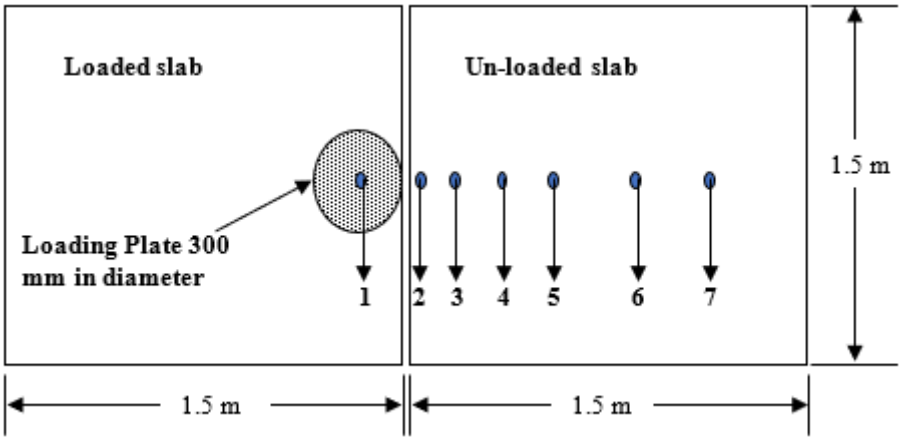

Figure 3.19 Load and deflection measurement arrangement in FWD

As shown in Figure 3.19, the first deflection sensor is at a distance of -150 mm away from the joint on the loaded slab, and the other six sensors are at a distance of +50 mm, +150 mm, +300 mm, +450 mm, +750 mm and +1050 mm away from the joint, on the unloaded slab. The load was applied thrice on the slab, and the corresponding

deflections of all seven sensors were recorded automatically in the computer connected to the device.

The deflection LTE is calculated using the following formula for the FWD data.

$$LTE = \beta \times \frac{D_{-150}}{D_{150}} \times 100 \tag{3.3}$$

where β is the correction factor when deflection sensors are at a distance of 300 mm apart, and its value lies between 1.05 and 1.15. D_{150} is the measured deflection of the unloaded slab at a distance of 150 mm away from the joint. D_{-150} is the measured deflection of the loaded slab at a distance of 150 mm away from the joint. The deflection response measured on the unloaded slab at a distance of +50 mm, +150 mm, +300 mm, +450 mm, +750 mm and +1050 mm away from the joint gives the deflection profile of the unloaded slab. The deflection value at the joint is obtained by interpolation. The value thus obtained is added with a factor of $(D_{-150} - D_{150}) \times 1.06$ to get the interpolated deflection value of the loaded slab at the joint. The deflection difference between these two interpolated points gives the vertical joint shear displacement at the joint.

3.10 ANN model

The ANN model was developed using MATLAB software. The detailed steps followed to improve the existing model to calculate joint stiffness directly from FWD data and various ANN models developed using the available analytical models determining the joint stiffness are presented in Chapter 7.

CHAPTER 4

LABORATORY EVALUATION OF SHEAR PARAMETERS OF AGGREGATE INTERLOCKED JOINTS

4.1 GENERAL

In this chapter, the laboratory evaluation of aggregate interlocked joints in terms of joint shear strength (τ), joint shear stiffness (K), and fracture energy in mode II (G_{IIF}) using the proposed direct shear test methodology is considered. The influence of nominal maximum aggregate size (NMAS) and groove depth (GD) on shear parameters of plain concrete mix and the influence of GD and varying dosages of micro and macro-fibers on shear parameters of fiber reinforced PQC mix are presented. The section aims to evaluate the influence of these parameters under fatigue shear loading at different higher stress levels. To evaluate the effect of NMAS and the influence of GD and varying dosages of micro and macro-fibers on the shear parameters of the concrete mixtures under static and fatigue loading, about 360 cylindrical specimens with two groove depths were considered. The statistical analysis of shear fatigue data is also carried out to understand the effect of stress level and groove depths on the shear fatigue response aggregate interlocked joints.

4.2 LABORATORY EXPERIMENTAL PLAN

The plain concrete specimens and micro and macro-fiber reinforced PQC cylindrical specimens with preformed groove were prepared, as explained in Chapter 3 of section 3.6.1. The details of the test specimens used for evaluating the shear parameters of aggregate interlocked joints are tabulated in Table 4.1.

Table 4.1 Details of test specimens for laboratory evaluation of shear parameters

Mix ID	NMAS Used (mm)	Fiber dosage		Number of specimens	
		Micro fiber	Macro fiber	For static direct shear test at two groove depths (37.5mm and 50 mm)	For fatigue shear test at three stress levels (80%, 85% and 90%) at two groove depths (37.5mm and 50 mm)
A19	19	-	-	5 × 2 = 10	5 × 3 × 2 = 30
A26.5	26.5	-	-	5 × 2 = 10	5 × 3 × 2 = 30
A31.5	31.5	-	-	5 × 2 = 10	5 × 3 × 2 = 30
F0.9	19	0.9kg/m^3	-	5 × 2 = 10	5 × 3 × 2 = 30
F2.1		2.1kg/m^3	-	5 × 2 = 10	5 × 3 × 2 = 30
F3.0		3.0kg/m^3	-	5 × 2 = 10	5 × 3 × 2 = 30
PF0.25		-	0.25%	5 × 2 = 10	5 × 3 × 2 = 30
PF0.50		-	0.50%	5 × 2 = 10	5 × 3 × 2 = 30
PF0.75		-	0.75%	5 × 2 = 10	5 × 3 × 2 = 30
				Total =	**360**

4.3 RESULTS AND DISCUSSIONS

The results and discussions of the present investigations are discussed in the following sections.

4.3.1 Static direct shear strength (τ)

The direct shear strengths of five samples each of concrete mix A19, A26.5, A31.5, F0.9, F2.1, F3.0, PF0.25, PF0.50 and PF0.75 with GD 1/4th of diameter and 1/3rd of diameter are tabularised in Table 4.2. From Table 4.2, it can be noticed that for a given concrete mix, whether plain or fiber reinforced, the static direct shear strength reduces with the increase in GD. This is due to the lower area of contact (resisting area) at the grooved cross-section (Rao et al. 2011). The concrete mix specimen prepared using the macro-fiber with a dosage of 0.75% having a groove depth of 37.5 mm (1/4th of diameter) showed the highest static direct shear strength compared to the other concrete mix. The obtained static direct shear strengths were lowest for the plain PQC mix prepared using 19 mm NMAS having a groove depth of 50 mm (1/3rd of diameter).

Table 4.2 Static mean shear strength of concrete mixtures

Type of concrete mix	Mix ID	Mean shear strength (MPa)	
		For Groove Depth = 37.5 mm (1/4th of diameter)	For Groove Depth = 50 mm (1/3rd of diameter)
Plain PQC	A19	1.31	1.06
	A26.5	1.43	1.29
	A31.5	1.61	1.45
Micro-fiber reinforced PQC	F0.9	1.34	1.29
	F2.1	1.42	1.35
	F3.0	1.32	1.26
Macro-fiber reinforced PQC	PF0.25	1.62	1.38
	PF0.50	1.78	1.52
	PF0.75	1.93	1.70

The shear strength increases with the increase in NMAS used in the PQC. This increase in shear strength is due to the use of a larger size of aggregates which improve the aggregate interlocking at the interface/joint (Walraven 1980). Similar findings have been reported by Yang *et al.* (2012) for monolithic concrete joints without transverse reinforcement and Yi *et al.* (2017) for beams without shear reinforcement after conducting push-off tests. The static shear strength of A31.5 concrete mix specimens with a GD of 1/3rd diameter is much closer to the value of shear strength obtained for A26.5 mix with a GD of 1/4th the diameter. This shows the significance of GD on the shear strength of PQC mixes when larger sized aggregate is used.

It is found from the test results that the shear strength of micro-fiber reinforced PQC mixes at the grooved cross-section increases with an increase in fiber dosage up to 2.1 kg/m^{3,} and the shear strength decreased for the dosage of 3.0 kg/m^3. This may be due to air entrapped at the cross-section with increased fiber dosage. The percentage increase in shear strength was highest for the fiber dosage of 2.1 kg/m^3 of about 8.40% and 27.36% for GD of 37.5 and 25mm, respectively, when compared to the A19 plain concrete specimens. The obtained results are in agreement with the findings reported by Xu et al. (2020).

The shear strength of macro-fiber reinforced PQC mixes at the grooved cross-section increases with an increase in fiber dosage irrespective of the groove depth.

Similar findings have been reported by Lakavath et al. (2021) for prestressed macro-fiber reinforced concrete beam specimens. For a GD of 37.5 mm, the addition of macro-fiber improves the shear strength of plain concrete A19 mix by 23.66%, 35.88% and 47.33%, and for a GD of 50 mm, by 30.19%, 43.40% and 60.38%, respectively, for the macro-fiber reinforced PQC mix PF0.25, PF0.50 and PF0.75, respectively. Also, it can be noticed that the shear strengths of all macro-fiber reinforced PQC mixtures are higher than the shear strengths of plain concrete mixes at a GD of 37.5 mm and a GD of 50 mm, except for PF0.25 mix, the other two macro-fiber reinforced PQC mixtures have higher shear strengths compared to the plain concrete mixes prepared using different NMAS.

4.3.2 Joint shear stiffness (K) and fracture energy mode II (G_{IIF})

The joint shear stiffness **(**K) and fracture energy mode II (G_{IIF}) of PQC, micro-fiber reinforced PQC and macro-fiber reinforced PQC mixtures with GD 1/4th of diameter (37.5 mm) and 1/3rd of diameter (50 mm) with 95% confidence interval are plotted in Figure 4.1 (a) & (b), (c) & (d) and (e) & (f), respectively.

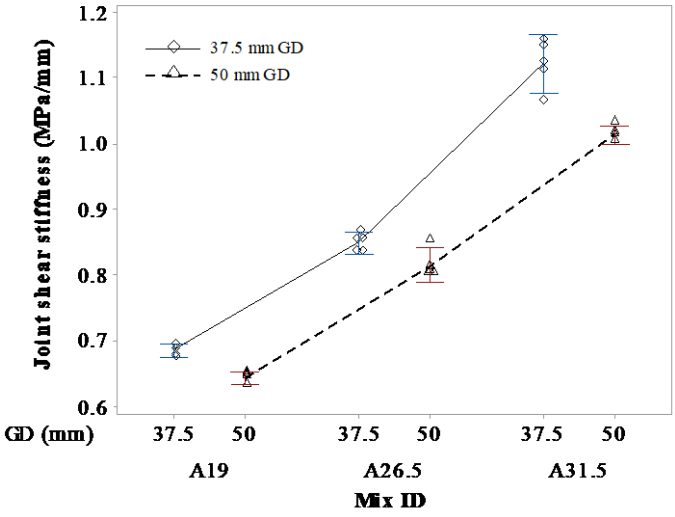

(a)

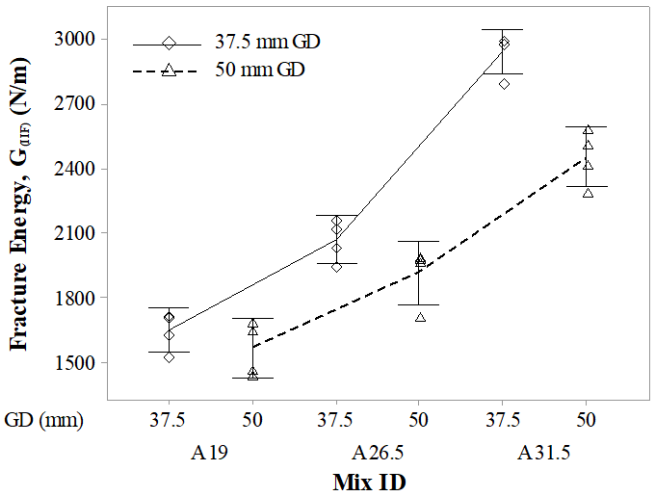
37.5 mm GD
50 mm GD
Fracture Energy, G(IF) (N/m)
3000
2700
2400
2100
1800
1500
GD (mm)
37.5
50
37.5
50
37.5
50
A19
A26.5
A31.5
Mix ID

(b)

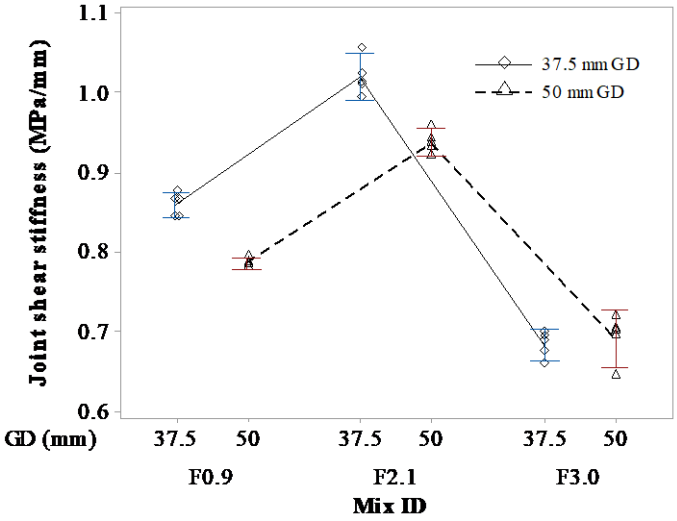
37.5 mm GD
50 mm GD
Joint shear stiffness (MPa/mm)
1.1
1.0
0.9
0.8
0.7
0.6
GD (mm)
37.5
50
37.5
50
37.5
50
F0.9
F2.1
F3.0
Mix ID

(c)

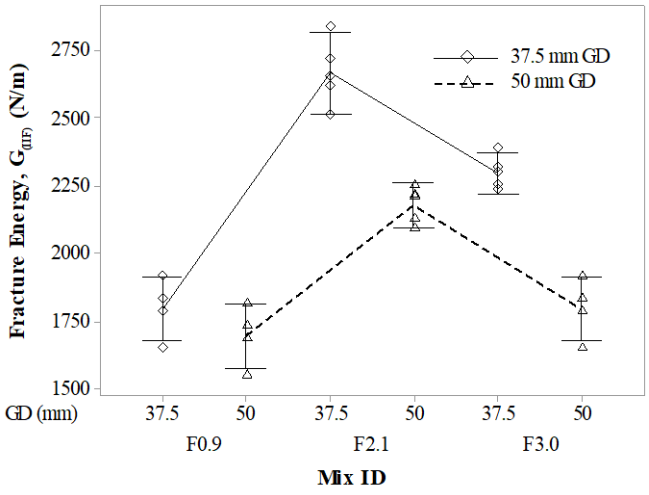
37.5 mm GD
50 mm GD
Fracture Energy, G(IF) (N/m)
2750
2500
2250
2000
1750
1500
GD (mm)
37.5
50
37.5
50
37.5
50
F0.9
F2.1
F3.0
Mix ID

(d)

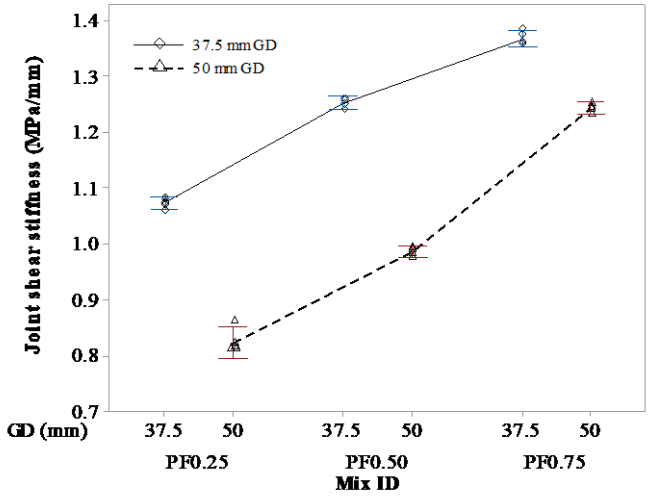

(e)

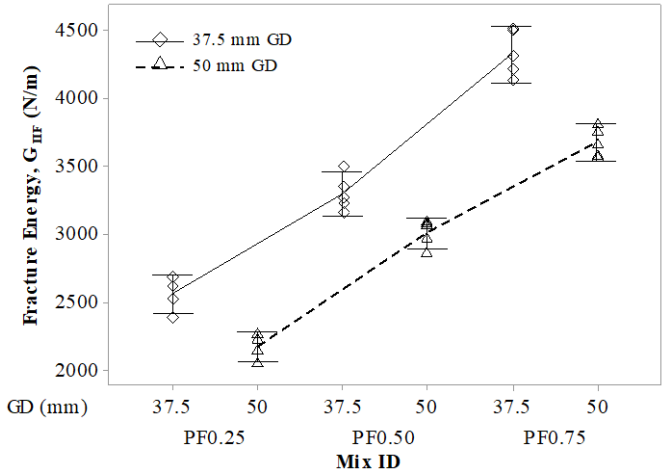

(f)

Figure 4.1 95% confidence interval plots of joint shear stiffness (K): (a), (c) and (e) and mode II fracture energy (G_{IIF}): (b), (d) and (f), respectively, for PQC, micro and macro-fiber reinforced PQC mixtures

As per the literature, 90%, 95%, and 99% CI are the most commonly used confidence intervals. A 90% CI would be narrower than a 95% CI. As the precision of the confidence interval increases, the CI width decreases. The reliability of an interval containing the actual mean decreases, which means that CI covers less of a range of mean. Also, in 99% CI, as the confidence level increases, the margin of error increases, which means that the interval is wider (Dekking et al. 2005). Thus, in the present study 95% CI is used to understand precision of obtained experimental data. The shear stress Vs shear displacement for all the PQC mixes is given in Appendix A from which the joint shear stiffness and fracture energy values were obtained.

It is seen from Figure 4.1 (a), (c), and (e) that for any concrete mix, whether it is plain or fiber reinforced, larger the GD, smaller is the K value. The increase in GD decreases the potential area of contact of aggregates at the grooved cross-section and results in lower K values in PQC specimens, whereas lower K values in FRC specimens with the increase in GD is due to the reduced the number of fibers contribution at the grooved cross-section.

It is observed that the percentage increase in K value, when GD is decreased from $1/3^{rd}$ to $1/4^{th}$ of the diameter is 5.93%, 4.19% and 9.66%, for the PQC mix A19, A26.5 and A31.5, respectively. In the case of the A31.5 PQC mix, GD significantly influences the K value. For a given GD, the K value increases with an increase in NMAS. When the GD is $1/4^{th}$ of diameter, the K value of A26.5 and A31.5 are 1.24 and 1.67 times that of A19 PQC mix, respectively. However, when the GD is $1/3^{rd}$ of diameter, the K values of A26.5 and A31.5 are 1.26 and 1.57 times that of A19 PQC mix, respectively. This shows that the use of larger NMAS has no significant improvement in the K value when GD is higher. The obtained results are in agreement with the test results of Wattar (2001). From the visual examination of cracked surfaces of the specimens, it is observed that the roughness of crack surfaces increased with the increase in NMAS, which improves the interlocking of two surfaces, thus increasing the K value. Similar findings can be seen in the study conducted by Yi *et al.* (2017).

From Figure 4.1 (c), it is seen that the K value increases with an increase in micro-fiber content up to 2.1 kg/m^3 and decreases with a further increase in fiber dosages. For the F0.9 mix, the K values increased by 21.87% and 25.46%, respectively, for the GD of 37.5 mm and 50 mm compared to A19 PQC mix specimens. With an increase in fiber dosage from 0.9 to 2.1 kg/m^3, the K value increased by 19.38% and 18.75%, respectively, for the GD of 37.5 mm and 50 mm and decreased by 26.29% and 33.08%, respectively, for the GD of 37.5 mm and 50 mm with an increase in dosage to 3.0 kg/m^3. The K value increases with an increase in fiber dosage in the case of macro-fiber reinforced PQC. From Figure 4.1 (c), it is observed that there is a significant improvement in K values of macro-fiber reinforced PQC specimens for lower GD. This is due to more number of fibers contributing to the bridging action across the grooved cross-section. When the GD is $1/4^{th}$ of diameter, the K value of PF0.25, PF0.50 and PF0.75 are 1.57, 1.83 and 1.99 times that of A19 PQC mix, respectively. However,

when the GD is 1/3rd of diameter, the K values of PF0.25, PF0.50 and PF0.75 are 1.28, 1.53 and 1.93 times that of A19 PQC mix, respectively. Also, the PF0.75 mix has the highest K value when compared to the other concrete mixtures under study. This shows that the higher the macro-fiber content improves the K value significantly, which indicates an improvement in the performance of aggregate interlocked joints.

From Figure 4.1 (b), it is seen that for any given PQC mix, G_{IIF} decreases with the increase in GD. The results are in line with the findings reported by the researchers both in mode I and mode II loading (Hillerborg 1985; Issa et al. 2003; Kumar and Rao 2010; Rao et al. 2011). The percentage increase in G_{IIF} values when GD is decreased from 1/3rd of diameter to 1/4th of diameter is 4.96%, 7.37% and 16.58% for PQC mix A19, A26.5 and A31.5, respectively. GD has a larger influence on the G_{IIF} in the case of the A31.5 PQC mix. It is reported in the literature that with the increase in NMAS, fracture energy increases for normal concrete in mode I (Elices and Rocco 2008; Hillerborg 1985; Issa et al. 2003; Nallathambi et al. 1984). In the present study, the G_{IIF} increased with the increase in NMAS, when GD is kept constant. When the GD is 1/4th of diameter, the G_{IIF} of A26.5 and A31.5 are 1.25 and 1.78 times that of A19 PQC mix, respectively. However, when the GD is 1/3rd of diameter, the G_{IIF} of A26.5 and A31.5 are 1.22 and 1.57 times that of A19 PQC mix, respectively. The same inference can be found in the literature for mode II fracture energy of double central notched plain concrete plates (Kumar and Rao 2010; Rao et al. 2011). The crack path is more zig-zag in nature in the case of PQC mix prepared using larger NMAS, thus increasing the fracture energy (Khalilpour et al. 2019; Nikbin et al. 2014; Rao and Prasad 2002; Siregar et al. 2017).

For fiber reinforced PQC mix (both micro and macro-fiber), the G_{IIF} decreases with the increase in GD. The results are in agreement with the findings reported by the researchers both in mode I and mode II loading (Abou El-Mal et al. 2015; Appa Rao and Sreenivasa Rao 2009; Reis and Ferreira 2004; Velazco et al. 1980). From Figure 4 (d), it is noticed that the G_{IIF} value increased with an increase in fiber dosage up to 2.1 kg/m^3 and then decreases with a further increase in dosages in the case of micro-fiber reinforced PQC. The G_{IIF} values of F0.9, F2.1 and F3.0 mix are 1.08, 1.39 and 1.15 times of A19 mix, respectively, for a GD of 1/3rd of diameter. For a GD of 1/4th of diameter, the G_{IIF} values of F0.9, F2.1 and F3.0 mix are 1.09, 1.62 and 1.39 times of

A19 mix, respectively. Similar results are reported by the authors Carpinteri et al. (2017) and Bencardino et al. (2010). The addition of fibers improve the crack bridging across the joint, thus improving the fracture energy. The decrement in G_{IIF} values for the fiber dosage of the F3.0 mix is due to aggregation and improper distribution of fibers. From Figure 4.1 (f), it is seen that the G_{IIF} value increased with an increase in fiber dosage for macro-fiber reinforced PQC mix. Similar findings were reported by Bhosale et al. (2019) for mode I fracture tests and by Hatami Jorbat et al. (2020) for mixed-mode fracture tests. The percentage increase in G_{IIF} values when GD is decreased from 1/3rd of diameter to 1/4th of diameter is 15.10%, 8.62% and 15.21% for PF0.25, PF0.50 and PF0.75 mixtures, respectively. GD has a larger influence on the G_{IIF} in the case of the lower and higher dosages of fiber reinforced PQC mix. In the present study, at a given GD, the G_{IIF} increased with the increase in fiber dosages. When the GD is 1/4th of diameter, the G_{IIF} of PF0.25, PF0.50 and PF0.75 are 1.55, 1.99 and 2.62 times that of A19 PQC mix, respectively. However, when the GD is 1/3rd of diameter, the G_{IIF} of PF0.25, PF0.50 and PF0.75 are 1.38, 1.91 and 2.34 times that of the A19 PQC mix, respectively. The results indicate that the addition of macro-fiber can substantially improve the fracture energy of aggregate interlocked joints.

The relationship between K and G_{IIF} is shown in Figure 4.2 (a), (b) and (c) for plain PQC, micro-fiber reinforced PQC and macro-fiber reinforced PQC mixes, respectively, at two different GDs. The three times error bars are shown for both K and G_{IIF} values.

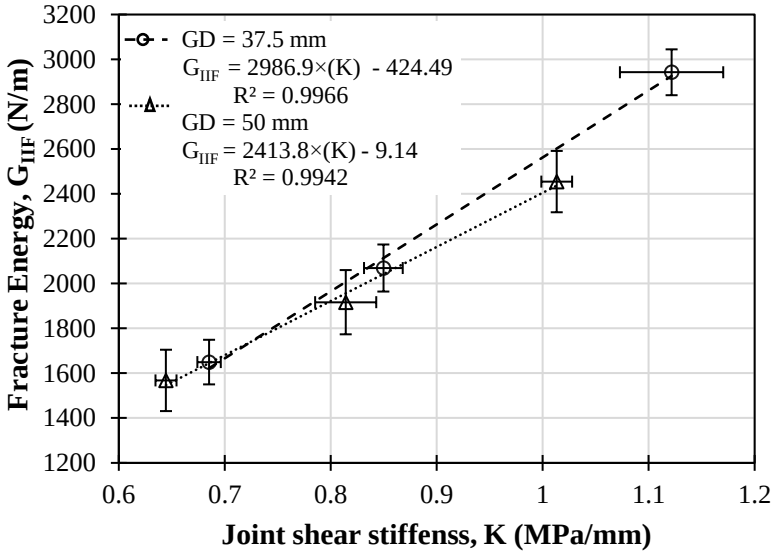

(a)

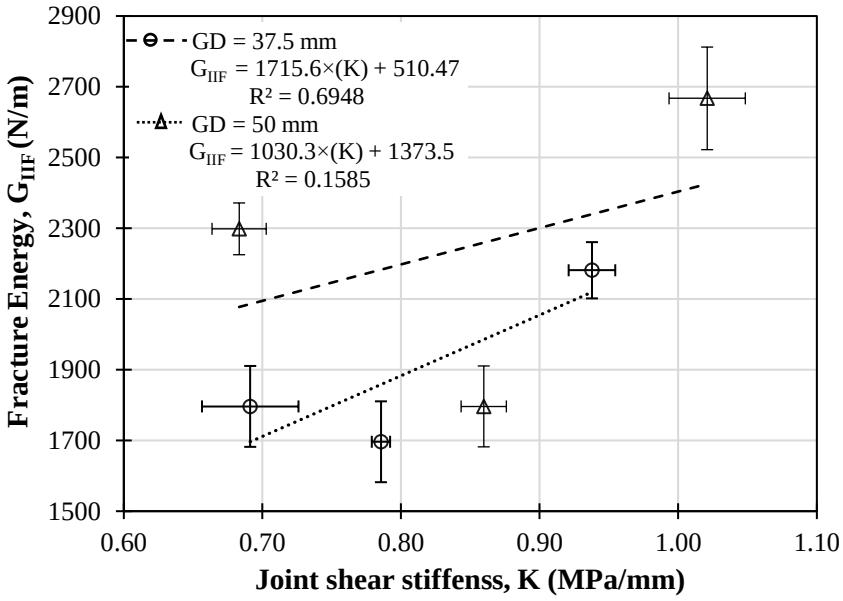

(b)

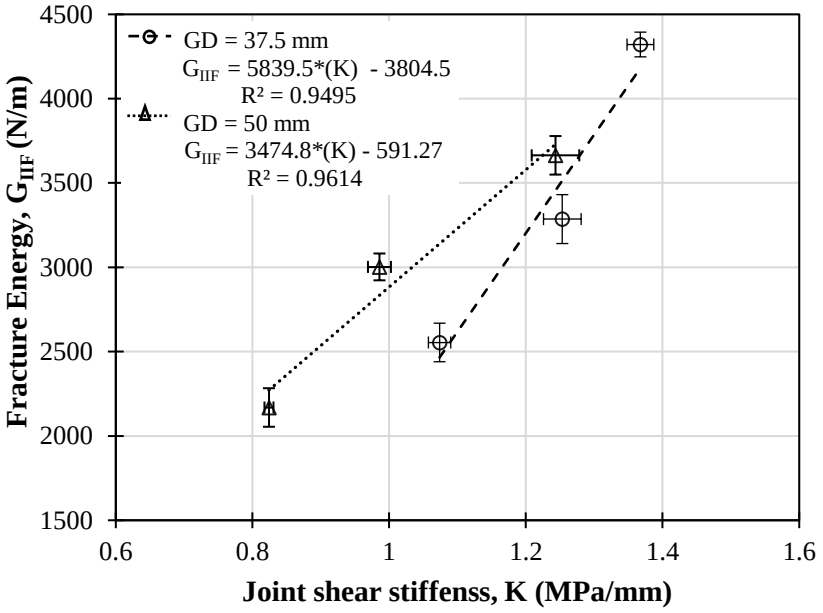

(c)

Figure 4.2 Relationship between fracture energy (G_{IIF}) and joint shear stiffness (K) at different GDs (a) for PQC mix, (b) for micro and (c) for macro-fiber reinforced PQC mixtures

4.4 FATIGUE BEHAVIOUR UNDER SHEAR LOADING

4.4.1 S-N plots

Fatigue life of the PQC, micro-fiber and macro-fiber reinforced PQC mixtures with GD 1/4th of diameter, and 1/3rd of diameter under shear loading at a frequency of 2 Hz are shown in Table 4.3, Table 4.4 and Table 4.5, respectively.

Table 4.3 Fatigue life cycles under shear loading of plain PQC mixtures

GD (mm)	90% stress level			85% stress level			80% stress level		
	A19	A26.5	A31.5	A19	A26.5	A31.5	A19	A26.5	A31.5
37.5 (1/4th of	1286	4682	8964	4628	10346	22468	6842	25684	54864
diameter)	1864	6842	10854	5284	13864	30640	8648	28648	58628
	2682	8964	12986	7544	15648	38948	12854	33548	62846
	3842	11874	16478	8648	20486	44684	14658	39684	68282
	4286	16982	18648	9874	22838	46824	17866	42636	71008
50 (1/3rd of	900	1574	4570	3458	6598	14586	3154	14858	22684
diameter)	1186	2254	8214	4340	9544	20546	8214	22584	44688
	1766	5478	10654	5686	12474	28474	12460	25478	53485
	2260	8160	11458	6758	14656	32548	14878	35476	59642
	2354	12170	14856	7254	18472	40856	16896	38744	62478

Table 4.4 Fatigue life cycles under shear loading of micro-fiber reinforced PQC mix

GD (mm)	90% stress level			85% stress level			80% stress level		
	F0.9	F2.1	F3.0	F0.9	F2.1	F3.0	F0.9	F2.1	F3.0
37.5 (1/4th	1482	3572	1088	4991	9346	3629	7841	21754	5741
of	1946	5742	1453	6598	12764	4373	8962	25898	7549
diameter)	2995	7864	2532	11247	13638	6433	14586	32488	11743
	4458	10894	3567	10258	19896	7642	18691	38644	13647
	4968	15682	3854	12005	21899	9595	23699	40586	16755
50 (1/3rd	1002	1284	540	4009	5986	2347	4315	12588	2152
of	1386	2986	1126	4214	8598	3230	10214	21840	7105
diameter)	2166	5268	1567	7683	11754	4574	14660	24878	12460
	2587	6150	2150	7896	13566	5639	18978	34576	13778
	2935	10890	2218	9896	17961	6123	20963	37844	15785

Table 4.5 Fatigue life cycles under shear loading of macro-fiber reinforced PQC mix

GD (mm)	90% stress level			85% stress level			80% stress level		
	PF0.25	PF0.50	PF0.75	PF0.25	PF0.50	PF0.75	PF0.25	PF0.50	PF0.75
37.5 (1/4th	2877	25487	31020	4874	21586	41020	9874	39487	48963
of	4621	8589	12583	7621	14568	22583	11621	38589	52583
diameter)	8897	12569	14896	8698	22569	34896	15898	31569	67896
	12586	20548	22689	15789	28548	32689	23581	38548	75789
	15782	18698	25864	25792	32986	45864	35792	42986	100189
50 (1/3rd	4782	12587	20478	6782	23587	40478	10782	43587	80478
of	6214	15478	28978	13214	34478	38978	28214	64478	68978
diameter)	10879	21589	25586	15870	20589	45586	35870	40589	85586
	15548	31847	37548	19545	43847	57548	49545	53847	105148
	25789	28963	35896	29781	38063	65896	29781	78063	141204

The geometric mean (GM) of shear fatigue life of five specimens for each mix is determined at different stress levels. Considering the large scatter in the fatigue data, a geometric mean will give the realistic mean of fatigue lives. Many researchers have shown that geometric mean can be used instead of arithmetic mean for fatigue life estimation when there is a large scatter in the fatigue data (Chandrappa and Biligiri 2019; Debnath and Pratim 2020; Kasu et al. 2020). Hence, the geometric mean was used instead of arithmetic mean in the present work. The GM of shear fatigue life of PQC, micro-fiber reinforced, and macro-fiber reinforced PQC mix specimens having the GD of 1/4th of diameter with variation in stress levels are plotted in Figure 4.3 (a), Figure 4.4 (a) and Figure 4.5 (a), respectively. The GM of shear fatigue life of PQC, micro-fiber reinforced, and macro-fiber reinforced PQC mix specimens having the GD of 1/3rd of diameter with variation in stress levels are plotted in Figure 4.3 (b), Figure 4.4 (b) and Figure 4.5 (b), respectively. A linear relationship exists between stress levels and GM of shear fatigue life for all the concrete mixes, irrespective of the GD. A similar trend can be found in the literature (Figueira et al. 2016) for the repeated push-off tests on the interfaces between concretes cast at different times.

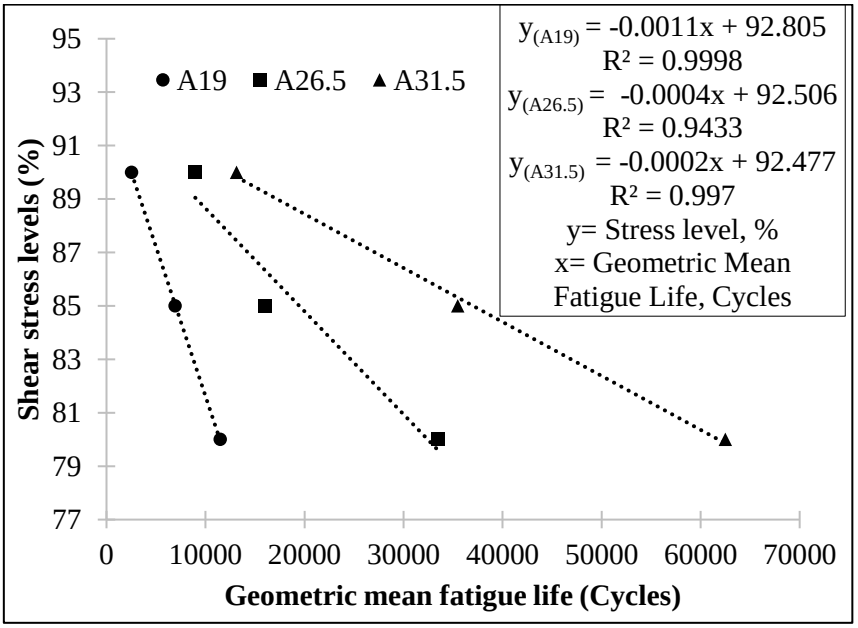

(a)

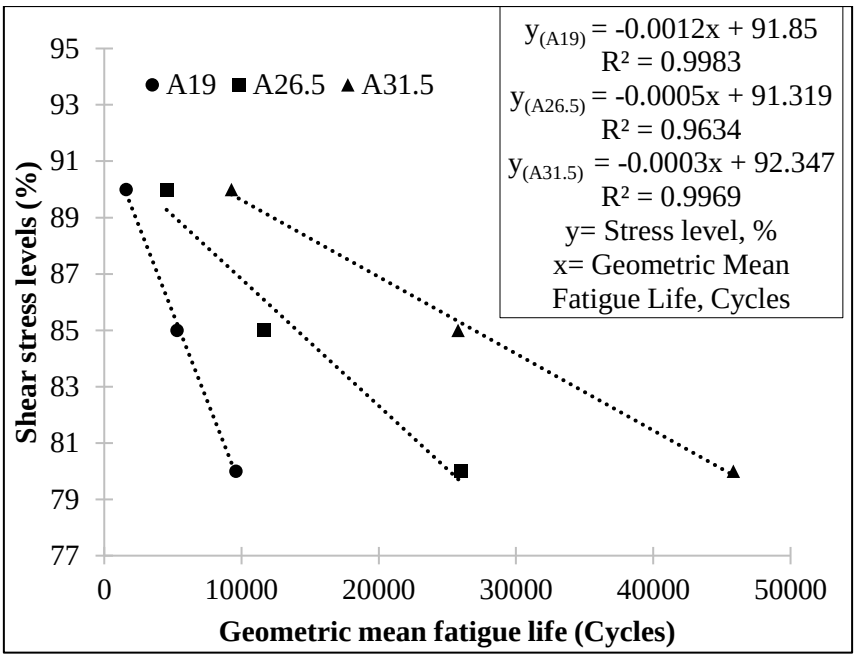

(b)

Figure 4.3 S-N plots for plain PQC mix: (a) GD: 1/4th of diameter (b) GD: 1/3rd of diameter

It is seen from the S-N plots that irrespective of the GD and stress levels, there is no significant difference in the fatigue life of A19 PQC mix specimens under shear fatigue loading. Whereas A26.5 and A31.5 PQC specimens with GD of 1/4th the diameter resulted in a much higher shear fatigue life for all the stress levels.

It is seen from the S-N plots that irrespective of the GD and stress levels, there is no significant difference in the fatigue life of A19 PQC mix specimens under shear fatigue loading. Whereas A26.5 and A31.5 PQC specimens with GD of 1/4th the diameter resulted in a much higher shear fatigue life for all the stress levels. With the reduction in GD, the number of coarse aggregates that participate in shear transfer increases, thus improving the aggregate interlocking at the grooved cross-section, resulting in higher fatigue life.

These experiments show that there is a higher probability that the undowelled joint would underperform in the field even though larger NMAS is used in the PQC mix when GD is higher. For all the three stress levels, irrespective of the GD, the shear fatigue life is in the increasing order of A19, A26.5 and A31.5, respectively. As the A31.5 concrete mix has large-sized aggregates, the path to be covered by the crack becomes longer, which in turn increases the fatigue life.

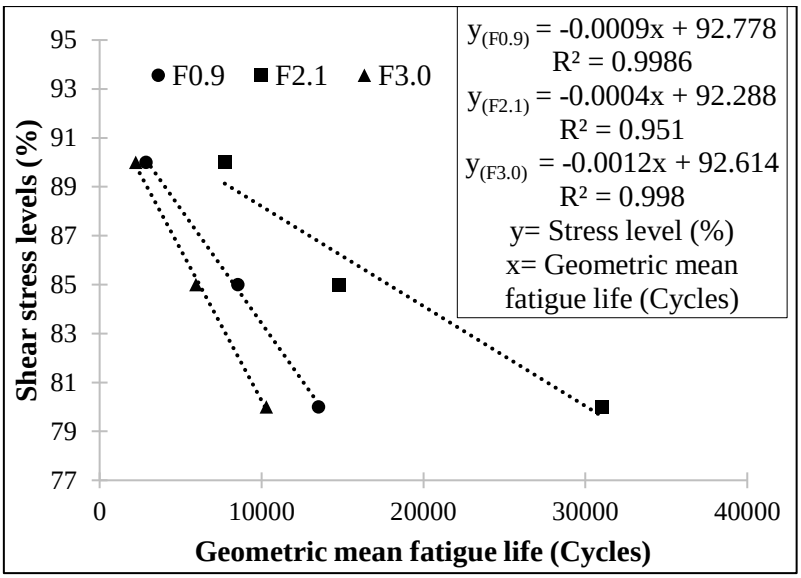

(a)

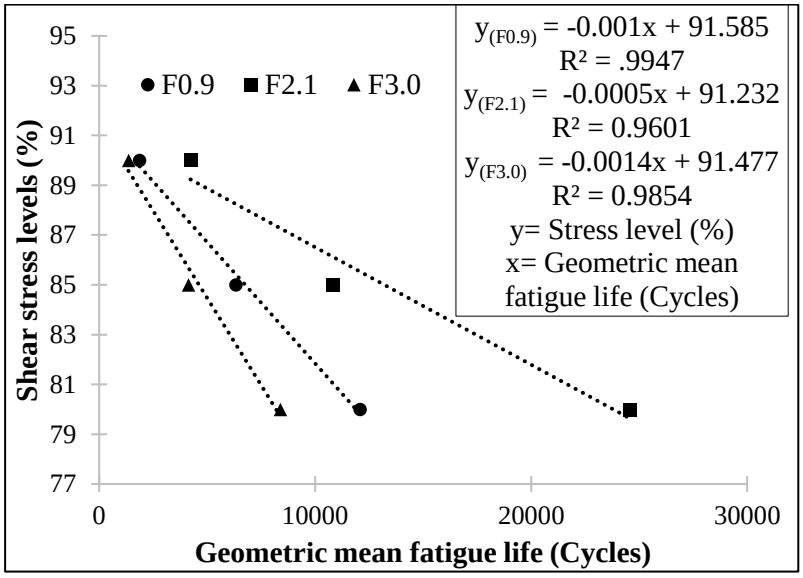

(b)

Figure 4.4 S-N plots for micro-fiber (a) GD of 1/4th of diameter (b) GD of 1/3rd of diameter

The shear fatigue life of F3.0 is the lowest in micro-fiber reinforced PQC mixtures. For all the stress levels at a given GD, the shear fatigue life is in the order of F0.9 < F3.0 < F2.1 in micro-fiber reinforced PQC. It may be attributed to the increase in the air content in the matrix with the addition of fibers (Kasu et al. 2020). It is found that the optimum fiber dosage of 2.1 kg/m^3 can improve the performance of aggregate interlocked joints in ultrathin whitetopping (UTW) layers.

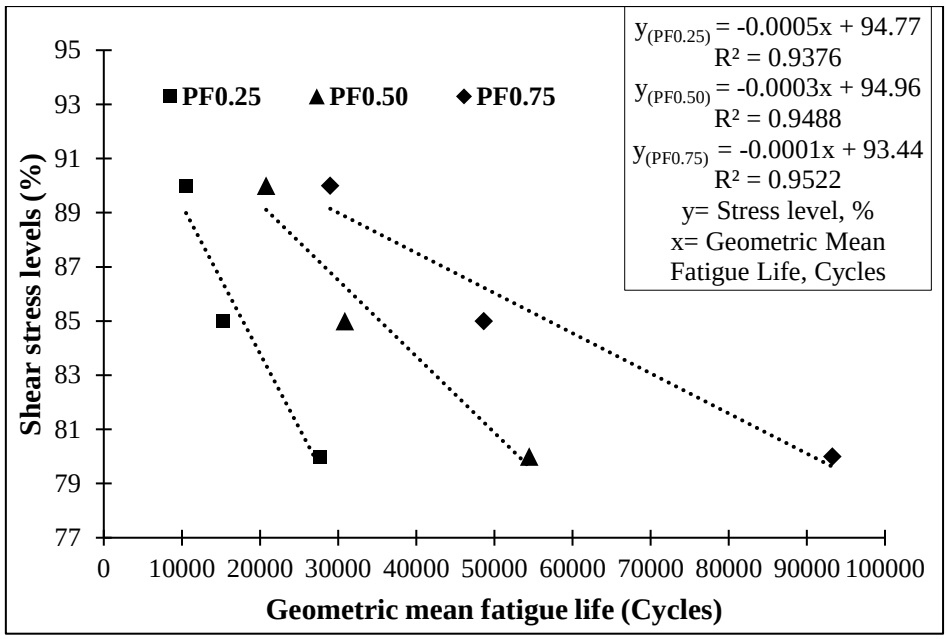

(a)

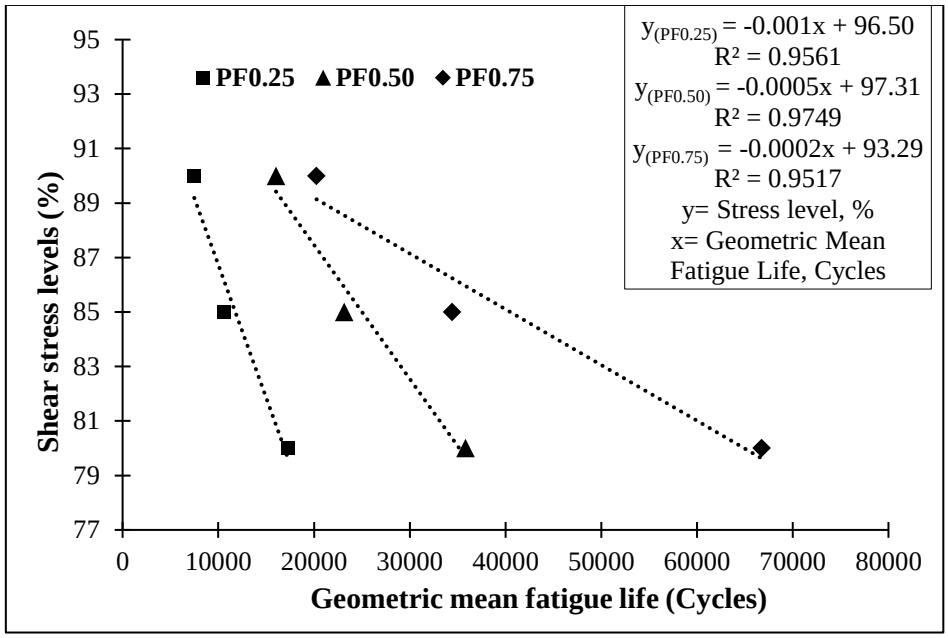

(b)

Figure 4.5 S-N plots for macro-fiber (a) GD of 1/4th of diameter (b) GD of 1/3rd of diameter

The shear fatigue life of PF0.75 is the highest among all the PQC, micro-fiber reinforced, and macro-fiber reinforced PQC mixtures at any stress level and GD. The shear fatigue life of PQC can be substantially improved with the addition of macro-fibers. The improvement is much greater than the A31.5 mixtures. The shear fatigue life is in the increasing order of PF0.25, PF0.50 and PF0.75. The crack bridging of

fibers across the joint can improve the performance of aggregate interlocked joints under repeated loads.

4.4.2 Effect of GD and stress levels on shear fatigue performance

The effect of GD and stress levels on shear fatigue performance of PQC, micro-fiber and macro-fiber reinforced PQC mixtures with GD 1/4th of diameter, and 1/3rd of diameter specimens under shear loading is studied using the Kaplan-Meir (K-M) survival analysis. This analysis estimates the fatigue life reliability of the specimens under shear loading and provides survival probability in the form of graphical abstract. K-M plots (Survival probability Vs Fatigue life) are shown in Figure 4.6 (a) – (f), Figure 4.7 (a) – (f), and Figure 4.8 (a) – (f), respectively, for PQC, micro-fiber reinforced and macro-fiber reinforced PQC mixtures. The stair-case shaped lines denote the evolution of occurrence of failure.

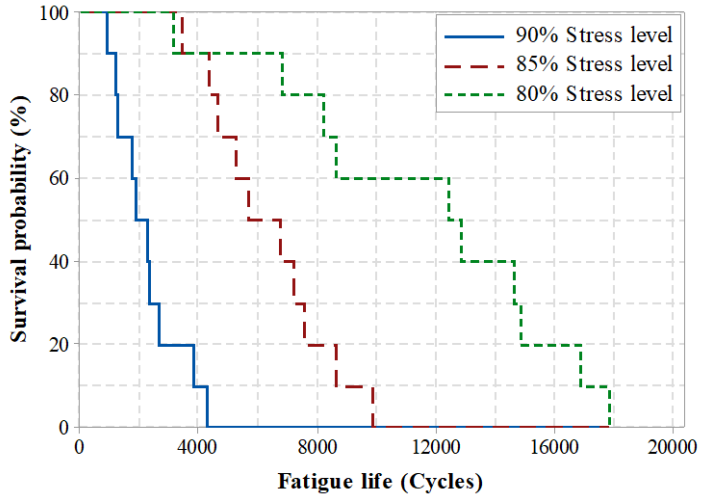

(a)

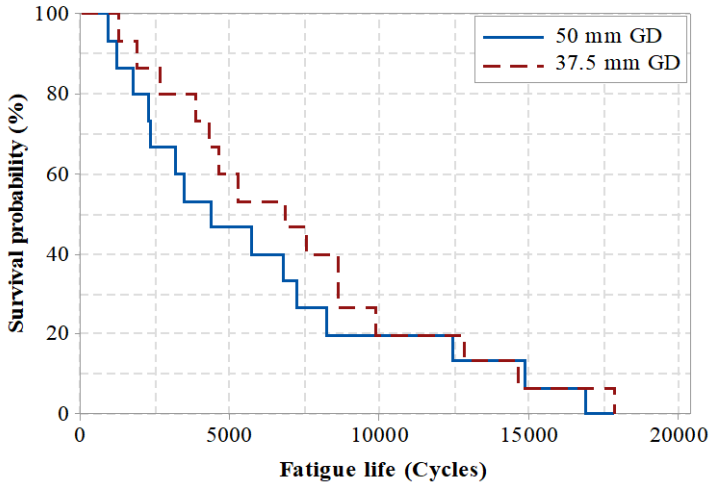

(b)

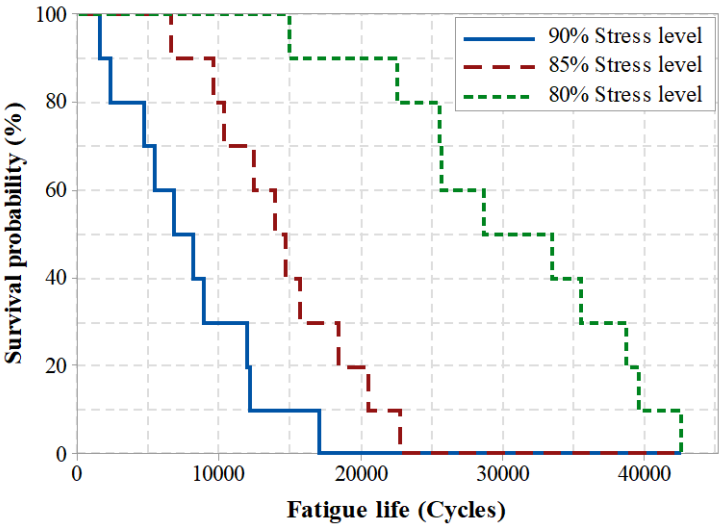
100
80
60
40
20
0
Survival probability (%)
0
10000
20000
30000
40000
Fatigue life (Cycles)
90% Stress level
85% Stress level
80% Stress level

(c)

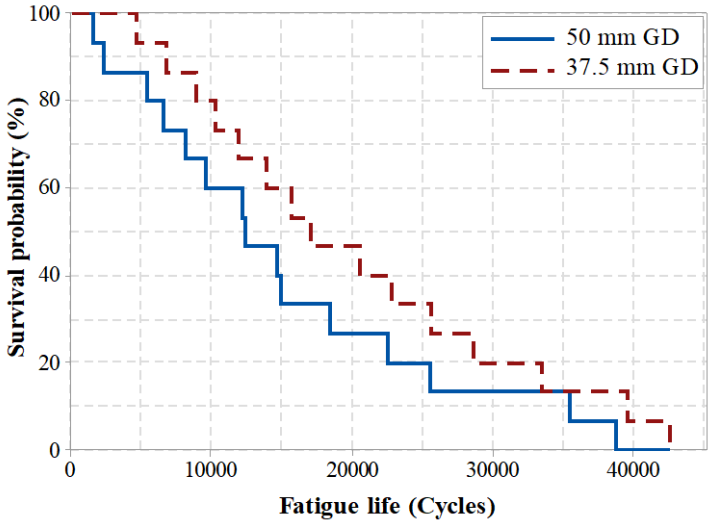
100
80
60
40
20
0
Survival probability (%)
0
10000
20000
30000
40000
Fatigue life (Cycles)
50 mm GD
37.5 mm GD

(d)

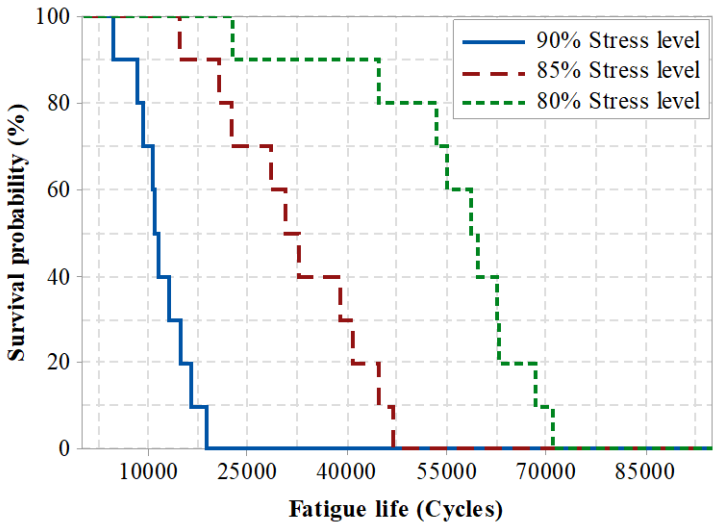
100
80
60
40
20
0
Survival probability (%)
10000
25000
40000
55000
70000
85000
Fatigue life (Cycles)
90% Stress level
85% Stress level
80% Stress level

(e)

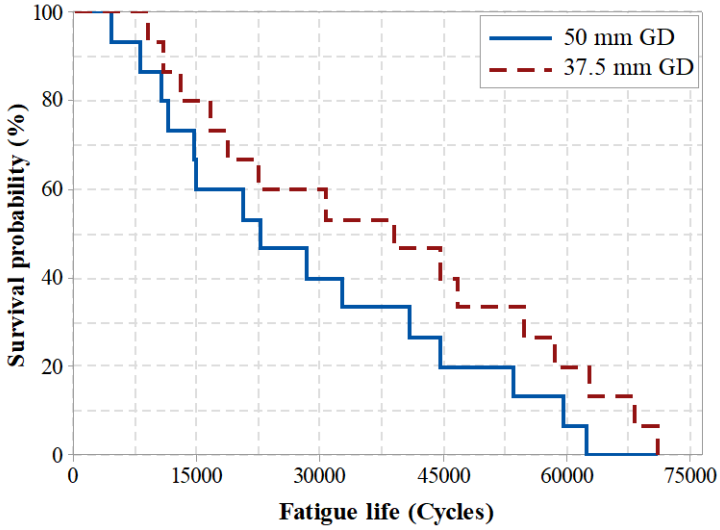

(f)

Figure 4.6 Kaplan-Meir (K-M) Survival plots: influence of stress levels and GD on survival probability (a) and (b) for A19, (c) and (d) for A26.5 and (e) and (f) for A31.5 plain PQC mixtures.

It is seen from the K-M plots shown in Figure 4.6 (a), (c), and (e) that irrespective of the type of NMAS used in the PQC mix, the survival probability is significantly higher in the case of 80% stress level when compared to 85% and 90% stress levels. At the survival probability of 50%, the shear fatigue life of all three PQC mix (A19, A26.5 and A31.5) specimens tested at 80% stress level are about two times of shear fatigue life of samples tested at 85% stress level. Similar variation is observed at 20% survival probability.

Moreover, it is seen from the K-M plots shown in Figure 4.6 (b), (d), and (f) that the survival probability is significantly higher in the case of GD of 1/4th diameter for a PQC mix of A26.5 and A31.5. However, in the A19 PQC mix, no significant difference in survival probability for the two GDs (1/4th of diameter and 1/3rd of diameter) is observed. At the survival probability of 50%, the shear fatigue life of the A31.5 PQC mix is largely dependent on the GD when compared to the other two PQC mixes. It is observed from K-M plots that at common stress level, GD and survival probability, the shear fatigue life of PQC mixes is in the decreasing order of A31.5, A26.5 and A19, respectively.

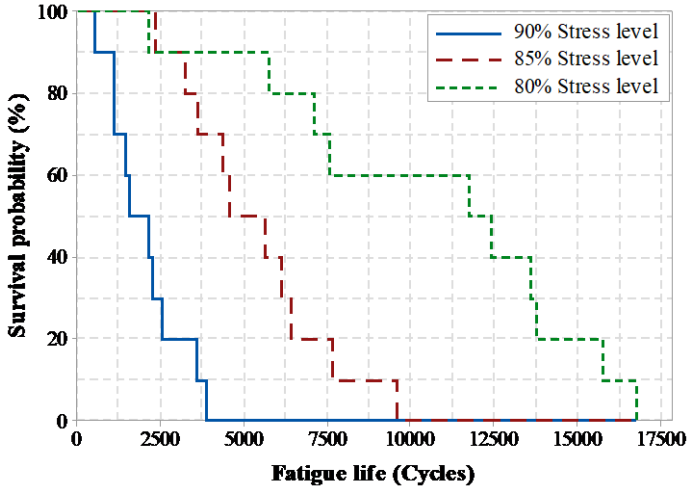
90% Stress level
85% Stress level
80% Stress level
Survival probability (%)
Fatigue life (Cycles)
0
20
40
60
80
100
0
2500
5000
7500
10000
12500
15000
17500

(a)

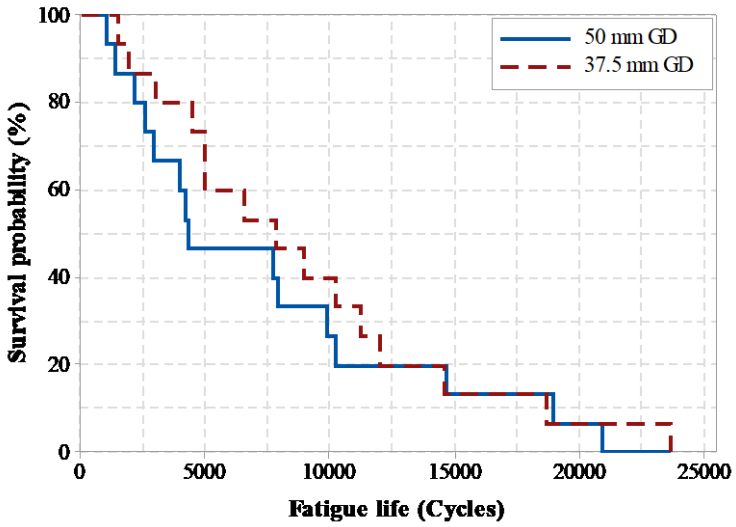
50 mm GD
37.5 mm GD
Survival probability (%)
Fatigue life (Cycles)
0
20
40
60
80
100
0
5000
10000
15000
20000
25000

(b)

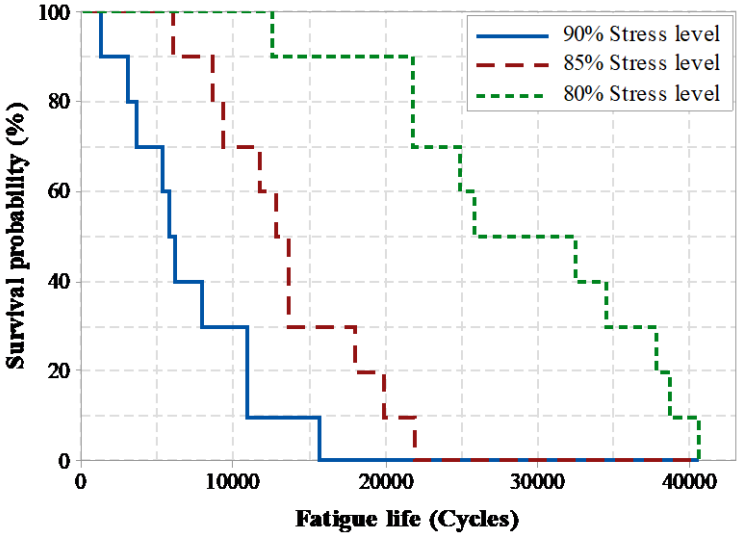
90% Stress level
85% Stress level
80% Stress level
Survival probability (%)
Fatigue life (Cycles)
0
20
40
60
80
100
0
10000
20000
30000
40000

(c)

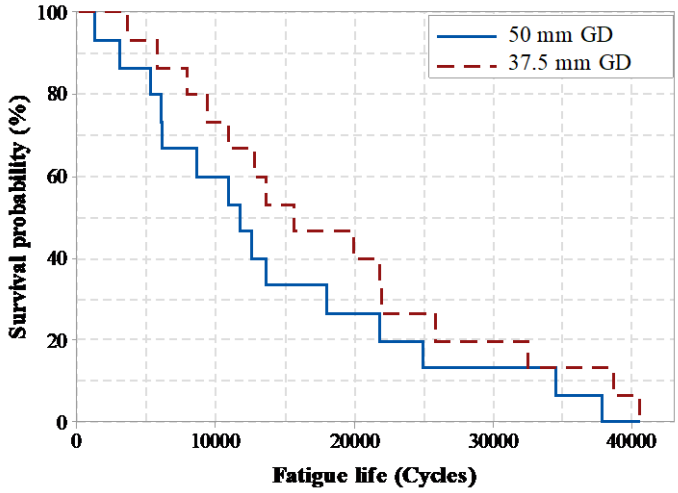

(d)

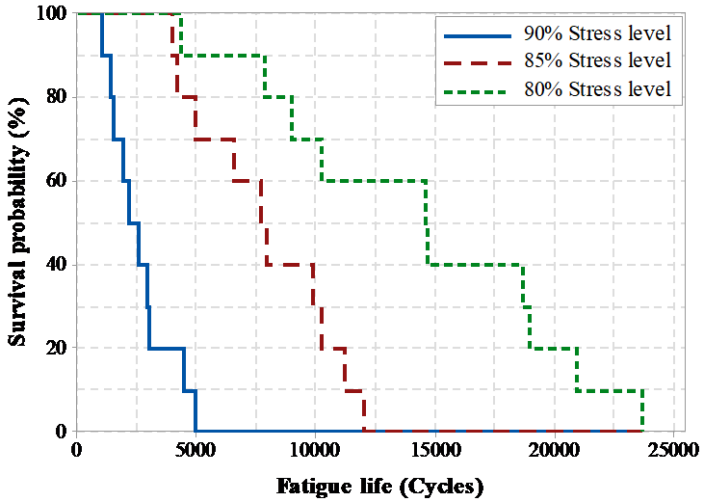

(e)

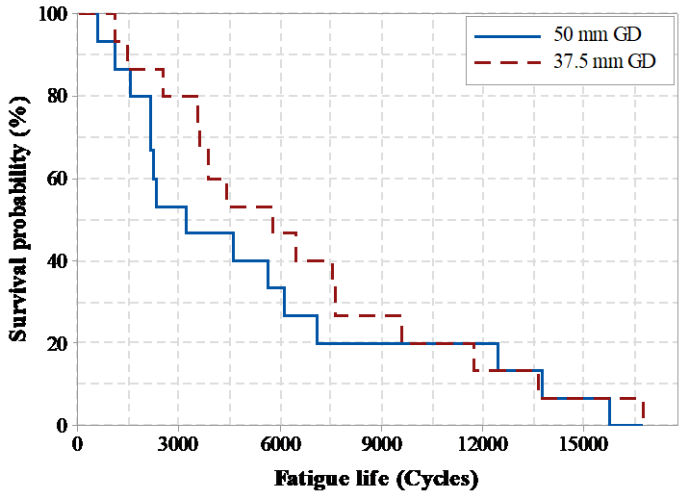

(f)

Figure 4.7 Kaplan-Meir (K-M) Survival plots: influence of stress levels and GD on survival probability (a) and (b) for F0.9, (c) and (d) for F2.1 and (e) and (f) for F3.0 micro-fiber reinforced PQC mixtures.

It can be noticed from the K-M plots shown in Figure 4.7 (b), (d), and (f) that the survival probability is significantly higher in the case of GD of 1/4th diameter for the F2.1 mix. However, no significant difference in survival probability for the two GDs (1/4th of diameter and 1/3rd of diameter) is observed in the other two micro-fiber reinforced PQC mixtures. It is observed from K-M plots that at common stress level, GD and survival probability, the shear fatigue life of micro-fiber reinforced PQC mix is in the decreasing order of F2.1, F0.9 and F3.0, respectively.

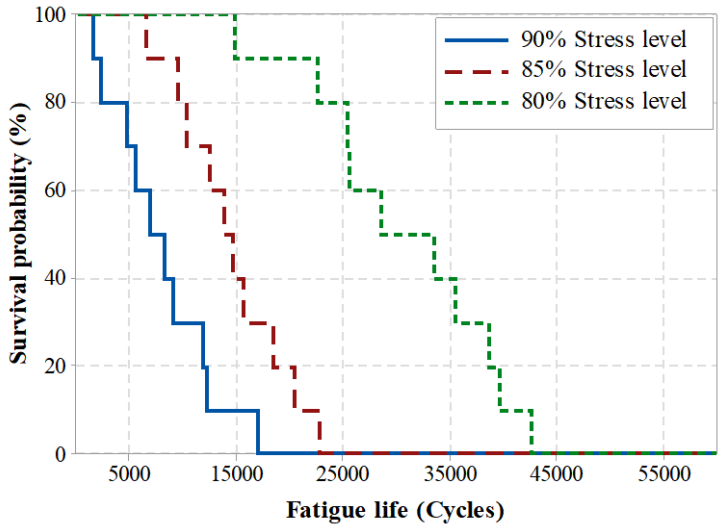

(a)

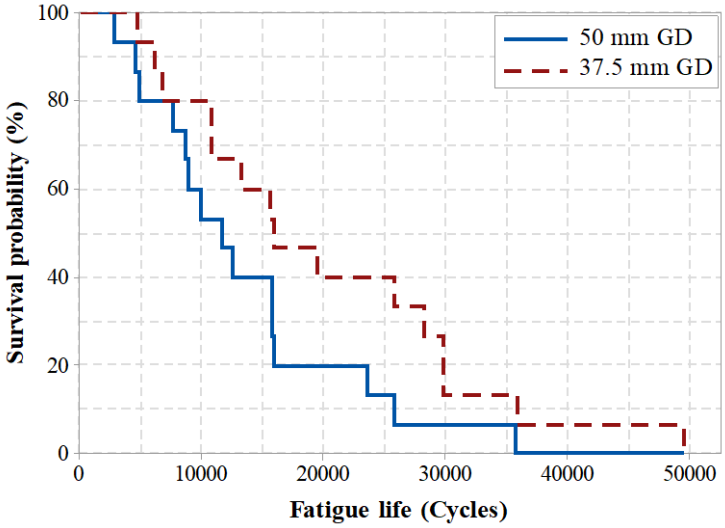

(b)

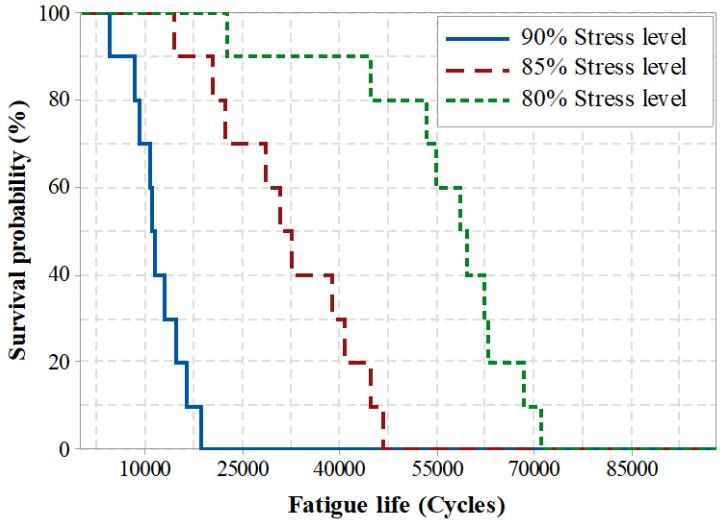
100
80
60
40
20
0
Survival probability (%)
10000
25000
40000
55000
70000
85000
Fatigue life (Cycles)
90% Stress level
85% Stress level
80% Stress level

(c)

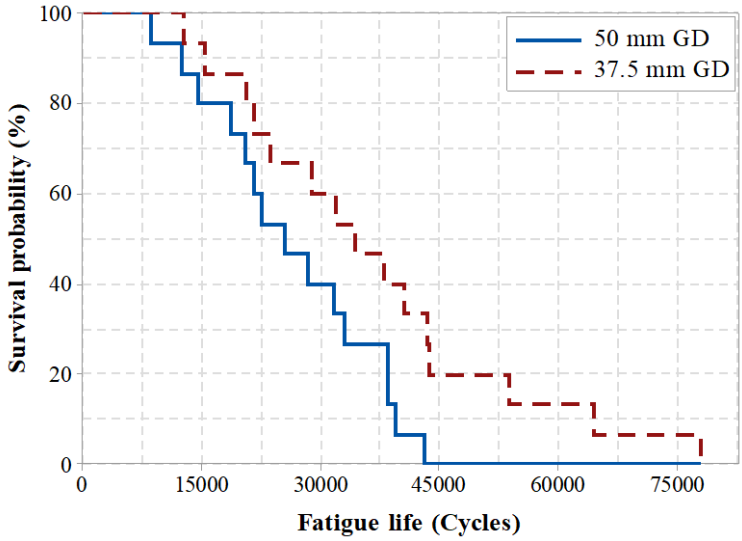
100
80
60
40
20
0
Survival probability (%)
0
15000
30000
45000
60000
75000
Fatigue life (Cycles)
50 mm GD
37.5 mm GD

(d)

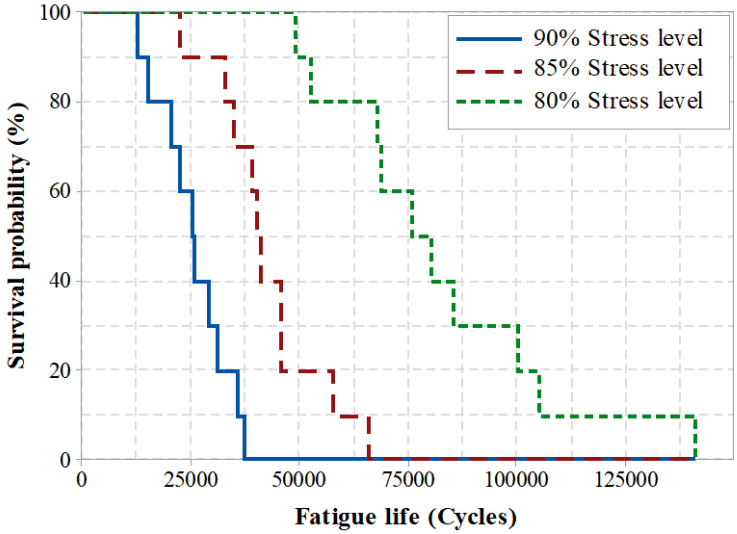
100
80
60
40
20
0
Survival probability (%)
0
25000
50000
75000
100000
125000
Fatigue life (Cycles)
90% Stress level
85% Stress level
80% Stress level

(e)

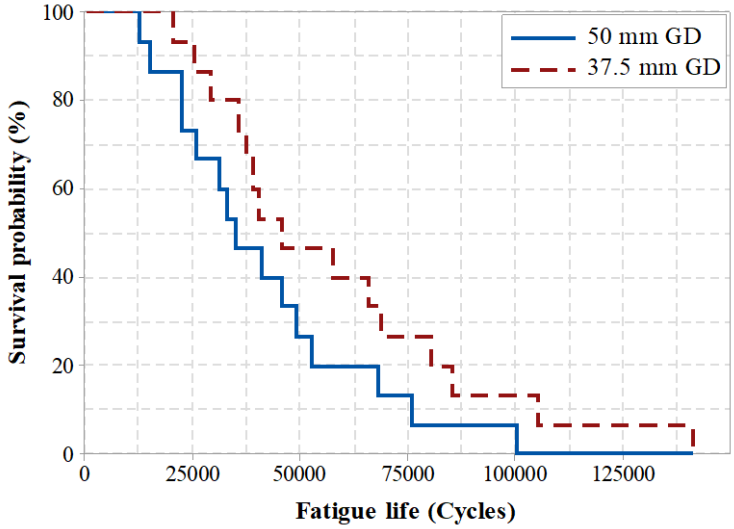

(f)

Figure 4.8 Kaplan-Meir (K-M) Survival plots: influence of stress levels and GD on survival probability (a) and (b) for PF0.25, (c) and (d) for PF0.50 and (e) and (f) for PF 0.75 macro-fiber reinforced PQC mixtures.

It is seen from the K-M plots shown in Figure 4.8 (a), (c), and (e) that irrespective of the fiber dosage, the survival probability is significantly higher in the case of 80% stress level when compared to 85%, and 90% stress levels for macro-fiber reinforced PQC mix specimens. At the survival probability of 20%, the shear fatigue life of macro-fiber reinforced PQC specimens PF0.25, and PF0.50 tested at 80% stress level are about two times of shear fatigue life of samples tested at 85% stress level. However, PF0.75 mix specimens tested at 80% stress level have three times of shear fatigue life of samples tested at 85% stress level.

It can be noticed from the K-M plots shown in Figure 4.8 (b), (d), and (f) that the survival probability is significantly higher in the case of GD of 1/4th diameter for PF0.75 mix. It is observed from K-M plots that at common stress level, GD and survival probability, the shear fatigue life of macro-fiber reinforced PQC mix is in the decreasing order of PF0.75, PF0.50 and PF0.25, respectively.

The log-rank test is a popular test being used to compare the survival curves. The null hypothesis of this statistic test is that the survival curves of all three PQC, micro-fiber reinforced, and macro-fiber mixes are the same, either for the three stress levels or for the two different GDs (Dudley *et al.* 2016). The null hypothesis is rejected

if there is a significant difference between the expected and observed failures. The log-rank test statistic is approximated to the Chi-square test with two degrees of freedom. The p-values of log-rank tests are zero for all the mixtures. This indicates that there is a significant effect of stress levels on the fatigue performance of PQC mixes under shear loading. The p-values of the log-rank test of A19, A26.5 and A31.5 PQC mixes are 0.291, 0.204 and 0.150, respectively. The p-values of the log-rank test of micro-fiber reinforced PQC mix F0.9, F2.1 and F3.0 are 0.504, 0.232 and 0.450, respectively. The p-values of the log-rank test of macro-fiber reinforced PQC mix PF0.25, PF0.50 and PF0.75 are 0.091, 0.033 and 0.134, respectively. This shows that the effect of GD is insignificant on the fatigue performance under shear loading at higher stress levels.

4.4.3 Distribution of fatigue life of concrete mixtures under shear loading

In the past, researchers have used lognormal distribution, 2-parameter and 3-parameter Weibull distributions for fitting the fatigue life cycles against the failure probability (Chandrappa and Biligiri 2017; Kasu et al. 2019). As the obtained shear fatigue data in the present study is scattered, the probabilistic analysis and distribution fitting techniques are used to understand the distribution of shear fatigue life of PQC, micro-fiber reinforced, and macro-fiber reinforced PQC mixes.

The 3-parameter Weibull distribution and lognormal distributions are used to fit the shear fatigue data. The probability density function (pdf) of 3-parameter Weibull distribution is given by:

$$f(s) = \frac{\beta}{\eta}\left(\frac{s-\lambda}{\eta}\right)^{\beta-1} e^{-\left(\frac{s-\lambda}{\eta}\right)^{\beta}} \quad (4.1)$$

Where s is the fatigue life of specimens; β is the shape parameter; η is the scale parameter, and λ is the location parameter (Kappenman 1985).

The probability density function (pdf) of the lognormal distribution is given by:

$$f(s) = \frac{1}{s\sigma\sqrt{2\pi}} e\left(-\frac{(ln\,(s)-\mu)^2}{2\sigma^2}\right) \quad (4.2)$$

where s is the shear fatigue life of specimens; σ is the standard deviation, and μ is the mean. The parameters are estimated using the maximum likelihood estimate (MLE) method (Kappenman 1985). The MLE of these two distributions for the PQC, micro-

fiber reinforced PQC and macro-fiber reinforced PQC mix fatigue data are tabulated in Table 4.6, Table 4.7 and Table 4.8, respectively.

Table 4.6 Maximum likelihood estimates (MLE) of distribution parameters for PQC mix

Distribution	Parameter	Value		
		A19	A26.5	A31.5
Three-parameter Weibull	Shape/slope, β	1.296	1.439	1.331
	Scale, η	6824	18393	31720
	Location/Threshold, λ	443.3	958.4	3939
Lognormal	Mean, μ	8.524	9.524	10.171
	Standard deviation, σ	0.830	0.810	0.756

Table 4.7 Maximum likelihood estimates (MLE) of distribution for micro-fiber reinforced PQC

Distribution	Parameter	Value		
		F0.9	F2.1	F3.0
Three-parameter Weibull	Shape/slope, β	1.246	1.372	1.096
	Scale, η	8332	17083	5676
	Location/Threshold, λ	495	900	518
Lognormal	Mean, μ	8.702	9.441	8.369
	Standard deviation, σ	0.863	0.827	0.886
	AD	0.286	0.324	0.232

Table 4.8 Maximum likelihood estimates (MLE) of distribution for macro-fiber reinforced PQC

Distribution	Parameter	Value		
		PF0.25	PF0.50	PF0.75
Three-parameter Weibull	Shape/slope, β	1.228	1.604	1.292
	Scale, η	15134	26952	41391
	Location/Threshold, λ	2706	7434	11913
Lognormal	Mean, μ	9.511	10.224	10.664
	Standard deviation, σ	0.706	0.507	0.583

Anderson-Darling test, popularly known as the AD test, is used for assessing the goodness of fit of these distributions (Chandrappa and Biligiri 2016; Zimmermann et al. 2012). The lower value of the AD test statistic is expected to provide better goodness of fit for the distribution under consideration (3-parameter Weibull and lognormal distribution). If the AD value is less than the critical value of 0.753, it means

that the null hypothesis is true and the data set follows the particular distribution under test at a 95% confidence level (Motamedi et al. 2015; Theodorsson 1988). The AD test statistic is given as

$$AD^2 = -n - \Phi \tag{4.3}$$

$$\Phi = n^{-1} \sum_{i=1}^{n} (2i-1)[\, ln(F(s_i) + ln\,(1 - F(s_{n+1-i})))] \tag{4.4}$$

$$Adjusted\ AD = AD\left(\frac{\sqrt{n}+0{\cdot}2}{\sqrt{n}}\right) \tag{4.5}$$

Where n is the sample size, i is the number assigned to the data points in order, F(s) is the cumulative distribution function (CDF) of the distribution under test and s_i is the shear fatigue data arranged in order. The AD test results of A19 PQC mix specimens fitted with 3-parameter Weibull distribution are shown in Table 4.9. Similarly, the AD test results are obtained for all the concrete mixtures.

Table 4.9 A-D goodness of fit test results of A19 PQC mixtures for 3-parameter Weibull distribution

i	Fatigue Cycles	$F(s_i)$	$F(s_{n+k-i})$	i^{th} term
1	900	0.03	0.97	0.2296
2	1186	0.05	0.96	0.6031
3	1286	0.06	0.93	0.8974
4	1766	0.11	0.92	1.1139
5	1864	0.12	0.89	1.2809
6	2260	0.16	0.88	1.4248
7	2354	0.17	0.78	1.4149
8	2682	0.21	0.72	1.4149
9	3154	0.26	0.72	1.4810
10	3458	0.29	0.69	1.5267
11	3842	0.33	0.65	1.5064
12	4286	0.38	0.63	1.5103
13	4340	0.38	0.60	1.5653
14	4628	0.41	0.60	1.6125
15	5284	0.47	0.51	1.4104
16	5686	0.51	0.47	1.3607
17	6758	0.60	0.41	1.1544
18	6842	0.60	0.38	1.1575
19	7254	0.63	0.38	1.1535
20	7544	0.65	0.33	1.0846
21	8214	0.69	0.29	0.9738
22	8648	0.72	0.26	0.9059
23	8648	0.72	0.21	0.8485
24	9874	0.78	0.17	0.6872
25	12460	0.88	0.16	0.5114
26	12854	0.89	0.12	0.4283
27	14658	0.92	0.11	0.3487
28	14878	0.93	0.06	0.2576
29	16896	0.96	0.05	0.1923
30	17866	0.97	0.03	0.1280
			Sum =	30.184
			AD =	0.184
			Adjusted AD =	0.191

The 3-parameter Weibull distribution is fitted to the shear fatigue data. It is shown in Figure 4.9, Figure 4.10 and Figure 4.11 for PQC (A19, A26.5 and A31.5), micro-fiber reinforced PQC (F0.9, F2.1 and F3.0) and macro-fiber reinforced PQC (PF0.25, PF0.50 and PF0.75) mixtures, respectively, along with the AD values and P-values.

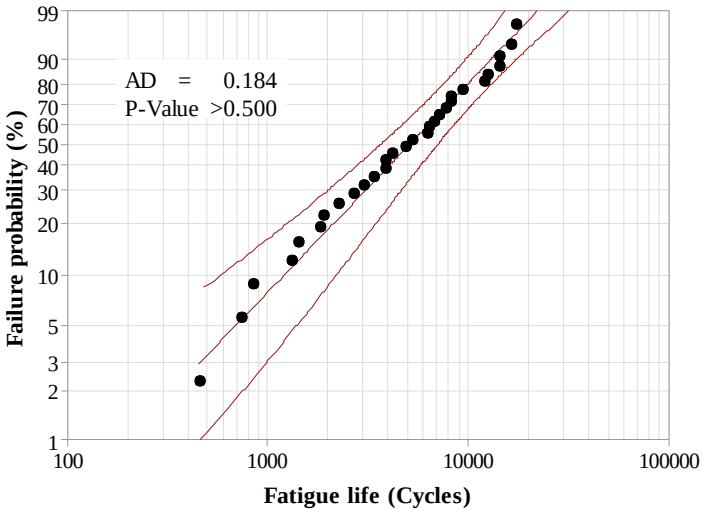

(a)

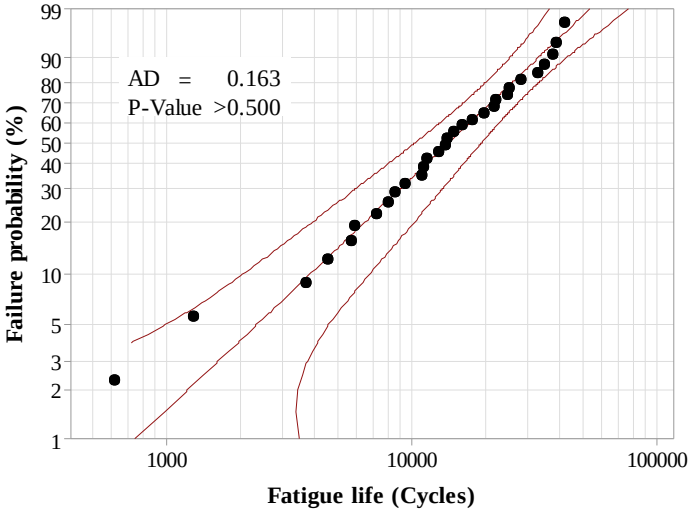

(b)

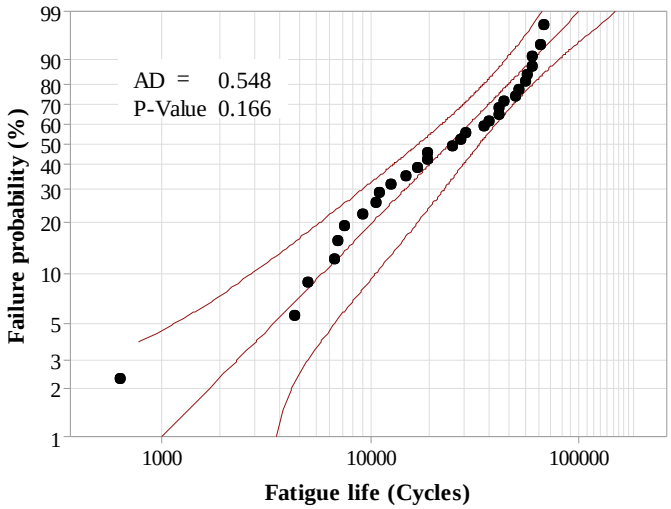

(c)

Figure 4.9 Three-parameter Weibull distribution fitted to shear fatigue data of PQC mixtures (a) A19, (b) A26.5 and (c) A31.5

For the obtained shear fatigue data, the AD values are lower (0.184, 0.163 and 0.548 for A19, A26.5 and A31.5 PQC mixtures, respectively) when fitted to Weibull distribution compared to the AD values (0.269, 0.388 and 0.614 for A19, A26.5 and A31.5 PQC mixtures, respectively) fitted to a lognormal distribution. It is observed from Figure 4.9 that the shear fatigue life of A31.5 PQC mixtures is about 24086 cycles at 50% failure probability. In contrast, at the same failure probability, the shear fatigue life of A26.5 and A19 PQC mixtures is 14257 and 5143, respectively. This shows that irrespective of GD and stress levels, A31.5 PQC blends have better shear fatigue life cycles when compared to A26.5 and A19 PQC mixtures.

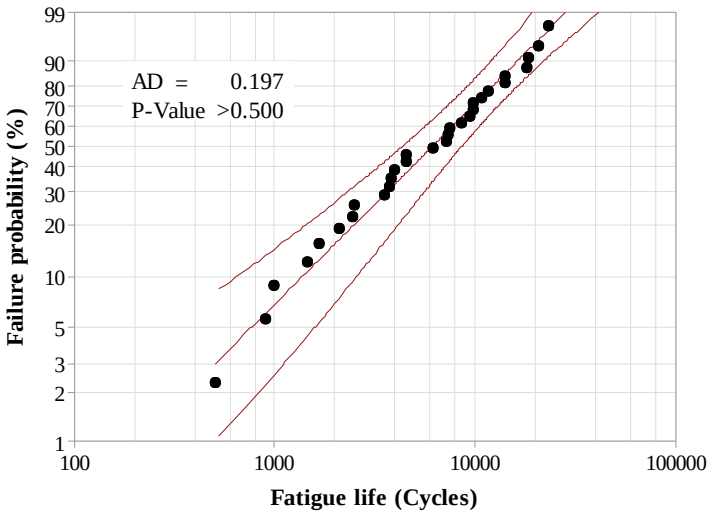

(a)

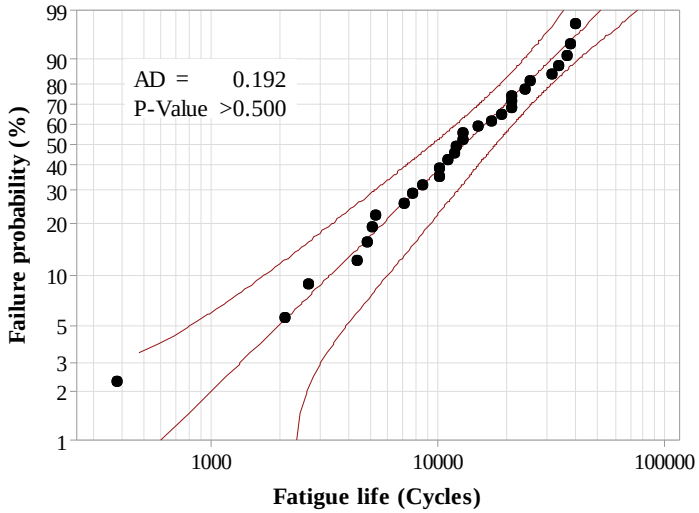

(b)

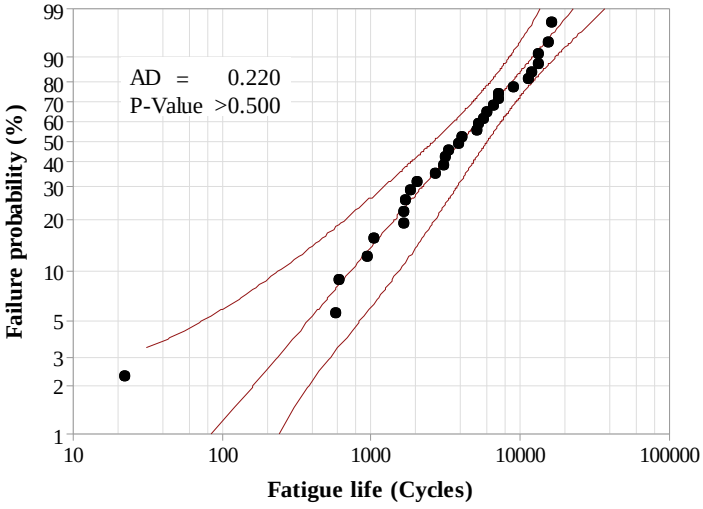

(c)

Figure 4.10 Three-parameter Weibull distribution fitted to shear fatigue data of micro-fiber reinforced PQC mixtures (a) F.9, (b) F2.1 and (c) F3.0

In the case of micro-fiber reinforced PQC specimens, the AD values are lower (0.197, 0.192 and 0.220 for F0.9, F2.1 and F3.0 mixtures, respectively) when fitted to Weibull distribution compared to the AD values (0.286, 0.324 and 0.232 for F0.9, F2.1 and F3.0 mixtures, respectively) fitted to a lognormal distribution for the obtained shear fatigue data. It is observed from Figure 4.10 that the shear fatigue life of F2.1 mixtures is about 13080 cycles at 50% failure probability. In contrast, at the same failure probability, the shear fatigue life of F0.9 and F3.1 mixtures is 6209 and 4063, respectively. This shows that irrespective of GD and stress levels, F2.1 mixtures have

better shear fatigue life cycles when compared to F0.9 and F3.0 micro-fiber reinforced PQC mixtures.

Also, for macro-fiber reinforced PQC specimens, the AD values are found to be lower (0.197, 0.219 and 0.149 for PF0.25, PF0.50 and PF0.75 mixtures, respectively) when fitted to Weibull distribution compared to the AD values (0.216, 0..256 and 0.184 for PF0.25, PF0.50 and PF0.75 mixtures, respectively) fitted to a lognormal distribution for the obtained shear fatigue data. It is observed from Figure 4.11 that the shear fatigue life of PF0.75 concrete mixtures is about 31167 cycles at 50% failure probability. In contrast, at the same failure probability, the shear fatigue life of PF0.50, PF0.25 and A19 concrete mixtures are 21445,11230 and 5143, respectively. This shows that irrespective of groove depths and stress levels, the PF0.75 concrete mixtures have better shear fatigue life cycles when compared to PF0.50, PF0.25 and A19 concrete mixtures.

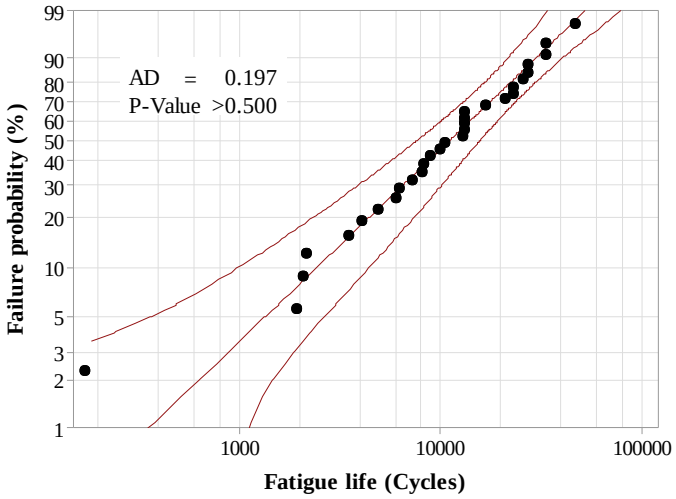

(a)

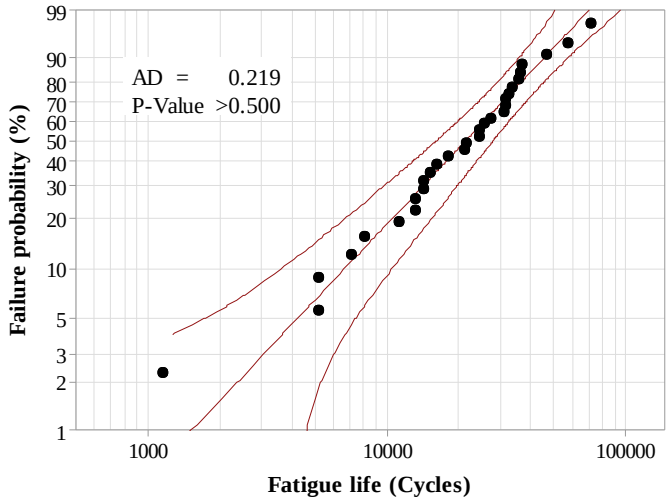

(b)

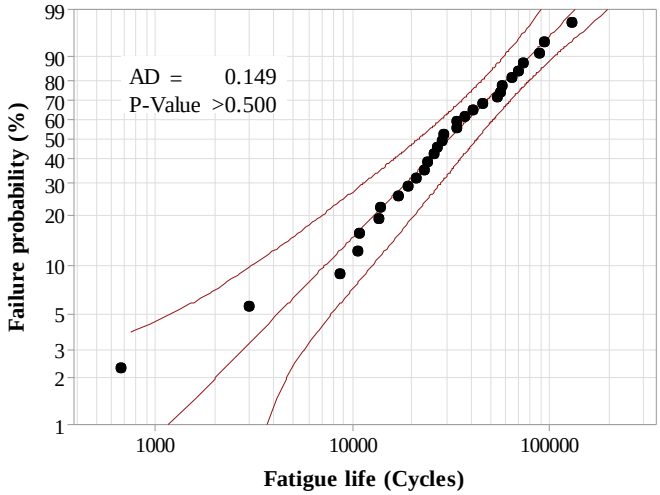

(c)

Figure 4.11 Three-parameter Weibull distribution fitted to shear fatigue data of macro-fiber reinforced PQC mixtures (a) PF0.25, (b) PF0.50 and (c) PF0.75

Also, for macro-fiber reinforced PQC specimens, the AD values are found to be lower (0.197, 0.219 and 0.149 for PF0.25, PF0.50 and PF0.75 mixtures, respectively) when fitted to Weibull distribution compared to the AD values (0.216, 0..256 and 0.184 for PF0.25, PF0.50 and PF0.75 mixtures, respectively) fitted to a lognormal distribution for the obtained shear fatigue data. It is observed from Figure 4.11 that the shear fatigue life of PF0.75 concrete mixtures is about 31167 cycles at 50% failure probability. In contrast, at the same failure probability, the shear fatigue life of PF0.50, PF0.25 and A19 concrete mixtures are 21445,11230 and 5143, respectively. This shows that irrespective of groove depths and stress levels, the PF0.75 concrete mixtures have better shear fatigue life cycles when compared to PF0.50, PF0.25 and A19 concrete mixtures.

The shape parameter of the 3-parameter Weibull distribution fitted to present shear fatigue data lies between 1 and 2 for all the concrete mixtures. This indicates that the rate of failure increases with the number of repetitions (with time), and failure occurs by wearing action in all concrete mixtures.

The PDF and CDF of 3-parameter Weibull plots for PQC, micro-fiber reinforced, and macro-fiber reinforced PQC specimens are shown in Figure 4.12, Figure 4.13 and Figure 4.14, respectively.

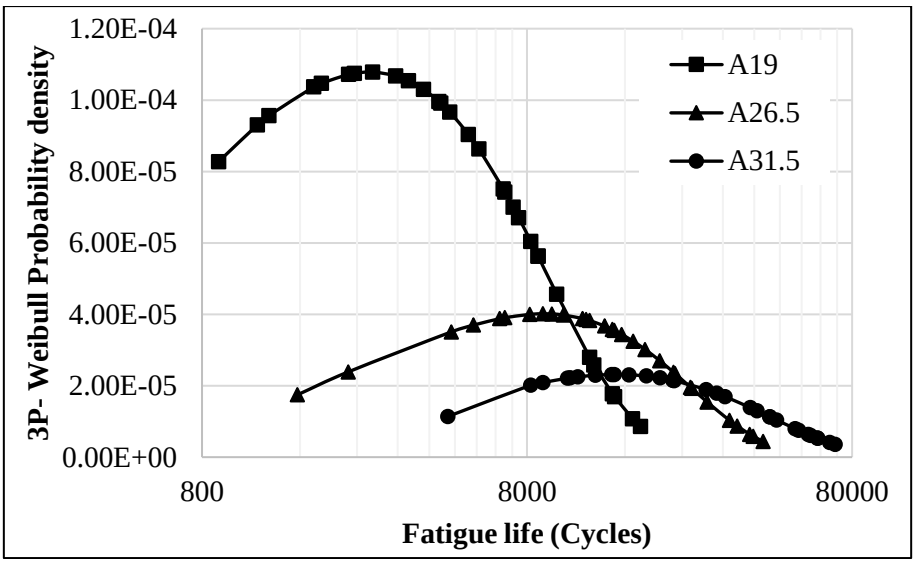

(a)

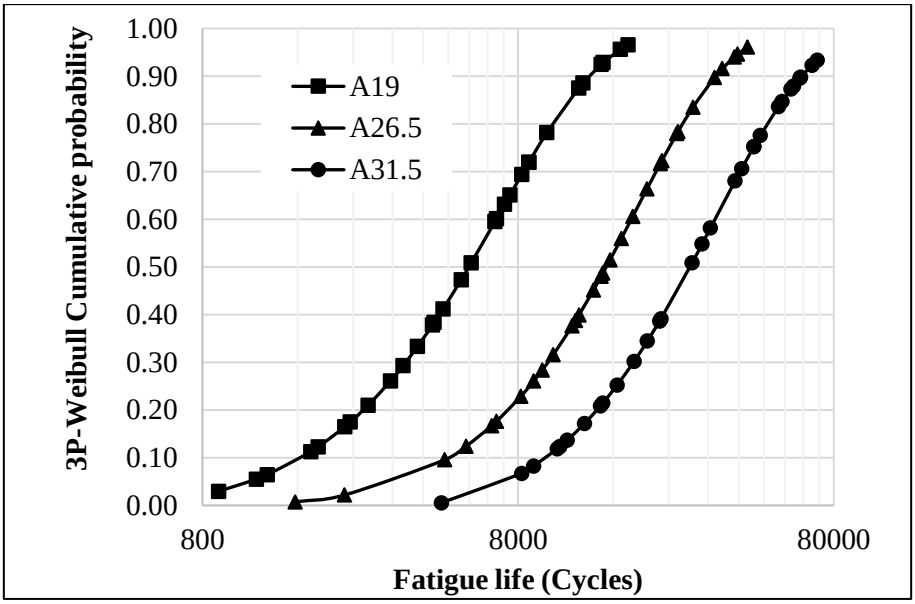

(b)

Figure 4.12 (a) PDF and (b) CDF plots of 3-parameter Weibull distribution for A19, A26.5 and A31.5 PQC mix

It is observed from Figure 4.12 a that the fatigue lives were in the range of 900 to 18000, 1500 to 43000 and 4500 to 71000 respectively for A19, A26.5 and A31.5 plain PQC mixtures. From Figure 4.12 b, it is seen that the failure probability is higher in the case of the A19 PQC mix when compared to A26.5 and A31.5 PQC mixtures. In other words, it means that the useful life of A31.5 PQC mixtures is higher than A19 and A26.5 PQC mixtures under shear fatigue. This increase in shear fatigue life of

A31.5 PQC mix is due to higher aggregate interlocking offered by larger NMAS at the grooved cross-section.

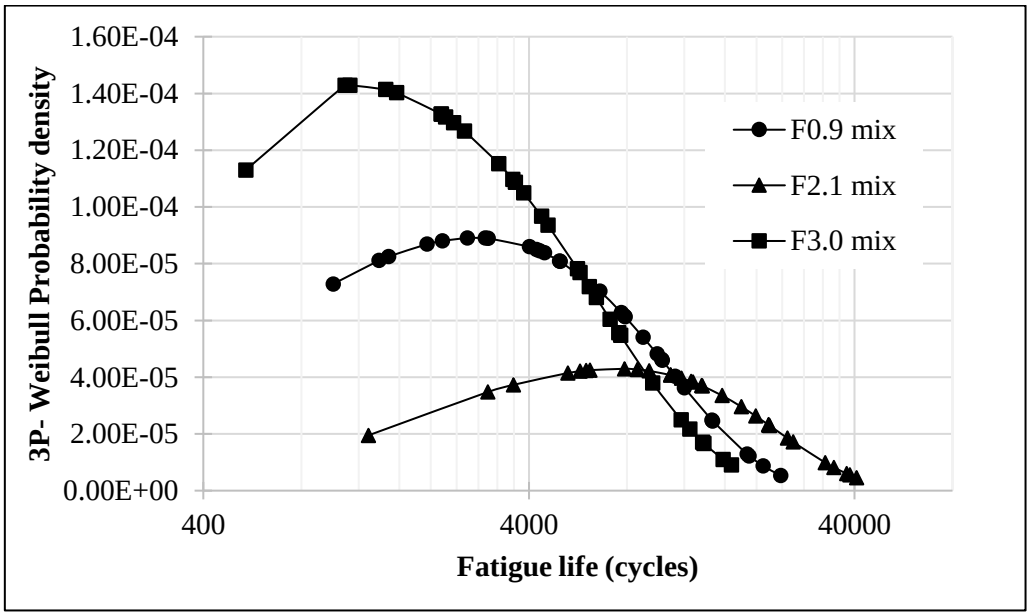

(a)

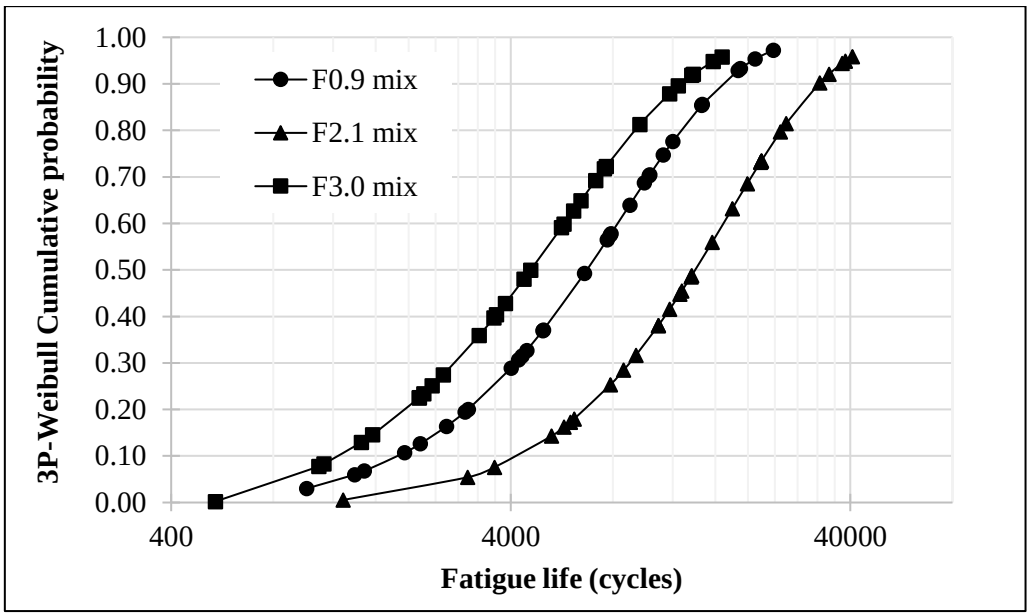

(b)

Figure 4.13 (a) PDF and (b) CDF plots of 3-parameter Weibull distribution for F0.9, F2.1 and F3.0 micro-fiber reinforced PQC mix

It is seen from Figure 4.13 a that the fatigue lives were in the range of 1000 to 24000, 1200 to 41000 and 540 to 17000, respectively for F0.9, F2.1 and F3.0 micro-fiber reinforced PQC mixtures. From Figure 4.13 b, it is observed that the failure

probability is higher in the case of the F3.0 mix when compared to F0.9, and F2.1 micro-fiber reinforced PQC mixtures. The useful life of micro-fiber reinforced PQC specimens increases with an increase in fiber dosage up to the optimum value of 2.1 kg/m^3. This increase in shear fatigue life is due to the improved load transfer through fibers.

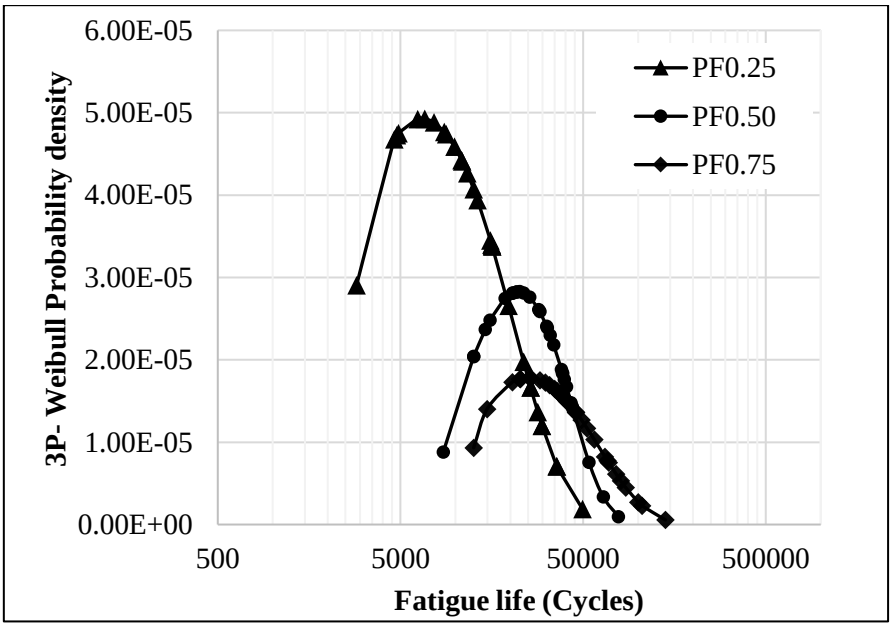

(a)

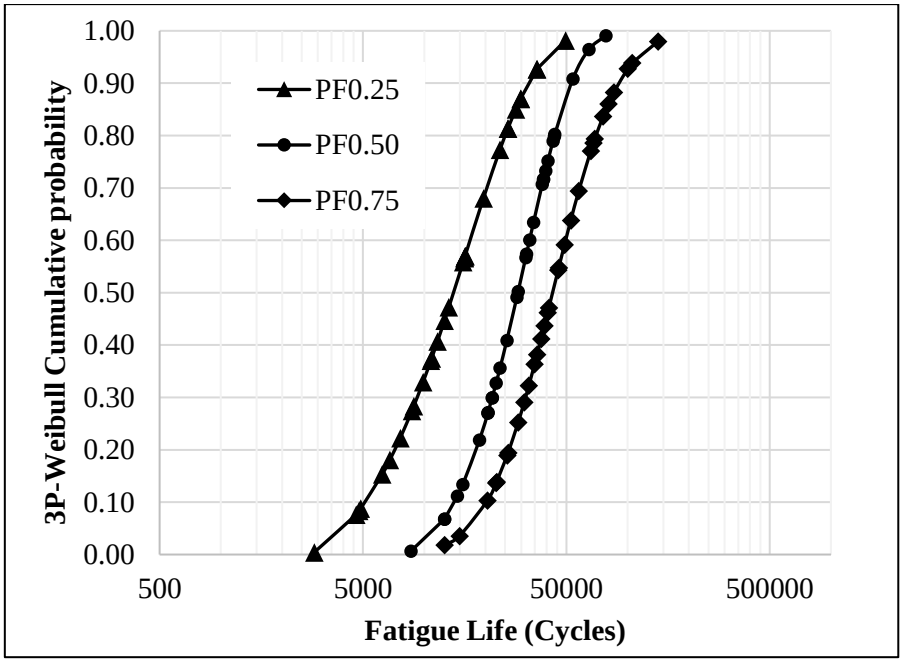

(b)

Figure 4.14 (a) PDF and (b) CDF plots of 3-parameter Weibull distribution for PF0.00, PF0.25, PF0.50 and PF0.75 concrete mix

It is observed from Figure 4.14 a that the fatigue lives were in the range of 2800 to 50000, 8500 to 78000 and 12500 to 141200, respectively, for PF0.25, PF0.50 and PF0.75 macro-fiber reinforced PQC mixtures. From Figure 4.14 b, it is found that the failure probability is lowest in the case of the PF0.75 mix when compared to other concrete mixtures. This shows that the addition of macro-fiber can improve the useful life of concrete mixture, improving the performance of aggregate interlocked joints in pavements. The improvement in useful life is due to crack bridging, and the polypropylene fibers can transfer the load across the crack.

CHAPTER 5

EVALUATION OF AGGREGATE INTERLOCKED JOINT USING THE SIMULATED SMALL-SCALE TEST SETUP

5.1 GENERAL

This chapter presents the laboratory evaluation of aggregate interlocked joints in terms of joint load transfer efficiency (LTE). The simulated test setup is used to evaluate the influence of GD, NMAS and different dosages of micro and macro-fibers on the performance of aggregate interlocked joints. The crack width and LTE relationships are determined and presented for each PQC mixture and GD.

5.2 LABORATORY EXPERIMENTAL PLAN

The beam specimens were prepared as explained in section 3.7.1 of chapter 3. The joint performance of aggregate interlocked joint was evaluated as described in section 3.7.2 of chapter 3. The details of specimens are tabulated in Table 5.1, Table 5.2 and Table 5.3, respectively, for plain PQC, micro-fiber-reinforced and macro-fiber reinforced PQC specimens.

Table 5.1 Details of test specimens for laboratory evaluation of LTE of plain PQC mix

Mix ID	NMAS Used (mm)	Groove depth (mm)		Number of specimens
		25 (1/4th of depth of beam)	33.33 (1/3rd of depth of beam)	
A19	19	3	3	3 × 2 = 6
A26.5	26.5	3	3	3 × 2 = 6
A31.5	31.5	3	3	3 × 2 = 6
			Total =	**18**

Table 5.2 Details of test specimens for laboratory evaluation of LTE of micro-fiber reinforced PQC specimens

Mix ID	Fiber Dosage (kg/m^3)	Groove depth (mm)		Number of specimens
		25 (1/4th of depth of beam)	33.33 (1/3rd of depth of beam)	
F0.9	0.9	3	3	3 × 2 = 6
F2.1	2.1	3	3	3 × 2 = 6
F3.0	3.0	3	3	3 × 2 = 6
			Total =	**18**

Table 5.3 Details of test specimens for laboratory evaluation of shear parameters of macro-fiber reinforced PQC specimens

Mix ID	Fiber Dosage (%)	Groove depth (mm)		Number of specimens
		25 (1/4th of depth of beam)	33.33 (1/3rd of depth of beam)	
PF0.25	0.25	5	5	5 × 2 = 10
PF0.50	0.50	5	5	5 × 2 = 10
PF0.75	0.75	5	5	5 × 2 = 10
			Total	**18**

5.3 RESULTS AND DISCUSSIONS

The results and discussions of the present investigations are discussed in the following sections.

5.3.1 Influence of NMAS and GD on crack width of plain PQC beam under repeated loading

In all the cases, up to ten thousand load cycles, the crack width increased gradually. After reaching ten thousand cycles, there was a rapid increase in crack width. The crack width was found to be increasing with an increase in the number of repetitions irrespective of the NMAS used and GD. In the A19 mix, the crack width was found to be higher at any given load repetition irrespective of GD. At any given load repetition, irrespective of the GD, the crack width is in the increasing order of A31.5, A26.5 and A19. Also, the smaller the GD smaller the crack width in all the three-concrete mixes at any load repetition. The test results are shown in Figure 5.1.

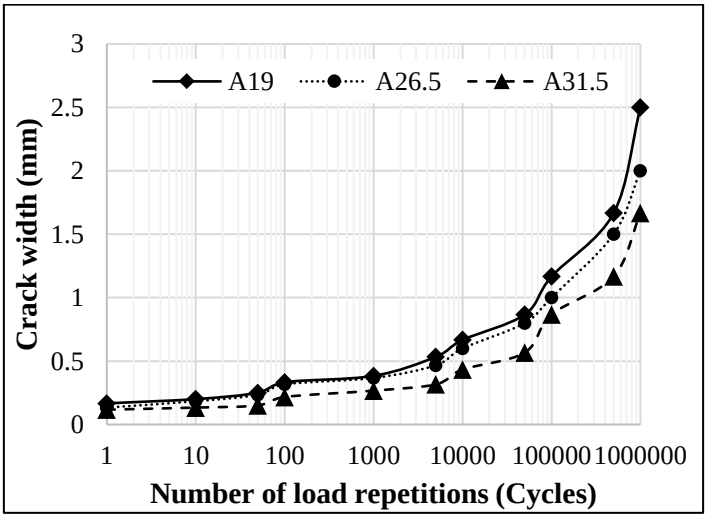

(a)

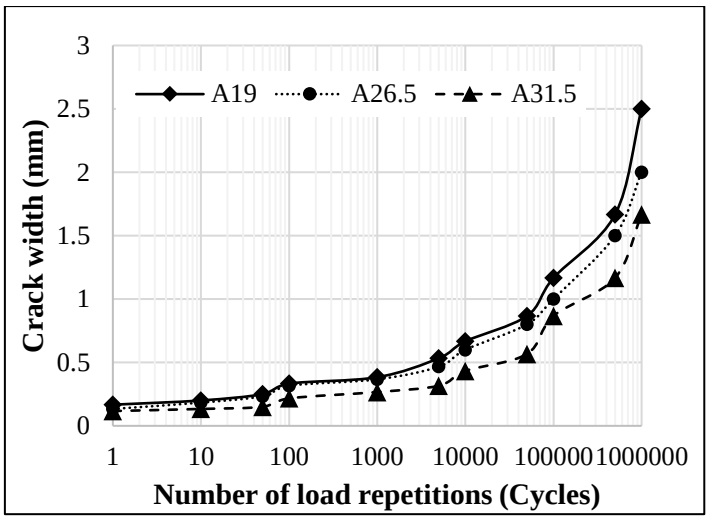

(b)

Figure 5.1 Influence of NMAS on crack width for (a) 1/4th GD (b) 1/3rd GD

5.3.2 Influence of NMAS and GD on the deflection of plain PQC beam under repeated loading

The deflection on the unloaded side and loaded side of the beam was measured using the LVDTs. The deflection on the loaded side is found to be increasing with an increase in the number of load repetitions irrespective of the GD and NMAS used in the concrete mix. However, the deflection on the unloaded side of the beam increased till there was sufficient interlocking at the joint with a further increase in the number of load cycles, the deflection on the unloaded side decreased. However, in no case up to one million cycles, the deflection of the unloaded side become zero. This shows that the rubber base still transferred the part of the load.

The maximum deflections on the loaded side observed in the concrete mix was lower in the beams with 1/4th GD, and the maximum deflections on the loaded side were found to decrease with the use of larger NMAS irrespective of the GD. The influence of NMAS on the deflections on the loaded and unloaded side of the beam with crack width and the number of load repetitions for a GD is plotted in Figure 5.2 and Figure 5.3.

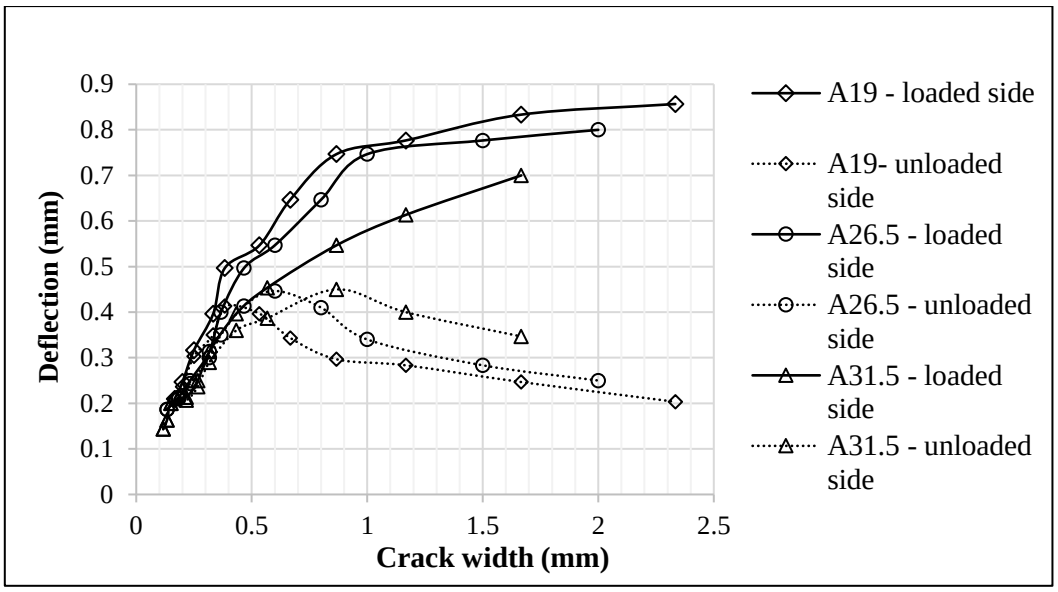

Figure 5.2 Influence of NMAS on deflections on loaded and unloaded sides with number of cycles at 1/4th of GD

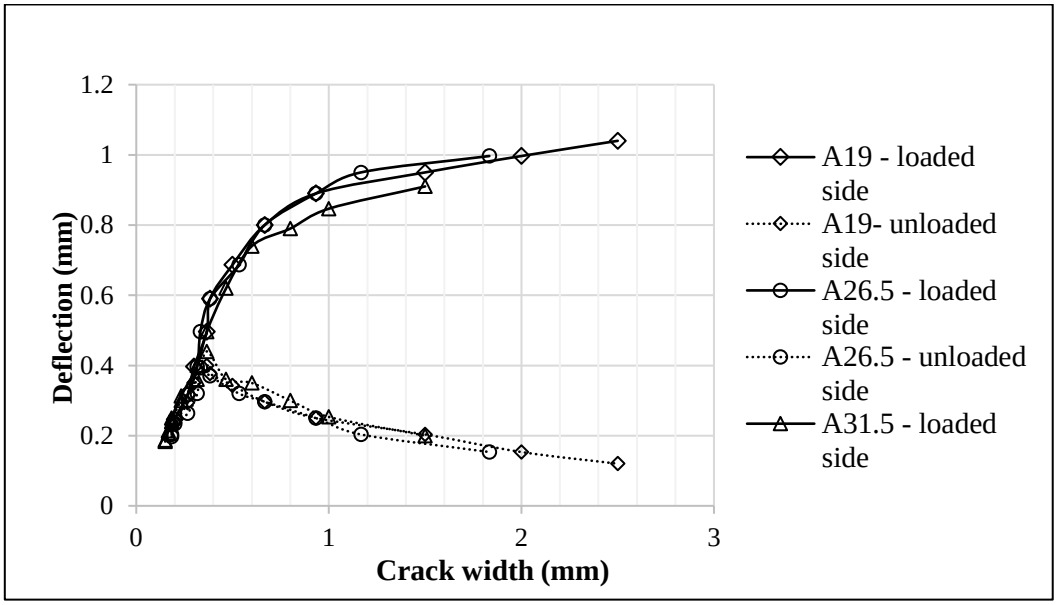

Figure 5.3 Influence of NMAS on deflections on loaded and unloaded sides with number of cycles at 1/3rd of GD

5.3.3 Relationship between LTE and relative movement (RM) of joint in plain PQC beams

The measured deflection values on the loaded and unloaded sides of the beam were used to calculate the LTE and RM of the joint at different crack widths. The relative movement is the difference in deflection of the loaded and unloaded side of the beam. The LTE is determined by taking the ratio of deflection of the unloaded side of

the beam to the loaded side deflection of the beam multiplied by 100.

The relationship between LTE and RM is plotted in Figure 5.4 (a) and (b) for GD 1/4th and 1/3rd of the depth of the beam, respectively.

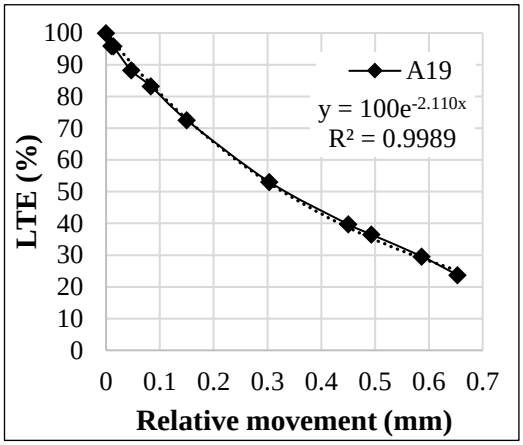

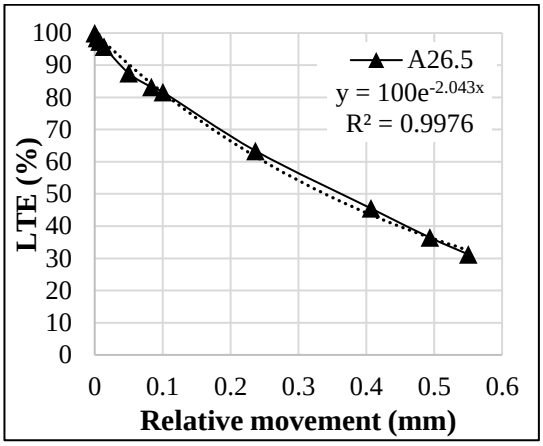

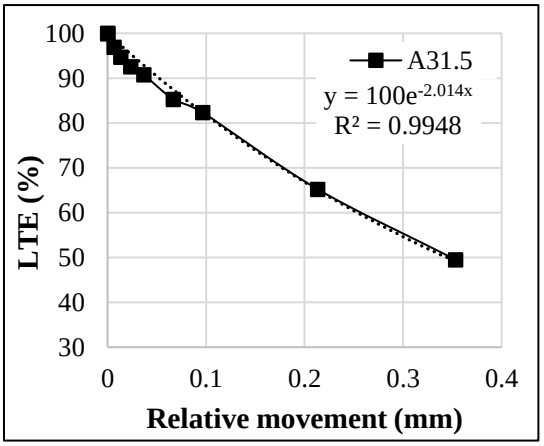

(a)

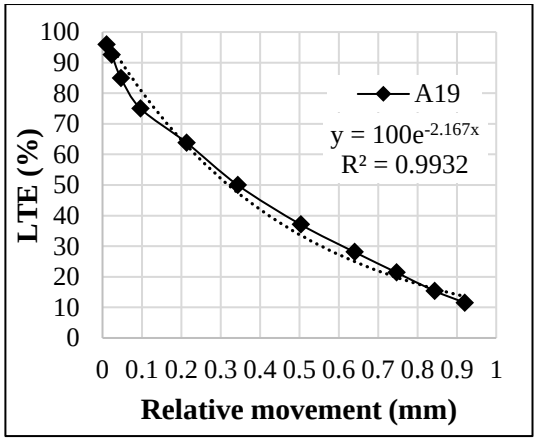

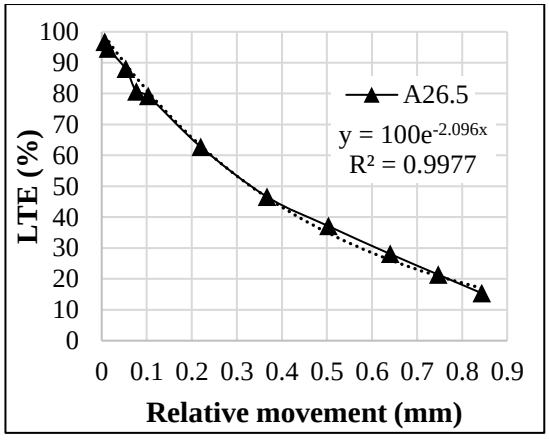

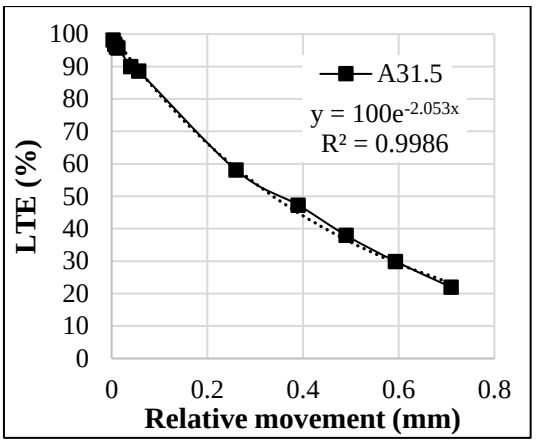

(b)

Figure 5.4 LTE Vs RM of plain PQC mix for (a) 1/4th GD (b) 1/3rd GD

It is seen from Figure 5.4 that irrespective of the GD and the NMAS used in the concrete mix, it is found that there exists an exponential relationship between the LTE and RM. The slope of the exponential curve determined the performance of aggregate interlocking in the beams. It is found that irrespective of the GD, the rate of decrease in LTE is higher in the case of beams with l/3rd GD. It is found that the performance of the joint improved with an increase in NMAS.

5.3.4 Influence of fiber dosages and GD on crack width under repeated loading

In both micro and macro-fiber reinforced PQC mixes, the crack width increased gradually up to twenty thousand load cycles, irrespective of GD and fiber dosages. After reaching twenty thousand cycles, there was a rapid increase in crack width. The crack width was found to be increasing with an increase in the number of repetitions irrespective of the amount of fiber used and GD. Irrespective of GD, the crack width is higher in the F3.0 micro-fiber reinforced PQC mix at any given load repetition. At any given load repetition, irrespective of the GD, the crack width is in the increasing order of F2.1, F0.9, and F3.1 in the case of micro-fiber reinforced PQC mixes. The addition of fibers beyond 2.1 kg/m^3 results in clustering of fibers which reduces the number of aggregates in contact at the joint, which results in an increase in crack width.

In the case of macro-fiber reinforced PQC mixes, the crack width is found to be higher at lower dosages. Irrespective of GD, the crack width is higher in the PF0.25 PQC mix at any given load repetition. At any given load repetition, irrespective of the GD, the crack width is in the increasing order of PF0.75, PF0.50 and PF0.25 in the case

of macro-fiber reinforced PQC mixes. Also, the smaller the GD smaller the crack width in all the fiber reinforced PQC mixes at any load repetition. The fibers across the joint are more in number, which helps to arrest the growth of crack width. The crack width against the number of load repetitions plots are shown in Figure 5.5 and Figure 5.6, respectively, for micro and macro-fiber reinforced PQC mixes.

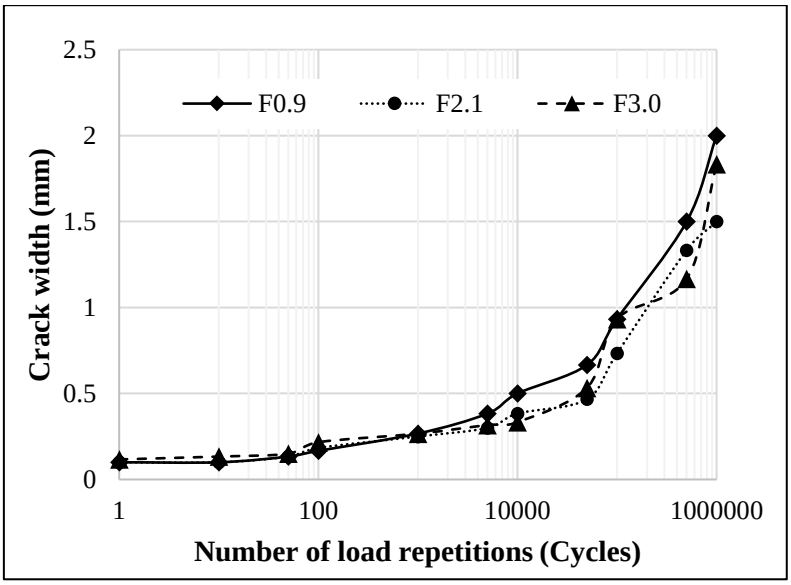

(a)

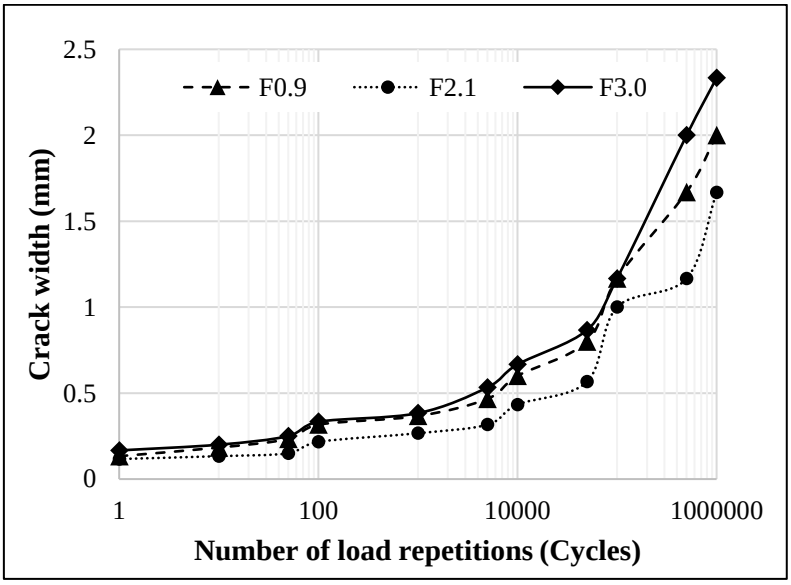

(b)

Figure 5.5 Influence of micro-fiber dosages on crack width for (a) 1/4th GD (b) 1/3rd GD

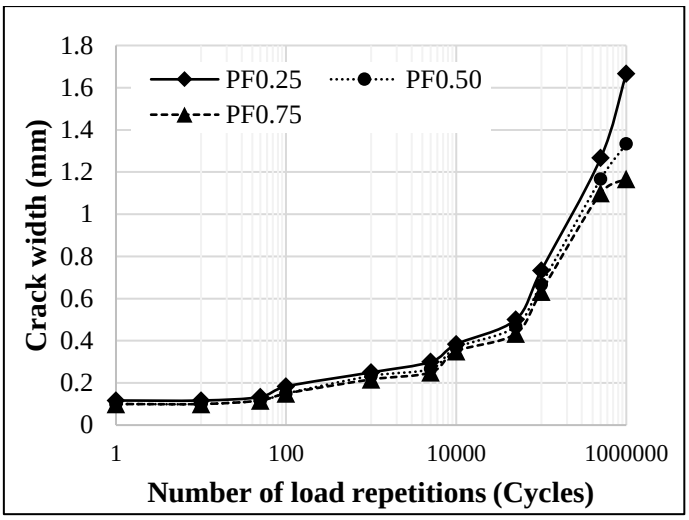

(a)

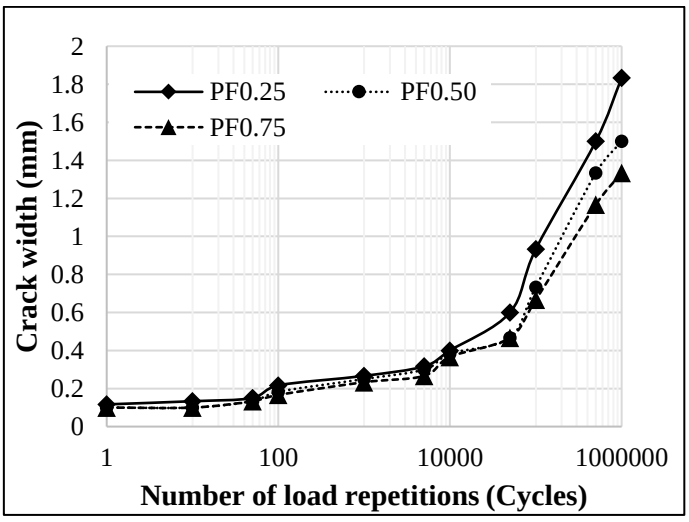

(b)

Figure 5.6 Influence of macro-fiber dosages on crack width for (a) 1/4th GD (b) 1/3rd GD

5.3.5 Influence of fiber dosages and GD on deflection of fiber reinforced PQC beam under repeated loading

The maximum deflections on the loaded side observed in the micro and macro-fiber reinforced PQC mixes were lower in the beams with 1/4th GD. The maximum deflections on the loaded side were found to decrease with the increase in macro-fiber dosages, irrespective of the GD in the case of macro-fiber reinforced PQC beam specimens. However, in the case of micro-fiber reinforced PQC specimens, the maximum deflections on the loaded side decreased with the increase in micro-fiber dosages up to 2.1kg/m^3, beyond which there was an increase in maximum deflection

on the loaded side of the beam. The influence of fiber dosages on the deflections on the loaded and unloaded side of the beam with crack width and the number of load repetitions for a GD are plotted in Figure 5.7 and Figure 5.8 for micro and macro-fiber reinforced PQC mixes, respectively.

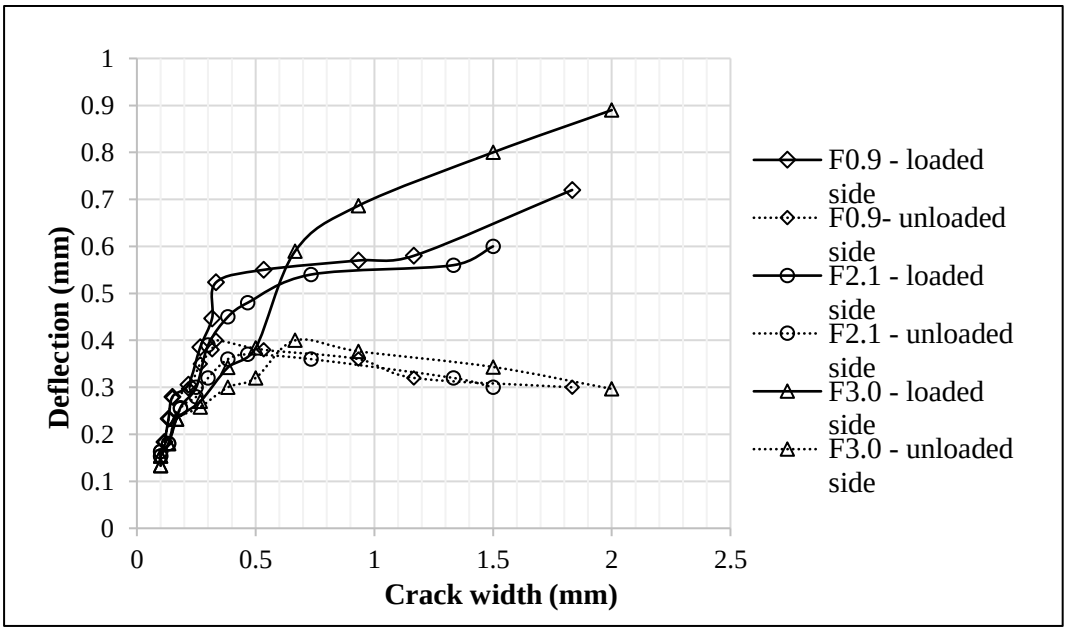

(a)

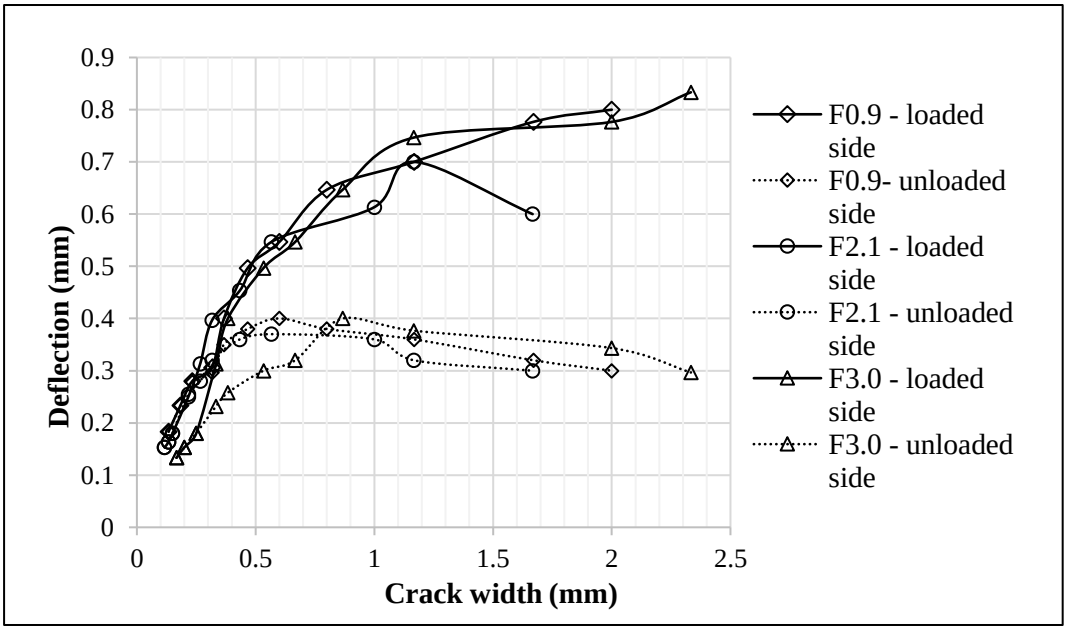

(b)

Figure 5.7 Influence dosage of micro-fiber on deflections on loaded and unloaded sides with crack width for (a) 1/4th GD and (b) 1/3rd GD

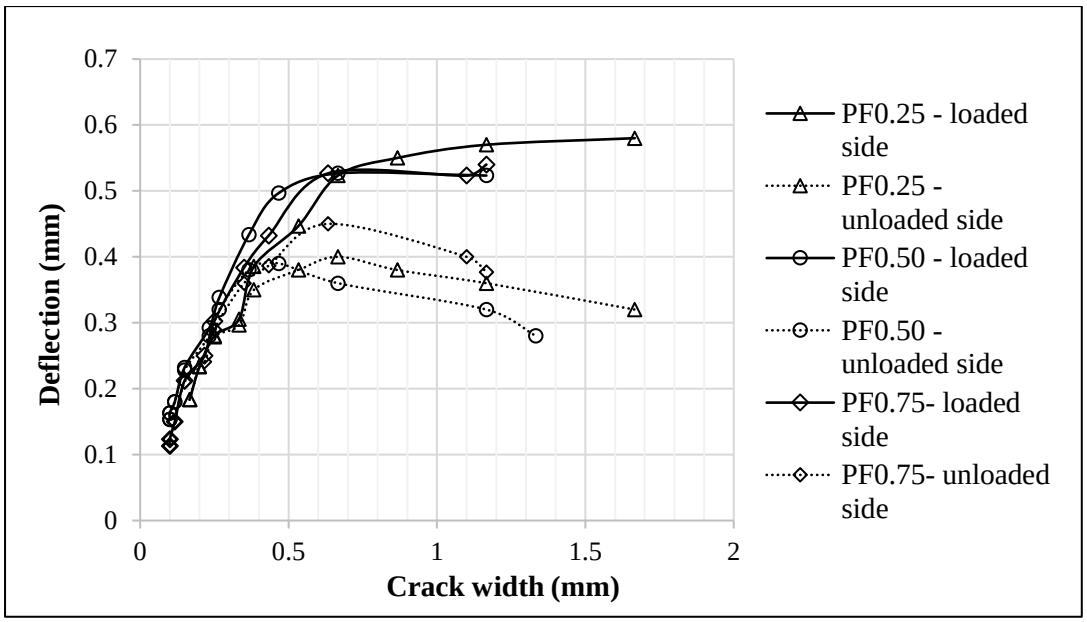

(a)

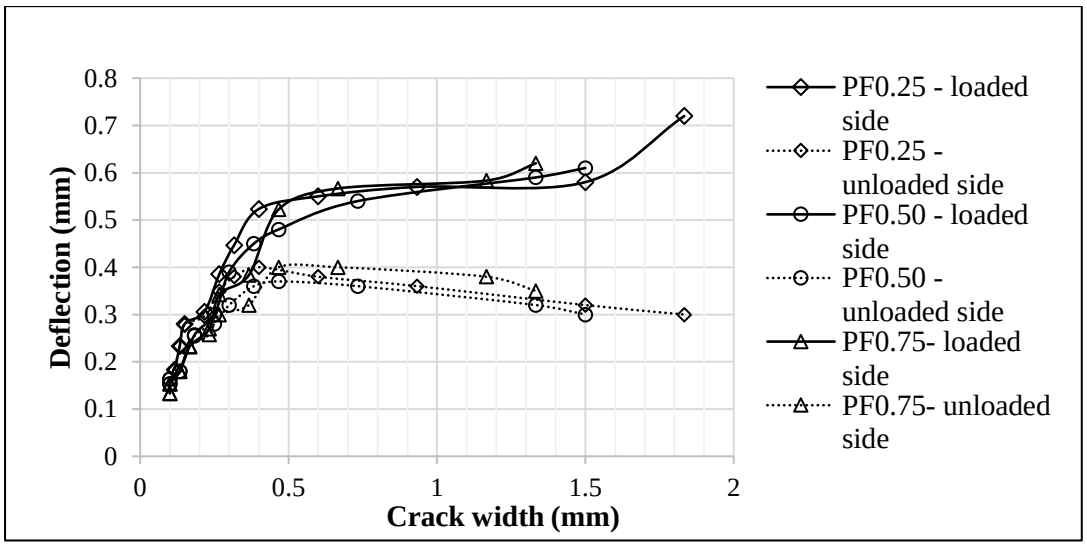

(b)

Figure 5.8 Influence of macro-fiber dosages on deflections on loaded and unloaded sides with crack width for (a) 1/4th GD and (b) 1/3rd GD

5.3.6 Relationship between LTE and relative movement (RM) of joint in fiber reinforced PQC beams

The relationship between LTE and RM for micro and macro-fiber reinforced PQC mixes are plotted in Figure 5.9 and Figure 5.10, respectively. It is observed that irrespective of the GD, type of fiber and the dosage of fibers added to the PQC mix, it is found that there exists an exponential relationship between the LTE and RM. The

slope of the exponential curve determines the performance of aggregate interlocking and the contribution of fibers in load transfer across the joint. The negative slope of the exponential curve is lower for lower GD for a given fiber reinforced PQC mix.

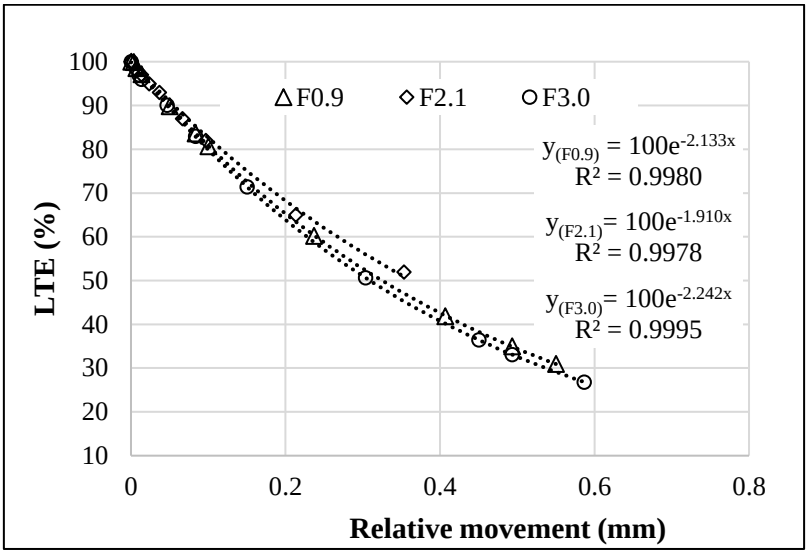

(a)

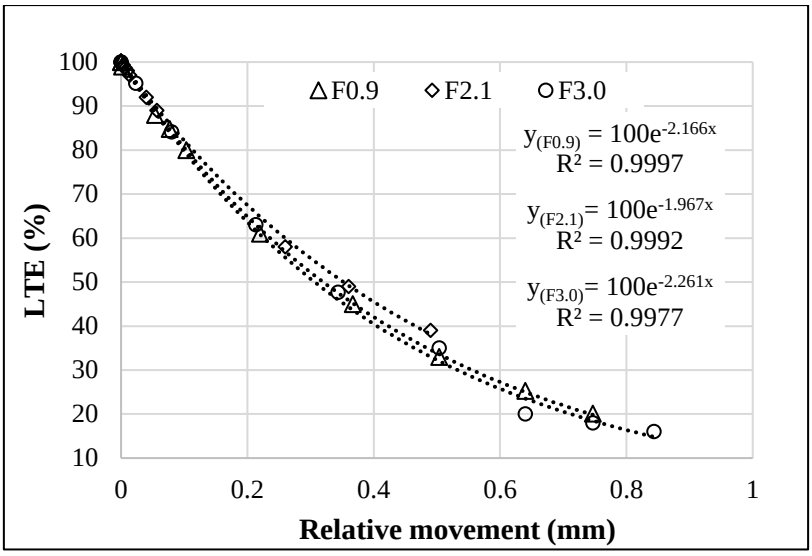

(b)

Figure 5.9 LTE Vs RM of micro-fiber reinforced PQC mix for (a) 1/4th GD (b) 1/3rd GD

From Figure 5.9, it is observed that the negative slope of the exponential curve is minimum for F2.1 mix specimens, which indicates that irrespective of the GD, the fiber dosage of 2.1 kg/m^3 can improve the load transfer performance substantially when compared to the other two dosages in micro-fiber reinforced PQC mix.

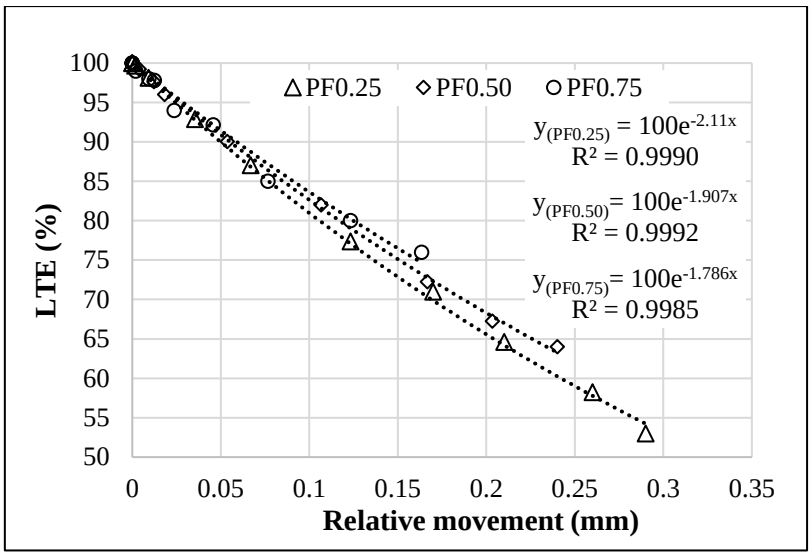

(a)

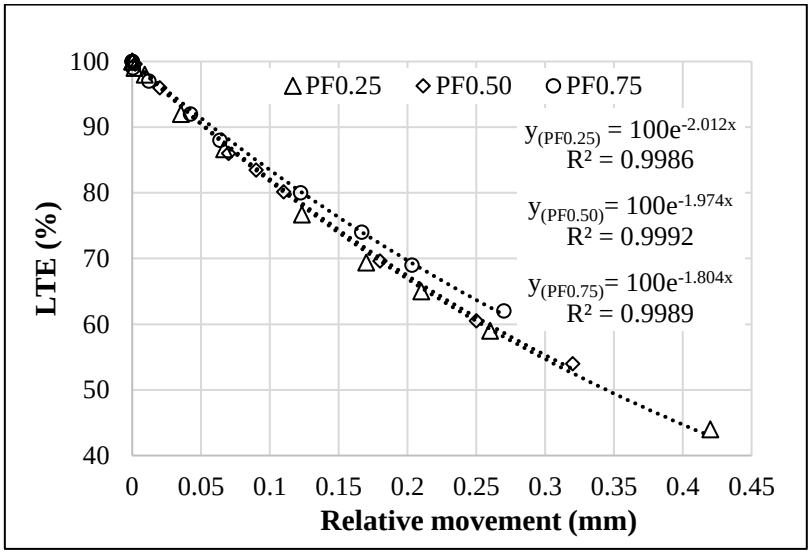

(b)

Figure 5.10 LTE Vs RM of macro-fiber reinforced PQC mix for (a) 1/4th GD (b) 1/3rd GD

From Figure 5.10, it is observed that the negative slope of the exponential curve is in the increasing order of PF0.75, PF0.50 and PF0.25 for macro-fiber reinforced PQC mix. The negative slope is minimum for PF0.75 mix specimens indicates that irrespective of the GD, the fiber dosage of 0.75% macro-fibers can substantially improve the load transfer performance compared to the other two dosages in macro-fiber reinforced PQC mix.

5.4 VALIDATION WITH FIELD FWD DATA

The simulated experimental results are compared with field FWD test results. The FWD study was carried out following the procedure described in section 3.9 of chapter 3. The relative movement is determined from the field FWD test data, and the corresponding LTE is determined using the LTE and RM relationship shown in Figure 5.4 (b) for the A19 PQC mix with 1/3rd GD. The LTE from the field is compared with the obtained LTE from the LTE and RM relationship equation. The comparison of plots is shown in Figure 5.11. A good linear correlation exists between the field LTE and the LTE measured from the simulated experimental small scale test setup.

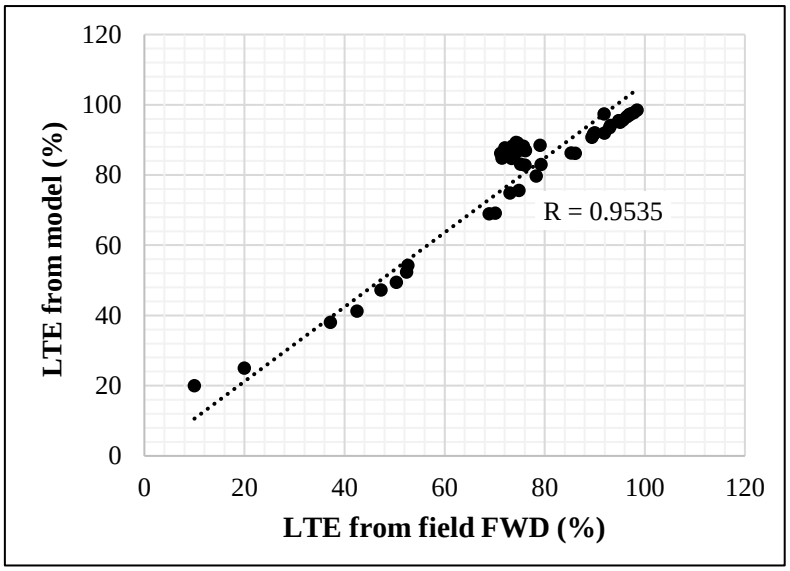

Figure 5.11 LTE from experiment Vs LTE from field FWD

CHAPTER 6

FINITE ELEMENT MODELLING

6.1 GENERAL

The 3-dimensional finite element approach was used to evaluate the influence of NMAS and fiber dosages on the shear strength of the aggregate interlocked joint, and the results were compared with the experimental results.

6.2 THREE-DIMENSIONAL FINITE ELEMENT (FE) MODEL FOR DIRECT SHEAR STRENGTH

The commercial FE software ANSYS Version 18.2 was used to simulate the test results. The concrete cylinders were modelled using the eight noded SOLID185 brick elements with three degrees of freedom. The aggregate interlocking was modelled using the COMBIN14 spring elements. The same elements were also used to model the fibers contributing to aggregate interlocking in fiber reinforced concrete mixtures. The spring stiffness is calculated by multiplying the effective area of aggregate interlocking with the joint stiffness value obtained from the direct shear test. The calculation of spring stiffness is shown in Appendix B.1. The calculated spring stiffness value ranged from 5027 N/mm to 19200 N/mm. The shear strength is computed and are compared with the experimental results.

A total of eighteen cylindrical models were analyzed for the direct shear strength. For these eighteen models, their respective mechanical properties of concrete were used while modelling. Also, the spring stiffness is calculated based on their respective joint stiffness values. The cylindrical concrete specimen with grooved cross-section is modelled as two separate components attached by the spring element representing the aggregate interlocking and crack bridging by the fibers, as shown in Figure 6.1. The fixed portion of the cylinder has a dimension of 150 in diameter and 100 mm in height, and the loaded portion of the cylinder has a dimension of 150 in diameter and 70 mm in height. A gap of 5 mm is created between these two cylindrical components connected by spring to simulate the grooved cross-section.

Different meshing schemes are available in the ANSYS software such as tetrahedral, hexahedral, polyhedral, pyramid, or wedge cells. In the past, many researchers have used the hexahedral meshing scheme for the analysis of concrete pavement joints (Davids et al. 1999; Maitra et al. 2010; Roesler and Wang 2008). Thus, in the present study, a hexahedron meshing scheme was adopted. This particular meshing scheme makes it convenient to attach the springs representing the joint between the two concrete blocks representing the two pavement slabs. The mesh size of 5 × 5 × 5 mm was adopted.

The boundary conditions for the direct shear test 3-D FE model are given below:

- The translation and rotation of the fixed portion of the cylinder was restricted in all directions.
- The rotation was restricted in all directions and translation was restricted in x and z direction for the portion of cylinder on which load is applied. The loaded portion of the cylinder was free to move in y direction.

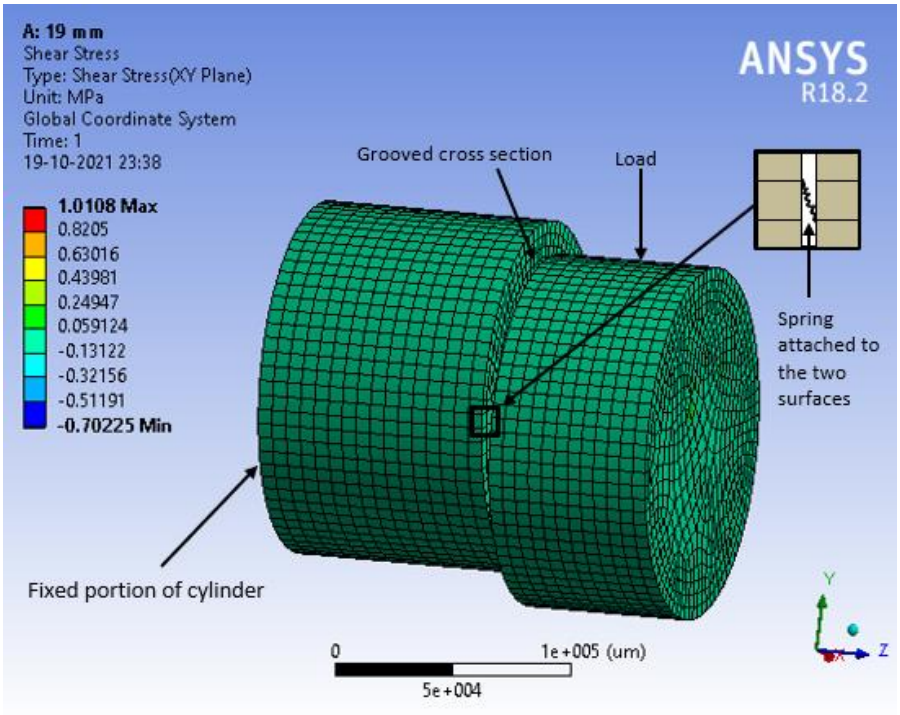

Figure 6.1 Shear stress at the joint for the concrete prepared using 19 mm NMAS with 1/3rd GD

The direct shear strengths from the experimental results and simulation were compared and are shown in Figure 6.2.

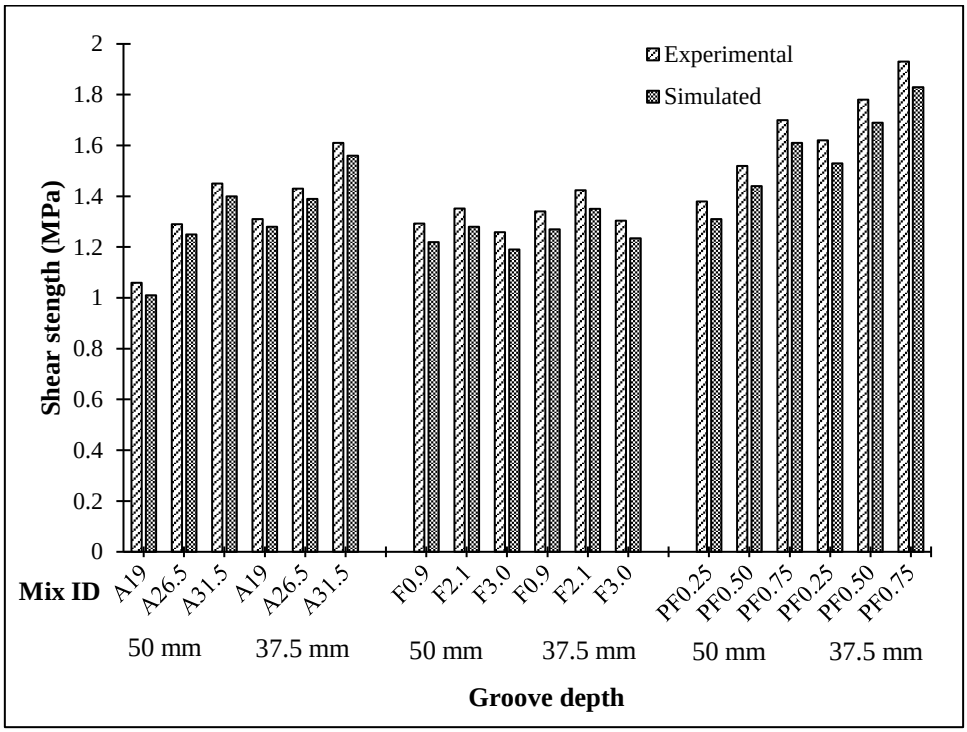

Figure 6.2 Comparison of direct shear strength of joint for different concrete mixes at different GDs.

From Figure 6.2, it can be observed that there are no much significant differences in the experimental and simulation results for all the concrete mixes under study. The error is about less than 5% for all the concrete specimens.

6.3 THREE-DIMESIONAL FINITE ELEMENT (FE) MODEL FOR CRACKED BEAM SPECIMEN SUBJECTED FLEXURE LOADING AT THE JOINT

The laboratory simulated experiment explained in section 3.3.4 of chapter 3 is modelled in ANSYS software. The concrete beam is modelled using SOLID185 eight noded brick elements, and the experimentally obtained mechanical properties were used to create engineering data in the software. The two separated halves of the beam were connected using the spring elements COMBIN14. The underlying rubber pad was modelled as a Winkler foundation with the modulus of subgrade reaction 1.4 MPa/mm. The moment resisting plates were modelled using the same brick elements. The materials properties of structural steel available in the material data library of ANSYS was used.

The boundary conditions for the cracked beam specimen subjected flexure loading at the joint are as follow:

- The translation and rotation of ends of the beam portions were restricted in all directions.
- The rotation was restricted in all directions and translation was restricted in x and z direction for the beams. The beam portions are free to move in y direction. The steel plates were restricted to translation and rotation in all directions.

The beam specimen subjected to flexural loading and deflection measurement on loaded and unloaded slabs of beam prepared using 31.5 mm NMAS with 1/3rd GD at a crack width of 1.5 mm is shown in Figure 6.3.

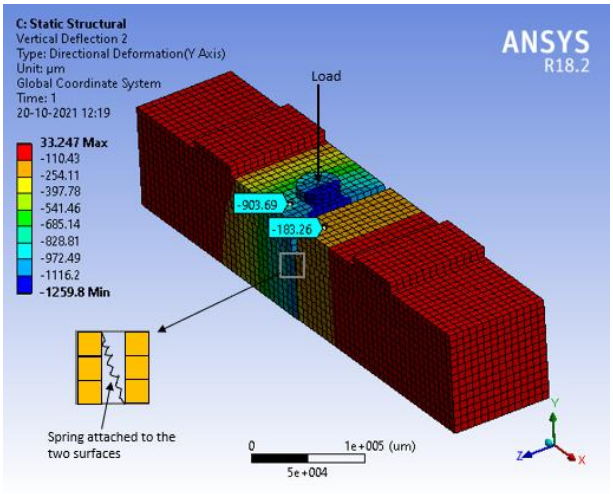

Figure 6.3 Beam specimen subjected to flexural loading and deflection measurement on loaded and unloaded slabs of beam prepared using 31.5 mm NMAS with 1/3rd GD with LTE of 20.28 %

Using the relationship between the non-dimensional joint stiffness AGG* and LTE developed by Ioannides and Korovesis (1990) shown in Figure 2.1 of chapter 2, the joint stiffness is obtained for the different concrete mixes from the experimentally obtained LTEs. The spring stiffness is obtained for various concrete mixes and their corresponding LTEs. The spring stiffness values are in the range of 400 N/mm to 4500000 N/mm. The calculation of spring stiffness is shown in Appendix B.2. Two LTEs were selected for each mix at maximum, and minimum value and the corresponding stiffness was determined. A total of 36 models for different concrete mixes. The experimentally obtained results, LTEs, deflection on the loaded and

unloaded side of the beam are compared with simulated results and is tabulated in Table 6.1.

Table 6.1 Comparison of experimental and simulation results

Groove Depth (mm)	Mix ID	Deflection on loaded side (mm) DL model		Deflection on unloaded side (mm)		Load Transfer Efficiency LTE (%)		Error (%)
		Experi--mental	Model	Experi--mental	Model	Experi--mental	Model	
50 mm	A31.5	0.187	0.204	0.183	0.186	98.21	91.46	6.88
	A31.5	0.910	0.904	0.200	0.183	21.98	20.28	7.73
	A26.5	0.203	0.223	0.197	0.200	96.72	89.70	7.26
	A26.5	0.997	1.088	0.153	0.156	15.38	14.33	6.83
	A19	0.247	0.269	0.237	0.241	95.95	89.36	6.87
	A19	1.040	1.134	0.120	0.121	11.54	10.69	7.33
	F3.0	0.237	0.259	0.223	0.227	94.37	87.70	7.06
	F3.0	1.032	1.135	0.120	0.122	11.63	10.76	7.44
	F2.1	0.223	0.244	0.206	0.210	92.09	86.06	6.54
	F2.1	0.780	0.852	0.310	0.314	39.74	36.85	7.27
	F0.9	0.237	0.260	0.232	0.235	97.89	90.31	7.74
	F0.9	1.010	1.101	0.160	0.163	15.84	14.80	6.60
	PF0.75	0.133	0.145	0.133	0.136	100.00	93.33	6.67
	PF0.75	0.620	0.680	0.350	0.355	56.45	52.17	7.59
	PF0.50	0.153	0.168	0.153	0.155	100.00	92.01	7.99
	PF0.50	0.610	0.671	0.300	0.304	49.18	45.32	7.84
	PF0.25	0.183	0.201	0.183	0.186	100.00	92.52	7.48
	PF0.25	0.720	0.790	0.300	0.305	41.67	38.67	7.18
37.5 mm	A31.5	0.143	0.157	0.143	0.145	100.00	92.28	7.72
	A31.5	0.700	0.764	0.347	0.353	49.52	46.19	6.74
	A26.5	0.187	0.204	0.187	0.189	100.00	92.55	7.45
	A26.5	0.800	0.873	0.250	0.255	31.25	29.21	6.51
	A19	0.210	0.230	0.210	0.214	100.00	93.13	6.87
	A19	0.857	0.935	0.203	0.205	23.74	21.98	7.41
	F3.0	0.227	0.248	0.214	0.218	94.61	87.97	7.02
	F3.0	1.025	1.122	0.121	0.123	11.80	10.93	7.44
	F2.1	0.233	0.256	0.226	0.229	96.71	89.62	7.34
	F2.1	0.785	0.863	0.350	0.357	44.59	41.36	7.25
	F0.9	0.236	0.259	0.236	0.240	100.00	92.41	7.59
	F0.9	1.015	1.111	0.180	0.183	17.73	16.43	7.36
	PF0.75	0.113	0.124	0.113	0.115	100.00	92.61	7.39
	PF0.75	0.540	0.592	0.377	0.381	69.75	64.28	7.85
	PF0.50	0.153	0.168	0.153	0.156	100.00	92.91	7.09
	PF0.50	0.523	0.574	0.320	0.324	61.15	56.41	7.75
	PF0.25	0.183	0.201	0.183	0.185	100.00	92.21	7.79
	PF0.25	0.590	0.648	0.300	0.306	50.85	47.20	7.18

From Table 6.1, it can be noticed that the results from FE simulated model are in good agreement with the experimental results. The error in the LTE measured from the laboratory to the FE model is below 8% in all the mixtures at all the groove depths.

CHAPTER 7

ANN MODEL TO PREDICT JOINT STIFFNESS OF WHITETOPPING USING FALLING WEIGHT DEFLECTOMETER (FWD) DATA

7.1 GENERAL

This chapter aims to improve the existing model in the literature to calculate the joint stiffness of whitetopping pavement directly from the field FWD data. The details of various models that are used to compute the joint stiffness and their applicability to the whitetopping pavement joints are presented in this chapter. The data generation from the limited field FWD studies, improvement to the existing models in the literature, development of ANN model to the analytical models available in the literature and the improved model in the present study and their accuracy along with the validation of proposed ANN model are presented.

7.2 DEFLECTION RESPONSE OF WHITETOPPING PAVEMENT JOINT

The field evaluation was carried out using the KUAB 70 vehicle-mounted falling weight deflectometer shown in Figure 3.16 as per the procedure described in section 3.8.2 of Chapter 3. The deflection values are noted automatically by the computer. Figure 7.1 shows the deflection response of the whitetopping joint having an LTE of 36%. The LTE is computed using equation 2.3 of Chapter 2.

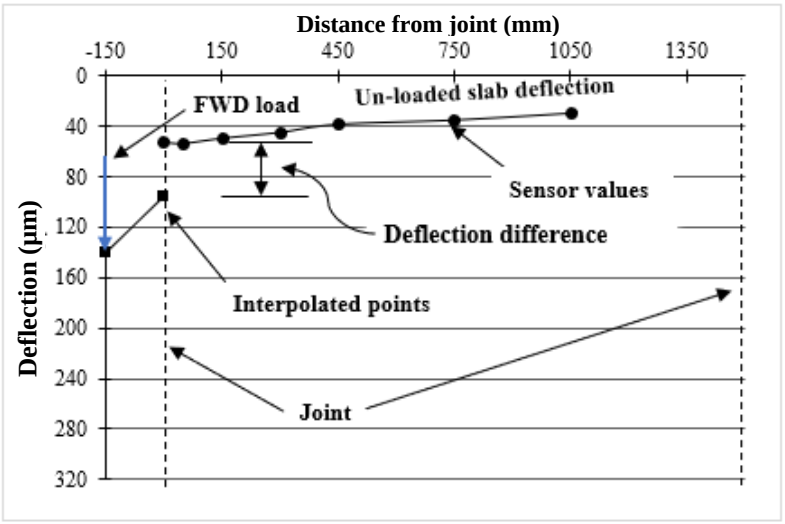

Figure 7.1 Deflection response of whitetopping pavement joint at LTE = 36 %

Since the obtained deflection data was limited, the Latin hypercube sampling (LHS) technique (discussed in the next section) was used to generate more realistic data to improve the existing analytical model.

7.3 LATIN HYPERCUBE SAMPLING (LHS)

Latin Hypercube Sampling (LHS) is a technique used to generate realistic random sampling data. The technique is more reliable than the Monte Carlo sampling method as the LHS sampling has memory. Ceylan et al. (2013) used the LHS technique to generate the input data for global sensitivity analysis of mechanistic performance predictions of jointed plain cement concrete pavements (JPCPs). In another study, Ostadi (2013) used this technique for generating the data for the development of ANN pavement performance prediction models.

In the present study, the LHS technique has been used to generate the deflection data of the loaded and unloaded whitetopping pavement slabs at different loading and pavement temperature conditions. To generate the data using the LHS technique, the lower bounds and upper bounds are estimated for each loading, pavement temperature, and deflections at each sensor from the field FWD data. The lower and upper bound values for each of these are tabulated in Table 7.1. LHS data was generated using MATLAB command *lhsdesign* within the lower and upper bounds.

Table 7.1 Lower bound and upper bound values obtained from FWD tests

Parameter	Lower bound	Upper bound
Load, kN	21.77	45.03
D1, µm	30.17	265.00
D2, µm	28.16	159.94
D3, µm	26.34	142.27
D4, µm	22.74	115.77
D5, µm	18.38	90.00
D6, µm	16.67	77.67
D7, µm	12.46	62.69
Temperature, °C	22.40	42.70

7.4 IMPROVEMENT TO EXISTING BYRUM MODEL

The steps followed to improve the Byrum (2012) model are presented for the field FWD data of the whitetopping pavement. In Byrum (2012) model, the author computed the

geometric parameters of deflection data of concrete pavement. Similarly, in the present study, the geometric parameters are calculated for whitetopping pavement joint deflection data and are shown in Figure 7.2. In Figure 7.2, L_R is the characteristic response length which is obtained by extrapolating the line joining the deflection points on the unloaded slab, and Φ is the response angle.

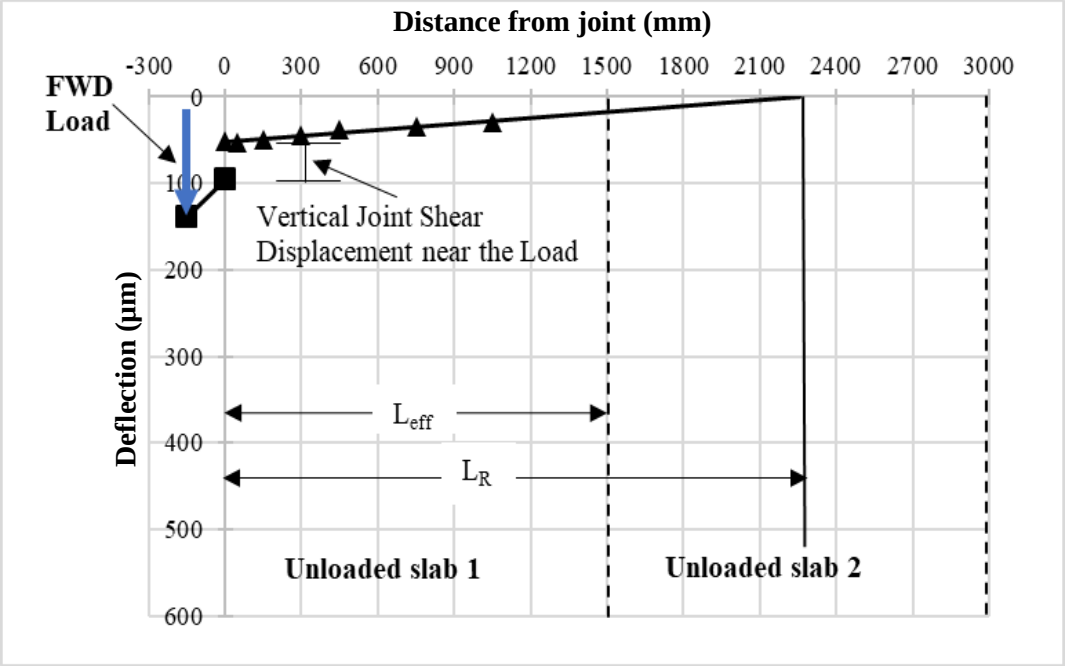

Figure 7.2 Geometric parameters of unloaded whitetopping pavement based on FWD deflection data

It is seen from Figure 7.2 that L_R extends beyond the unloaded slab of the joint for field FWD deflection data of the whitetopping pavement joint. For the joint under consideration, when the L_R of the unloaded slab exceeds its length, the response length cannot be true response length. The L_R of the unloaded slab adjacent to the loaded slab has to be considered for computing the joint stiffness. But, according to Byrum (2012) model, the entire length has to be considered as L_R, which leads to an overestimation of joint stiffness in the case of whitetopping pavement joints. In Figure 7.2, L_{eff} is the response length of the unloaded slab that is adjacent to the loaded slab. If L_R is greater than or equal to the length of the slab, L_{eff} is equal to L_R; otherwise, L_{eff} is equal to the length of the slab. The parameters Φ and L_R are calculated using the following formula.

$$\Phi = tan^{-1}\left[\frac{D_{150} - D_{1050}}{900}\right] \quad (7.1)$$

$$L_R = 1050 + \left[\frac{D_{150}}{\tan\phi}\right] \quad (7.2)$$

The geometric parameters are utilized to develop a linear approximation of the joint relative shear displacement area. The approximated area of the joint relative shear displacement of a whitetopping pavement slab having a length lower than the L_R is shown in Figure 7.3. The unloaded slab deflection has been deducted on both sides so that the unloaded slab deflection is at zero reference. The approximated area shown in Figure 7.3 is for the FWD deflection data of whitetopping pavement. This area is the key factor in determining the amount of shear transfer across the joint.

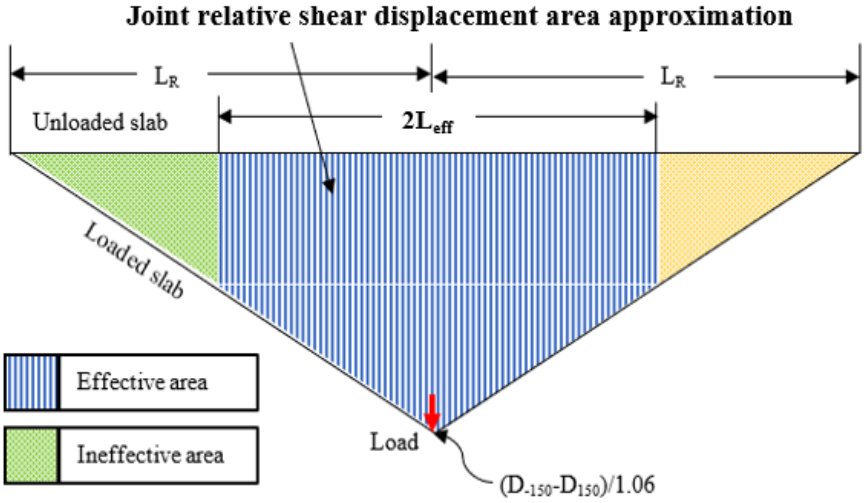

Figure 7.3 Total linearly approximated joint vertical shear displacement area mobilized along joint face (Byrum 2012)

The total joint vertical shear force is calculated by multiplying the joint stiffness (k_j) expressed in N/mm^2 and the integrated area under the deflection difference profile. In case, if the $L_R \leq$ length of the slab, the total joint vertical shear force is calculated by

Total vertical joint shear force = $[L_R \times k_j \times (D_{-150} - D_{150}) \times 1.06]$ (7.3)

when $L_R >$ length of the slab, the total joint vertical shear is calculated by

Total vertical joint shear force =

$$\{2L_{eff} \times D_{Leff} + [0.5 \times (2L_{eff}) \times ((D_{-150} - D_{150}) \times 1.06 - D_{Leff})]\} \times k_j \quad (7.4)$$

where L_{eff} is the effective length equal to the length of the slab, and D_{Leff} is the deflection of the unloaded slab at the unloaded edge and is given by

$$D_{Leff} = [L_{eff} \times [(D_{-150} - D_{150}) \times 1.06 / L_R] \quad (7.5)$$

There are two unknown parameters, one being k_j and the other being the total vertical shear force at the joint, in the equation obtained from geometrical interpretation of

deflection difference profile. In order to solve these unknowns, one more equation is required. The total joint vertical shear force must be equal to the total FWD load applied on the joint. Another equation that can be used to determine the joint vertical shear force is obtained by drawing the free body diagram at the joint. Figure 7.4 shows the free body diagram of the joint loaded on one side of the slab and the deflection of the adjacent slab due to load transfer. Applying the equilibrium equations in the vertical direction, the total FWD load is given by

$$P = (R + R \times LTE) \tag{7.6}$$

Total vertical shear force $= \frac{P \times (LTE)}{(1+LTE)}$ (7.7)

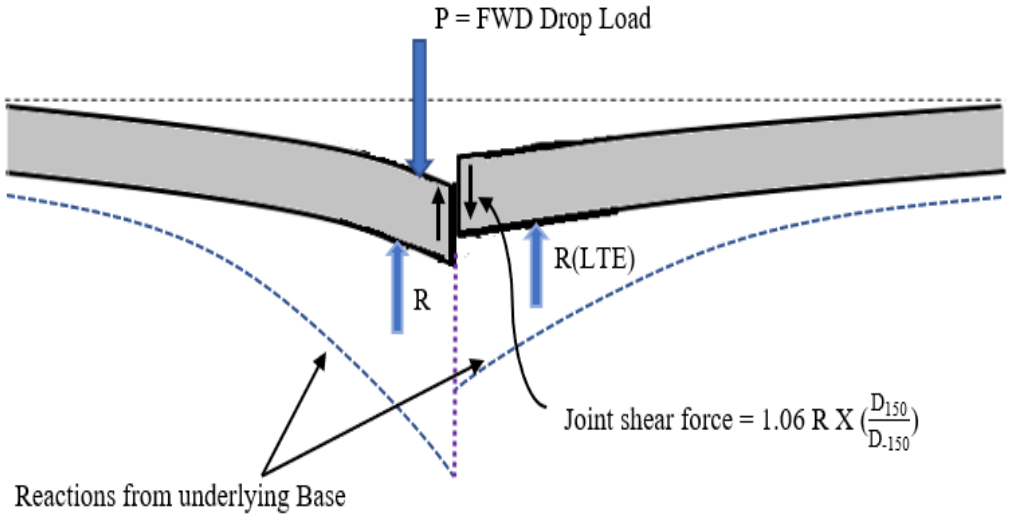

Figure 7.4 Free body diagram of whitetopping pavement at the loaded joint (Byrum 2012)

The equations (7.3) and (7.7) are rearranged and solved to obtain the equation (7.8) for $L_R \leq$ length of the unloaded slab.

$$k_j = \frac{(P \times 10^6) \times (D_{150}^2 - D_{150} D_{1050})}{[(D_{-150}^2 - 1.06 D_{150}^2) \times \lambda \times 900 D_{150}]} \tag{7.8}$$

For the case, $L_R >$ length of the slab, the equations (7.4) and (7.7) are rearranged and solved to obtain equation (7.9).

$$k_j = \frac{(P \times 10^6) \times (1050 D_{150}^2 - 150 D_{150} D_{1050})}{(D_{-150}^2 - 1.06 D_{150}^2) \times \lambda \times L_{eff} [L_{eff} \times (D_{150} - D_{1050}) + (1050 D_{150} - 150 D_{1050})]} \tag{7.9}$$

where $\lambda = \frac{deflection\ of\ loaded\ slab}{average\ deflection\ on\ unloaded\ slab}$

From the field FWD data of whitetopping pavement joints, the geometric parameters were determined, and it was found that the response length was always greater than the length of the whitetopping pavement slab. Thus, equation (7.9) can be used as a modified Byrum model to determine the joint shear stiffness directly from the field FWD data for whitetopping concrete pavement joints.

7.5 DEVELOPMENT OF ANN PREDICTION MODEL FOR ANALYTICAL MODELS AVAILABLE IN THE LITERATURE AND IMPROVED BYRUM MODEL

The ANN architecture generally comprises of three layers: input layer, hidden layer and output layer. The architecture used in this study is 9-10-1-1 and is shown in Figure 7.5. In this study, nine input parameters are used. The nine input parameters are D1, D2, D3, D4, D5, D6, D7 (defelections measured by seven senors), the load applied by the FWD and the temperature at the time of testing. Since the data set was small, less training data resulted in the higher variance in performance of ANN model during training. The less testing and validation data resulted in the higher variance in performance of ANN model during testing and validation. Thus, an optimal split of 70 % for training, 15% for testing and 15% for validation was used in the development of ANN model in the present study. Also, most of the researchers have obtained optimum results using the same split of data (Alatoom and Al-Suleiman (Obaidat) 2021; Fakhri and Shahni Dezfoulian 2019; Hossain et al. 2019; Kallannavar et al. 2021; Nivedya and Mallick 2020b). For the development of the ANN model, ten neurons are used in the hidden layer, and one neuron is used in the output layer. Bayesian regularization technique is used for training the network in all the ANN prediction models as this technique provides better performance than other training techniques (Albatayneh et al. 2020; Heravi and Eslamdoost 2015).

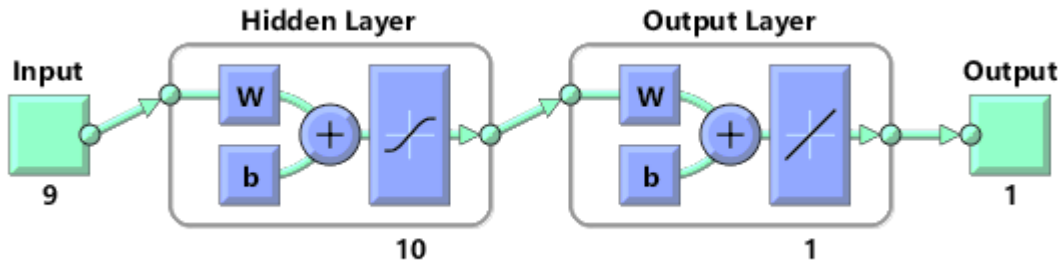

Figure 7.5 ANN architecture used in the present study

In this study, the ANN prediction models for the three most popular analytical models have been developed and presented along with the ANN prediction model for the improved Byrum model. The three analytical models used in the present work are proposed by Ioannides and Korovesis (1990), Maitra et al. (2010) and Byrum (2012).

7.5.1 ANN prediction model for Ioannides and Korovesis (1990) analytical model

Ioannides and Korovesis (1990) proposed an analytical model that provides the relationship between LTE and joint stiffness (AGG) using FE and dimension analysis techniques. The model can be used to back-calculate the joint stiffness of conventional concrete pavement and is given in equation (7.10).

$$AGG = kl\left(\frac{\frac{l}{LTE} - 0.01}{0.012}\right)^{-1.17786} \tag{7.10}$$

where AGG is the joint stiffness in psi;

k is the effective modulus of subgrade reaction in psi/inch;

l is the radius of relative stiffness in inches;

LTE is the load transfer efficiency in percentage.

Using equation 2.3 of Chapter 2, LTE corresponding to each LHS sample was computed. The joint stiffness is calculated for each sample using the Ioannides and Korovesis (1990) model. The joint stiffness predicted using the Ioannides and Korovesis ANN model and the corresponding joint stiffness computed by the analytical model are plotted as shown in Figure 7.6.

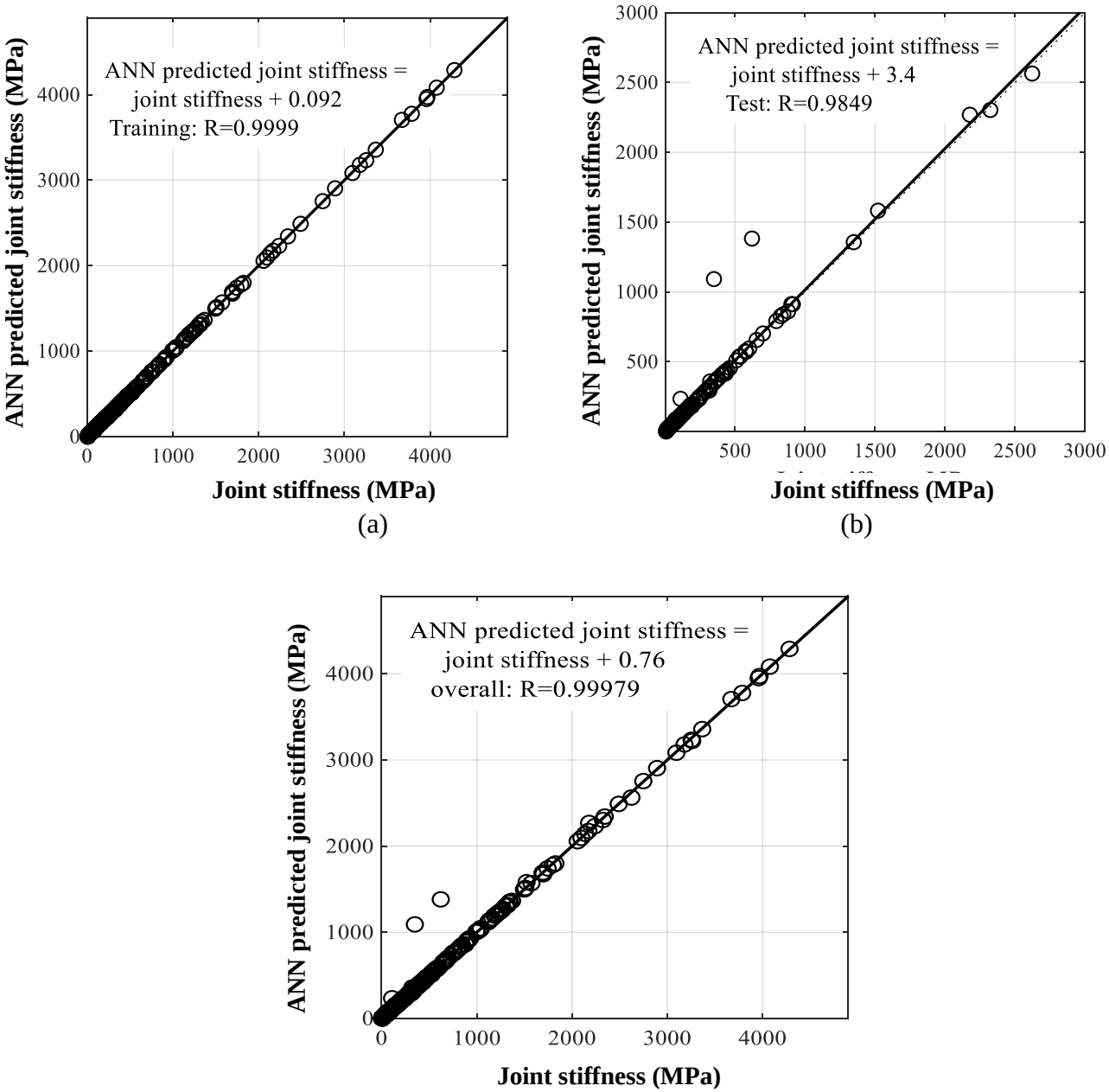

Figure 7.6 ANN predicted joint stiffness Vs joint stiffness computed by Ioannides and Korovesis (1990) analytical model (a) Training, (b) Testing and (c) Overall

7.5.2 ANN prediction model for Maitra et al. (2010) analytical model

Maitra et al. (2010) introduced a new parameter, modulus of joint stiffness (K_j), to characterize the efficiency of the aggregate interlocked joints. The authors developed a model based on the experimental studies conducted by Brink (2003) using the FE method. The parameter depends mainly on the size of the aggregate used in the pavement and joint opening. The joint stiffness can be obtained by multiplying the

length/width of the slab depending on the direction of the joint. The equation used for calculating K_j is as follow

$$K_j = 0.4568 \times x^{-0.7493} \times exp\,(0.0643 \times IR) \quad (7.11)$$

where K_j is the modulus of joint stiffness in MPa/mm; the joint stiffness is obtained by multiplying the thickness of the concrete slab; x = crack or joint width in mm; and IR = interlocking ratio (IR = agg/x; agg = nominal size of 20% of the biggest particles in the concrete mix in mm).

Using equation 2.3 of Chapter 2, LTE corresponding to each LHS sample was computed. The joint stiffness is calculated for each sample using the equation (7.11). The joint stiffness predicted using the Maitra et al. ANN model and the corresponding joint stiffness computed by the analytical model are plotted as shown in Figure 7.7.

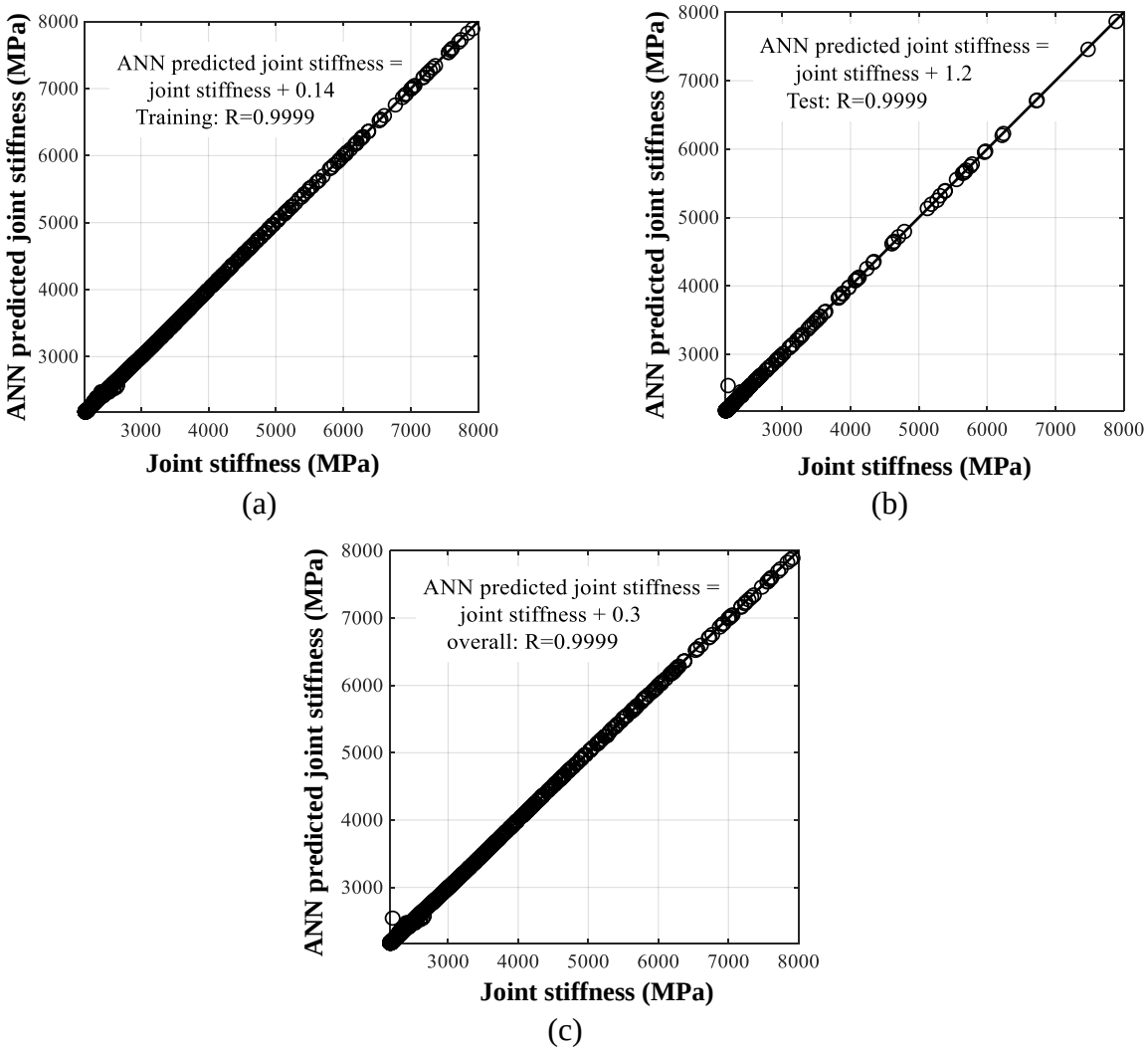

Figure 7.7 ANN predicted joint stiffness Vs joint stiffness computed by Maitra et al. (2010) analytical model (a) Training, (b) Testing and (c) Overall

7.5.3 ANN prediction model for Byrum (2012) analytical model

Byrum (2012) developed a joint stiffness model for aggregate interlocked concrete pavement joints based on the FWD data. The model is shown in equation (7.12)

$$k_j = \frac{P \times LTE}{\left[(1+LTE) \times (D_{-6}-D_6) \times (1+i\%) \times \Omega \times \left(\frac{66+D_{66}}{D_6-D_{66}}\right)\right]} \quad (7.12)$$

where k_j is the joint stiffness in psi;

P is the FWD load in pounds;

LTE is the load transfer efficiency in percentage;

D_{-6} is the deflection in mils on loaded slab 6 in. away from the joint;

D_6 is the deflection in mils on unloaded slab 6 in. away from the joint;

i is the constant;

Ω is the unknown function;

D_{66} is the deflection in mils on unloaded slab 66 in. away from the joint.

LTE corresponding to each LHS sample was computed using equation (2.3) of Chapter 2. The joint stiffness is calculated for each sample using the equation (7.12). The joint stiffness predicted using the Byrum ANN model and the corresponding joint stiffness computed by the analytical model are plotted as shown in Figure 7.8.

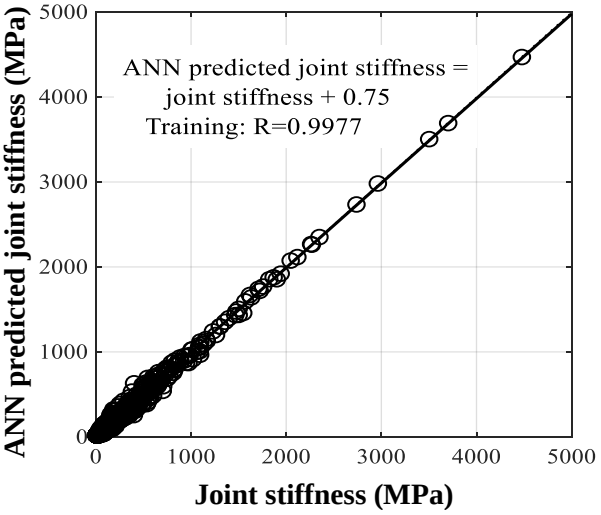

(a)

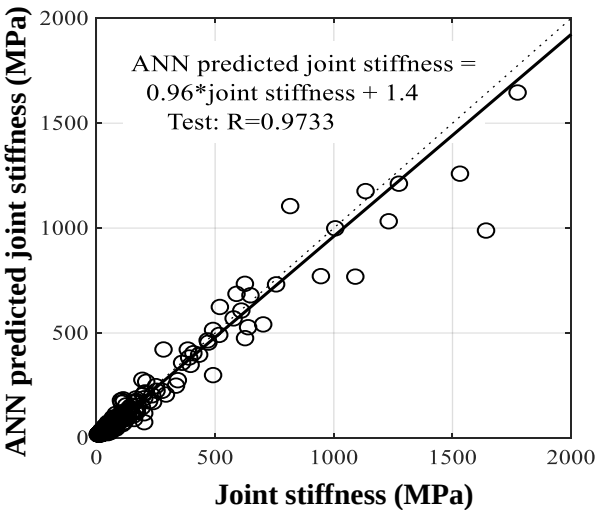

(b)

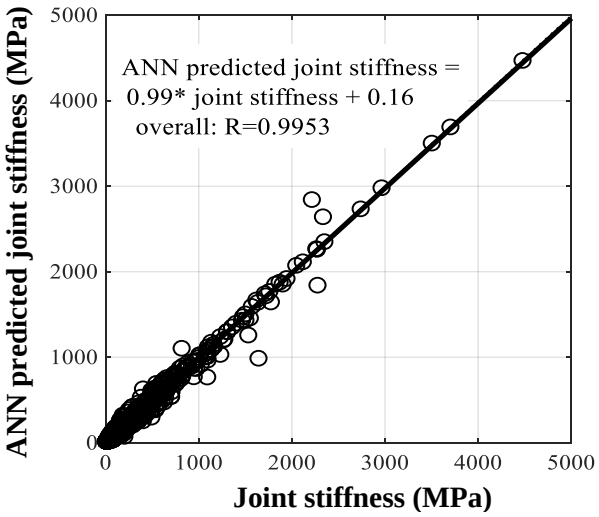

(c)

Figure 7.8 ANN predicted joint stiffness Vs joint stiffness computed by Byrum (2012) analytical model (a) Training, (b) Testing and (c) Overall

7.5.4 ANN prediction model for improved Byrum model

The joint stiffness values computed using equation (7.9) were used as target values for developing the ANN prediction model. The joint stiffness predicted using the improved Byrum ANN model and the corresponding joint stiffness computed by the analytical model is plotted as shown in Figure 7.9.

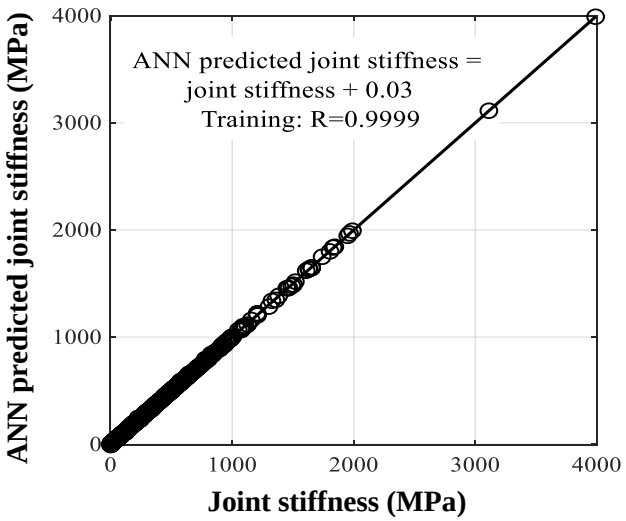

(a)

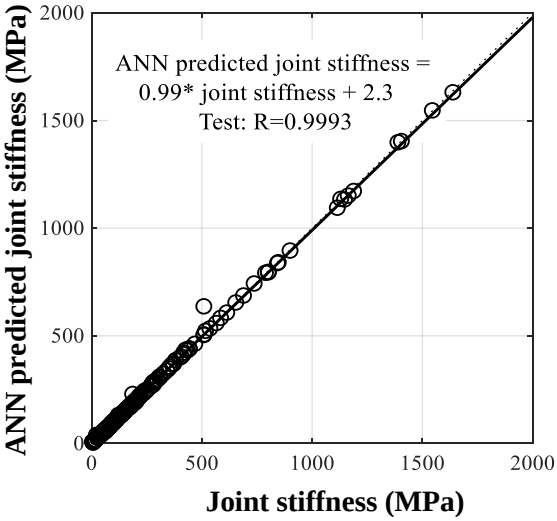

(b)

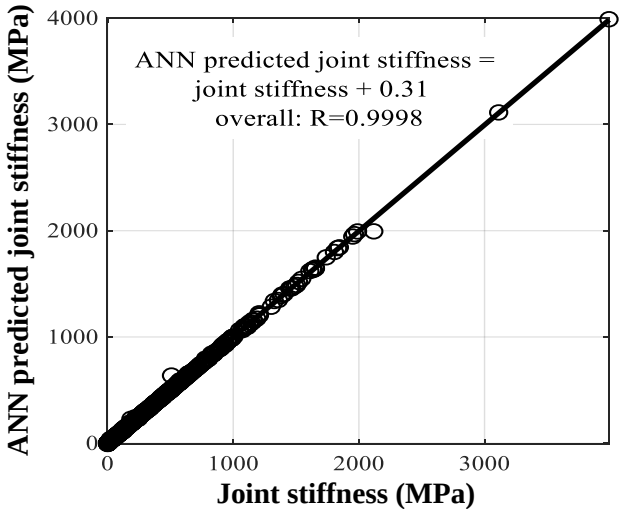

(c)

Figure 7.9 ANN predicted joint stiffness Vs joint stiffness computed by improved Byrum model (a) Training, (b) Testing and (c) Overall

The mean square error (MSE) of each model is computed using equation (14). The comparison of MSE of the models during the training, testing and overall is tabulated in Table 7.2.

$$MSE = \frac{1}{n}\sum_{i=1}^{n}(y_i - y_i^1)^2 \tag{7.13}$$

where, y_i is the predicted joint stiffness of individual ANN models;

y_i^1 is the calculated joint stiffness from the corresponding analytical models;

n is the number of samples.

Table 7.2 MSE of different ANN prediction models developed using analytical models

ANN prediction models developed using analytical model	MSE		
	Training	Testing	Overall
Ioannides and Korovesis (1990)	13.46	160.05	24.23
Maitra et al. (2010)	47.17	202.03	70.38
Byrum (2012)	6.88	81.55	17.06
Improved Byrum model (2021)	5.67	30.94	11.33

From Table 7.2, it can be noticed that the MSE of the ANN model is lower for the one developed using the improved Byrum model in all three cases (training, testing and overall). The MSE is highest for the ANN model developed using Maitra et al. analytical model compared to the other models for all three cases. The reason for this

could be that this model was developed solely based on numerical studies. It is seen from the plots Figure 7.6 to 7.9 that the ANN model developed using Ioannides and Korovesis (1990) model, Maitra et al. (2010) model, and Byrum (2012) model overpredicted the joint stiffness of whitetopping pavements when compared to the ANN model developed using the improved Byrum model. The LTE is compared with field experiments using the joint stiffness computed from the ANN model created from the proposed analytical model as an input parameter in the FE model for further validation.

7.6 3-D FINITE ELEMENT (FE) MODEL AND ACCURACY OF ANN PREDICTION MODEL

The joint stiffness is computed from the improved Byrum ANN prediction model. The joint stiffness is used as an input in the 3-D Finite Element (FE) model to compare the LTE from the FE model and field studies. The whitetopping pavement (1.5 m × 1.5 m each slab) is modelled in the commercially available 3-D finite element software ANSYS. The details of the FE model are tabulated in Table 7.3.

Table 7.3 Details of 3-D FE whitetopping pavement model

Layer	Elements used to model	Material properties and Dimensions
Layers below bituminous concrete	Winkler foundation	Thickness = 500 mm Modulus of Subgrade reaction (k) = 0.03 MPa/mm
Bituminous concrete layer	Eight noded brick elements	Thickness = 190 mm Effective Modulus of Subgrade reaction (k) = 0.09 MPa/mm
Whitetopping concrete	Eight noded brick elements	Thickness = 200 mm Compressive strength of concrete, f_{ck} = 40 MPa Modulus of elasticity, E = 30000 MPa
Aggregate joint	Spring elements	Spring stiffness, N/mm (from improved Byrum ANN prediction model for different LTEs)

The whitetopping concrete slab and underlying bituminous layer were modelled as linear elastic and isotropic materials. The eight noded brick elements (SOLID 185) were used to model both layers. The subgrade below the bituminous layer was modelled as a Winkler foundation using the linear spring elements (COMBIN 14). The aggregate

interlock between the whitetopping concrete slab was modelled using two series of spring elements (COMBIN 14). A total number of 17572 elements were used for meshing the entire model. The ANSYS FE model is shown in Figure 7.10.

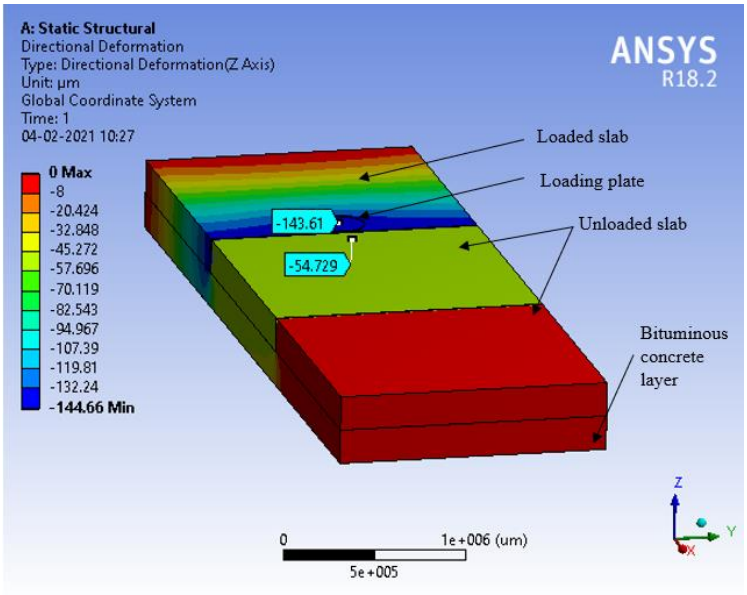

Figure 7.10 3-D FE model of whitetopping pavement

The spring stiffness was calculated by multiplying the width of the slab with the joint stiffness obtained from the improved Byrum ANN prediction model. The 3-D FE simulation was carried out to validate the improved Byrum ANN prediction model by comparing the LTEs obtained from the simulation and the field data.

The accuracy of the improved Byrum ANN prediction model is determined by calculating the root mean square error (RMSE), mean absolute error (MAE) and mean absolute percentage error (MAPE), also called mean absolute percentage deviation (MAPD). Many authors have used these statistical parameters effectively and efficiently to assess the performance of the ANN models developed for predicting the cracks on flexible pavements (Inkoom et al. 2019), IRI of flexible pavements (Hossain et al. 2019), and predicting the compressive strengths of high-performance concrete (Chou et al. 2014), geopolymer concrete (Nazari and Sanjayan 2015), FRP-confined concrete circular columns (Cascardi et al. 2017) and shear strength of reinforced concrete beams (Chou et al. 2020). The statistical error parameters MAE, RMSE and MAPE are calculated using equations (7.14), (7.15) and (7.16), respectively.

$$MAE = \frac{\sum_{j=1}^{n} \left| y_j - y_j^1 \right|}{n} \tag{7.14}$$

$$RMSE = \sqrt{\frac{\sum_{j=1}^{n} \left(y_j - y_j^1 \right)^2}{n}} \tag{7.15}$$

$$\text{MAPE} = \frac{100\,\%}{n} \sum_{j=1}^{n} \left| \frac{y_j - y_j^1}{y_j} \right| \tag{7.16}$$

where, y_j is the LTE computed from the 3-D FE model;

y_j^1 is the LTE computed from field FWD data;

n is the total number of field observation samples.

The MAE, RMSE and MAPE are found to be 0.78, 1.01 and 1.13, respectively.

CHAPTER 8

SUMMARY AND CONCLUSIONS

8.1 SUMMARY

8.1.1 Shear parameters of aggregate interlocked joints

In the present study, a simple and reliable test methodology is proposed to evaluate the performance of aggregate interlocked joints in plain, micro-fiber reinforced, and macro-fiber reinforced PQC mix cylindrical specimens. It is found that the test methodology used in the present study can be effectively used to evaluate the aggregate interlocking in terms of shear strength (τ), joint shear stiffness (K), and mode II fracture energy (G_{IIF}) of concrete mixes at the grooved cross-section under static shear loading. Also, the same test apparatus can be used for evaluating the shear fatigue performance of aggregate interlocking in these PQC mixes. The obtained shear fatigue life cycle data of these mixtures at different stress levels is used for statistical analysis. The findings from this test are summarized below.

- The static shear strength (τ), joint shear stiffness (K), and mode II fracture energy (G_{IIF}) were found to be increasing with an increase in the NMAS and fiber dosages used in the plain and macro-fiber reinforced PQC mixes, respectively, irrespective of groove depths under study.
- There exists a linear relationship between joint shear stiffness (K) and mode II fracture energy (G_{IIF}) for all plain and macro-fiber reinforced PQC mixes at both the groove depths under study. However, a poor linear relationship exists in micro-fiber reinforced PQC mixtures.
- The fatigue performance of aggregate interlocked joints improves with an increase in NMAS and macro-fiber dosages. However, in the case of micro-fiber reinforced PQC mix specimens, the performance increases up to 2.1kg/m^3, beyond which further addition of micro-fiber deteriorates the aggregate interlocked joint performance.
- The failure probability against fatigue life plots fits well with the three-parameter Weibull distribution for all the PQC mixtures when compared to the

lognormal distribution. This has been demonstrated using the Anderson-Darling (AD) statistic test.

- The 3-parameter Weibull shape parameter (β) is greater than one for all the concrete mixtures, indicating that all PQC specimens fail by wearing action under shear fatigue loading.
- The PDF and CDF plots of 3-parameter Weibull illustrate that the useful life of plain PQC increases with an increase in NMAS, and the useful life of macro-fiber reinforced PQC increases with an increase in macro-fiber dosages under shear fatigue loading.

8.1.2 Aggregate interlocked joint performance in terms of LTE

A small-scale test setup is developed to simulate the aggregate interlocked joint in concrete pavements in the present study. The developed small-scale test setup was used to evaluate the performance of aggregate interlocked joints in plain, micro-fiber reinforced, and macro-fiber reinforced PQC mix beam specimens in terms of LTE. The influence of NMAS and fiber dosages on PQC beam specimens at two GDs were studied. The findings from this test are summarized below.

- The crack width increased with an increase in the number of load repetitions irrespective of the type of PQC mix and GD. The increase in crack width was gradual for plain PQC specimens up to ten thousand load repetition cycles. However, for the fiber reinforced PQC specimens, the increase in crack width was gradual up to twenty thousand load repetition cycles.
- The maximum deflection on the loaded side of the beam is highest for A19, F3.0, and PF0.25 mix among the plain, micro and macro-fiber reinforced PQC mixtures, respectively.
- The relationship between the LTE and RM was determined for each PQC mixture, which follows an exponential curve. The slope of the exponential curve determines the extent of load transfer across the joint, thus quantifying the aggregate interlocking at the joint. Based on the slope values, it is found that the performance of the undowelled joint is in the increasing order of A19, A26.5 and A31.5 for plain PQC mix, F3.1, F0.9, and F2.1 for micro-fiber reinforced

PQC mix and PF0.25, PF0.50 and PF0.75 for macro-fiber reinforced PQC mix, respectively.

- The field test results of LTE of whitetopping pavement joints are compared with LTE obtained from the relationship between LTE and RM of the A19 plain PQC mix with a GD of 1/3rd of the depth of the beam. The comparison of LTE values indicates that the proposed small-scale test setup can be effectively used to evaluate the performance of aggregate interlocked joints.

Overall, from the mentioned two tests, it was found that the use of 31.5 NMAS and macro-fiber dosage of 0.75% by volume of PQC mix can significantly improve the performance of undowelled joints in short-panelled concrete pavements. Also, the use of micro-fiber dosages of 2.1 kg/m^3 can improve the undowelled joint performance in Ultrathin Whitetopping (UTW) pavements.

8.1.3 3-D Finite element model

The ANSYS software was used to model the two test methodologies proposed in the present study. Following are the findings of the 3-D FE analysis.

- The static shear strength values from the simulated 3-D FE model are in good agreement with the obtained experimental static direct shear test results.
- The small-scale test setup was modelled in ANSYS, and the LTE values from the model are compared with the experimental results.

8.1.4 ANN model to predict joint shear stiffness of whitetopping pavement joints

In the present study, an improvement to the existing analytical model is presented that can be used to compute the joint stiffness of whitetopping pavements directly from the FWD deflection data. ANN models have been developed using the Bayesian regularization technique for the proposed and previously available analytical models in the literature. The joint stiffness calculated from the ANN model developed from the proposed analytical model is used as an input parameter in the FE model. LTE is compared with the field studies. The following observations are made for the developed ANN model.

- It was found that the ANN model developed from the proposed analytical model can predict the joint stiffness of whitetopping pavement accurately when compared to the ANN model developed from other analytical models available in the literature.
- ANN prediction model proposed in this study is simple, efficient and accurate enough to calculate the joint stiffness directly from FWD deflection data. In addition, the ANN model saves the cost of conducting large scale field studies and saves computational time.

8.2 CONCLUSIONS

Based on the research work carried out, the following conclusions are made:

1. The larger NMAS (31.5 mm) provides better aggregate interlocking in plain PQC mix irrespective of the groove depth, and the useful life of plain PQC specimens increases with the increase in NMAS under shear fatigue loading. This is due to the greater area of contact for aggregate interlocking across the grooved cross-section.
2. The use of micro polypropylene fibers in the PQC mix significantly improves the aggregate interlocked joint performance under both static and cyclic shear loading for a dosage of 2.1 kg/m^3. Further increase in fiber dosage has detrimental effects on joint performance due to entrapment of voids at the cross-section. The use of macro polypropylene fibers in the PQC mix significantly improved the performance of aggregate interlocked joints under both static and cyclic loading with an increase in the dosages. This is due to the larger number of fibers participating in load transfer across the grooved cross-section, improving the aggregate interlocking.
3. The LTE and crack width results from the developed small scale test setup also indicate that the aggregate interlocking performance improves for larger NMAS and lower groove depth. From the present study, it is concluded that the aggregate interlocked joint performance can be improved with the addition of 2.1 kg/m^3 of micro-fiber and 0.75% of macro polypropylene fiber to the PQC mix.

4. The results from the 3-D finite element model are in good agreement with the experimental results for both the cylindrical specimens and simulated beam specimens prepared using plain and fiber reinforced concrete mixes.
5. The comparison of the field FWD results with the experimental results obtained from the simulated test setup indicates that the proposed small-scale test setup can be effectively used to evaluate the aggregate interlocked joint performance in terms of LTE.

Further, it is concluded that the improved Byrum model presented in this study can be used to compute the joint stiffness directly from FWD deflection data. The statistical parameters indicate that the difference in LTE of the field FWD data and the LTE computed from the 3-D FE model is minimal. It is concluded that the proposed improved Byrum ANN model is simple, efficient and accurate enough to estimate the joint stiffness directly from FWD deflection data.

The limitations of the present study are that the comparison of test results of the proposed small-scale test setup was limited only to the pavement constructed using 19 mm NMAS, the experiments carried out in the present study were not temperature controlled, and the FE analysis carried out was limited only to static loading.

8.3 SCOPE FOR FUTURE RESEARCH WORK

Following are the scope for future research work:

- The present study can be extended to include the influence of temperature variation parameters on the performance of the aggregate interlocked joints in concrete pavements as the pavements are subjected to both temperature and traffic loads.
- There is a scope to conduct extensive field studies on whitetopping pavements constructed using macro-fiber reinforced PQC mix to validate small-scale test setup results for these PQC mixtures.
- The FE model can be improved to model the degradation of aggregate interlocked joints under shear fatigue loading.
- There is a scope to use different optimization techniques to analyse and predict the joint stiffness of aggregate interlocked joints of whitetopping pavement constructed using different PQC mixtures.

REFERENCES

Abdi Moghadam, M., and Izadifard, R. (2019). "Evaluation of shear strength of plain and steel fibrous concrete at high temperatures." *Construction and Building Materials*, Elsevier Ltd, 215, 207–216.

Abellán García, J., Fernández Gómez, J., and Torres Castellanos, N. (2020). "Properties prediction of environmentally friendly ultra-high-performance concrete using artificial neural networks." *European Journal of Environmental and Civil Engineering*, Taylor & Francis, 0(0), 1–25.

Abou El-Mal, H. S. S., Sherbini, A. S., and Sallam, H. E. M. (2015). "Mode II Fracture Toughness of Hybrid FRCs." *International Journal of Concrete Structures and Materials*, Korea Concrete Institute, 9(4), 475–486.

Al-Oraimi, S. K., Taha, R., and Hassan, H. F. (2006). "The effect of the mineralogy of coarse aggregate on the mechanical properties of high-strength concrete." *Construction and Building Materials*, 20(7), 499–503.

Alatoom, Y. I., and Al-Suleiman (Obaidat), T. I. (2021). "Development of pavement roughness models using Artificial Neural Network (ANN)." *International Journal of Pavement Engineering*, Taylor & Francis, 0(0), 1–16.

Albatayneh, O., Moomen, M., Farid, A., and Ksaibati, K. (2020). "Complementary Modeling of Gravel Road Traffic-Generated Dust Levels Using Bayesian Regularization Feedforward Neural Networks and Binary Probit Regression." *International Journal of Pavement Research and Technology*, 13(3), 255–262.

Alberti, M. G., Enfedaque, A., and Gálvez, J. C. (2014). "On the mechanical properties and fracture behavior of polyolefin fiber-reinforced self-compacting concrete." *Construction and Building Materials*, Elsevier Ltd, 55, 274–288.

Appa Rao, G., and Sreenivasa Rao, A. (2009). "Toughness indices of steel fiber reinforced concrete under mode II loading." *Materials and Structures*, 42(9), 1173–1184.

Arnold, S., Fleming, P., Austin, S., and Robins, P. (2005). "A test method and deterioration model for joints and cracks in concrete slabs." *Cement and concrete research*, *35*(12), 2371-2383.

Asteris, P. G., Kolovos, K. G., Douvika, M. G., and Roinos, K. (2016). "Prediction of self-compacting concrete strength using artificial neural networks." *European Journal of Environmental and Civil Engineering*, Taylor & Francis, 20, s102–s122.

Aure, T. W., and Ioannides, A. M. (2015). “Fracture analysis of aggregate interlock jointed slabs-on-grade.” *Construction and Building Materials*, Elsevier Ltd, 77, 340–348.

Ball, C. G., and Childs, L. D. (1975). "Tests of joints for concrete pavements," *Research and Development Bulletin RD-26, 01P, Portland Cement Association*, Skokie.

Barman, M. (2014). “Joint Performance Characterization of Bonded Concrete Overlays.” Doctoral dissertation, University of Pittsburgh.

Barman, M., Vandenbossche, J. M., and Li, Z. (2017). “Influence of Interface Bond on the Performance of Bonded Concrete Overlays on Asphalt Pavements.” *Journal of Transportation Engineering, Part B: Pavements*, 143(3), 04017008.

Barman, M., and B. Hansen. (2018).“Comparison of Performances of Structural Fibers and Development of a Specification for Using Structural Fibers in Thin Concrete Overlays.” Final Report. Minnesota Department of Transportation, St. Paul.

Bayrak, M. B., and Ceylan, H. (2008). “Neural Network-Based Approach for Analysis of Rigid Pavement Systems Using Deflection Data.” *Transportation Research Record: Journal of the Transportation Research Board*, 2068(1), 61–70.

Bazant, Z.P. and Pfeiffer, P.A., (1986). “Shear fracture tests of concrete.” *Materials and* Structures, 19 (2), 111–121.

Belshe, M., Mamlouk, M. S., Kaloush, K. E., and Rodezno, M. (2011). “Temperature Gradient and Curling Stresses in Concrete Pavement with and without Open-Graded Friction Course.” *Journal of Transportation Engineering*, 137(10), 723–729.

Bencardino, F., Rizzuti, L., Spadea, G., and Swamy, R. N. (2010). “Experimental evaluation of fiber reinforced concrete fracture properties.” *Composites Part B: Engineering*, Elsevier Ltd, 41(1), 17–24.

Bhosale, A., Rasheed, M. A., Prakash, S. S., and Raju, G. (2019). “A study on the efficiency of steel vs. synthetic vs. hybrid fibers on fracture behavior of concrete in flexure using acoustic emission.” *Construction and Building Materials*, Elsevier Ltd, 199, 256–268.

Blazy, J., and Blazy, R. (2021). “Polypropylene fiber reinforced concrete and its application in creating architectural forms of public spaces.” *Case Studies in Construction Materials*, Elsevier Ltd., 14, e00549.

Brink, A. C. (2003). “Modelling aggregate interlock load transfer at concrete pavement joints.” Doctoral dissertation, University of Pretoria, South Africa.

Broek, D. (1986). *Elementary engineering fracture mechanics*. Springer Netherlands, Dordrecht.

Bruinsma, J. E., Snyder, M. B., and Vandenbossche, J. M. (1995). “Factors Affecting The Deterioration Of Transverse Cracks in JRCP.” Michigan Department of Transportation and Great Lakes Center for Truck Transportation Research University of Michigan.

Buch, N., and Frabizzio, M. (2000). “Impact of Aggregate Type on Performance of Transverse Cracks in Jointed Concrete Pavements-A Field Study.” *International Journal of Pavement Engineering*, 1(2), 97–106.

Byrum, C. (2012). “Falling weight deflectometer joint load tests used for direct calculation of pavement joint stiffness.” *Transportation Research Record*, (2306), 95–104.

Carpinteri, A., Fortese, G., Ronchei, C., Scorza, D., and Vantadori, S. (2017). “Mode I fracture toughness of fibre reinforced concrete.” *Theoretical and Applied Fracture Mechanics*, Elsevier Ltd, 91, 66–75.

Cascardi, A., Micelli, F., and Aiello, M. A. (2017). “An Artificial Neural Networks model for the prediction of the compressive strength of FRP-confined concrete circular columns.” *Engineering Structures*, Elsevier Ltd, 140, 199–208.

Ceylan, H., Gopalakrishnan, K., Kim, S., Schwartz, C. W., and Li, R. (2013). “Global Sensitivity Analysis of Jointed Plain Concrete Pavement Mechanistic–Empirical Performance Predictions.” *Transportation Research Record: Journal of the Transportation Research Board*, 2367(1), 113–122.

Chandrappa, A. K., and Biligiri, K. P. (2016). “Influence of mix parameters on pore properties and modulus of pervious concrete: an application of ultrasonic pulse velocity.” *Materials and Structures/Materiaux et Constructions*, Springer Netherlands, 49(12), 5255–5271.

Chandrappa, A. K., and Biligiri, K. P. (2017). “Flexural-fatigue characteristics of pervious concrete: Statistical distributions and model development.” *Construction and Building Materials*, Elsevier Ltd, 153, 1–15.

Channakeshava, C., Barzegar, F., and Voyiadjis, G. Z. (1993). “Nonlinear FE Analysis of Plain Concrete Pavements with Doweled Joints.” *Journal of Transportation Engineering*, 119(5), 763–781.

Chattaraj, R., and B.B.Pandey. (2014). “Short panelled Concrete pavement in Built-Up Area.” *Indian Highways*, 42(1), 11–18.

Chatti, K., and Lim, T. (2001). “Dynamic Analysis of Rigid Pavements with Different Subgrade Support Models.” In *Seventh International Conference on Concrete Pavements. The Use of Concrete in Developing Long-Lasting Pavement Solutions for the 21st Century International Society for Concrete Pavements* (Vol. 1).

Chou, J.-S., Pham, T.-P.-T., Nguyen, T.-K., Pham, A.-D., and Ngo, N.-T. (2020). "Shear strength prediction of reinforced concrete beams by baseline, ensemble, and hybrid machine learning models." *Soft Computing*, Springer Berlin Heidelberg, 24(5), 3393–3411.

Chou, J.-S., Tsai, C.-F., Pham, A.-D., and Lu, Y.-H. (2014). "Machine learning in concrete strength simulations: Multi-nation data analytics." *Construction and Building Materials*, Elsevier Ltd, 73, 771–780.

Chupanit, P., and Roesler, J. (2005). "Part 1: Aggregates: Quality Assurance Tests and Performance Prediction Models: Improvement of Concrete Cracking Resistance and Joint Load Transfer Through Coarse Aggregate Selection." *Transportation Research Record: Journal of the Transportation Research Board*, 1913, 2–10.

Chupanit, P., and Roesler, J. R. (2008). "Fracture Energy Approach to Characterize Concrete Crack Surface Roughness and Shear Stiffness." *Journal of Materials in Civil Engineering*, 20(4), 275–282.

Colley, B. E., and Humphrey, H. A. (1968). "Aggregate Interlock at Joints Concrete Pavements." *Portland Cement Association Research and Development Laboratories*, 18, 1–18.

Covarrubias V., J. P. (2012). "Design of concrete pavement with optimized slab geometry." *Revista ingeniería de construcción*, 27(3), 181–197.

Darter, M. I., Khazanovich, L., Snyder, M., Rao, S., and Hallin, J. (2001). "Development and Calibration of a Mechanistic Design Procedure for Jointed Plain Concrete Pavements." Proceedings of the 7th international conference on concrete pavements, Orlando (FL), No. 1; 2001. p. 113–31.

Davids, W. (1998). "Modeling of Rigid Pavements: Joint Shear Transfer Mechanisms and Finite Element Solution Strategies." Doctoral Dissertation, University of Washington.

Davids, W. G., Turkiyyah, G. M., and Mahoney, J. P. (1998). "EverFE: Rigid Pavement Three-Dimensional Finite Element Analysis Tool." *Transportation Research Record: Journal of the Transportation Research Board*, 1629(1), 41–49.

Debnath, B., and Pratim, P. (2020). "Prediction and model development for fatigue performance of pervious concrete made with over burnt brick aggregate." *Materials and Structures*, Springer Netherlands, 53(4), 1–20.

Elices, M., and Rocco, C. G. (2008). "Effect of aggregate size on the fracture and mechanical properties of a simple concrete." *Engineering Fracture Mechanics*, 75(13), 3839–3851.

Elshafey, A. A., Dawood, N., Marzouk, H., and Haddara, M. (2013). “Crack width in concrete using artificial neural networks.” *Engineering Structures*, Elsevier Ltd, 52, 676–686.

Fakhri, M., and Shahni Dezfoulian, R. (2019). “Pavement structural evaluation based on roughness and surface distress survey using neural network model.” *Construction and Building Materials*, Elsevier Ltd, 204, 768–780.

Fallah, S., and Nematzadeh, M. (2017). “Mechanical properties and durability of high-strength concrete containing macro-polymeric and polypropylene fibers with nano-silica and silica fume.” *Construction and Building Materials*, Elsevier Ltd, 132, 170–187.

Fenwick, R. C. (1966). "Shear strength of reinforced concrete beams," Doctoral thesis, University of Canterbury, Christchurch, New Zealand.

Figueira, D., Sousa, C., Calçada, R., and Neves, A. S. (2016). “Push-Off Tests in the Study of Cyclic Behavior of Interfaces between Concretes Cast at Different Times.” *Journal of Structural Engineering*, 142(1), 04015101.

Frabizzio, M. A., and Buch, N. J. (1999). “Performance of Transverse Cracking in Jointed Concrete Pavements.” *Journal of Performance of Constructed Facilities*, 13(November), 172–180.

Frénaij, J. W (1989). “Time-dependent shear transfer in cracked reinforced concrete.” Doctoral Thesis, University of Delft, Delft.

Ghanizadeh, A. R., Abbaslou, H., Amlashi, A. T., and Alidoust, P. (2019). “Modeling of bentonite/sepiolite plastic concrete compressive strength using artificial neural network and support vector machine.” *Frontiers of Structural and Civil Engineering*, 13(1), 215–239.

Giaccio, G., and Zerbino, R. (1998). “Failure Mechanism of Concrete.” *Advanced Cement Based Materials*, 7(2), 41–48.

Han, C., Ma, T., Chen, S., and Fan, J. (2021). “Application of a hybrid neural network structure for FWD backcalculation based on LTPP database.” *International Journal of Pavement Engineering*, Taylor & Francis, 0(0), 1–14.

Hatami Jorbat, M., Hosseini, M., and Mahdikhani, M. (2020). “Effect of polypropylene fibers on the mode I, mode II, and mixed-mode fracture toughness and crack propagation in fiber-reinforced concrete.” *Theoretical and Applied Fracture Mechanics*, Elsevier, 109(May), 102723.

Heravi, G., and Eslamdoost, E. (2015). “Applying Artificial Neural Networks for Measuring and Predicting Construction-Labor Productivity.” *Journal of Construction Engineering and Management*, 141(10), 04015032.

Hillerborg, A. (1985). “Results of three comparative test series for determining the fracture energyG F of concrete.” *Materials and Structures*, 18(5), 407–413.

Hossain, M., Gopisetti, L. S. P., and Miah, M. S. (2020). “Artificial neural network modelling to predict international roughness index of rigid pavements.” *International Journal of Pavement Research and Technology*, 13(3), 229–239.

Hossain, M. I., Gopisetti, L. S. P., and Miah, M. S. (2019). “International Roughness Index Prediction of Flexible Pavements Using Neural Networks.” *Journal of Transportation Engineering, Part B: Pavements*, 145(1), 04018058.

Huang, Y.H. and Wang, S.T., (1973). “Finite-element analysis of concrete slabs and its implications for rigid pavement design.” *Highway Research Record*, (466).

Huang, Y. H., and S. T. Wang. (1974) "Finite-element analysis of rigid pavements with partial subgrade contact." *Transportation Research Record*, 485, 39-54.

Huang, Y. H., and Deng, X. (1983). “Finite Element Analysis of Jointed Concrete Pavements.” *Journal of Transportation Engineering*, 109(5), 689–705.

Huang. Y. H. (2004). *Pavement Analysis Design*, second ed., Pearson Prentice Hall, Upper Saddle River, NJ, USA.

Hussain, F., Ali, Y., and Irfan, M. (2021). “Quantifying the Differential Phase Angle Behaviour of Asphalt Concrete Mixtures Using Artificial Neural Networks.” *International Journal of Pavement Research and Technology*, Springer Singapore.

Inkoom, S., Sobanjo, J., Barbu, A., and Niu, X. (2019). “Prediction of the crack condition of highway pavements using machine learning models.” *Structure and Infrastructure Engineering*, Taylor & Francis, 15(7), 940–953.

Ioannides, A. M., and Korovesis, G. T. (1990). “Aggregate Interlock : A Pure-Shear Load Transfer Mechanism.” *Transportation Research Record*, 1286(11), 14–24.

IRC 44. (2017). “Guidelines for Cement Concrete Mix Design for Pavements.” *Indian Road Congress, New Delhi*.

IRC: SP-76. (2015). “Guidelines for conventional, thin and ultrathin whitetopping.” *Indian Road Congress, second revision*, New Delhi.

IS: 269. (2015). "Ordinary Portland cement- specifications.” *Bureau of Indian Standards*, New Delhi.

IS: 383. (2016). “Coarse and fine aggregate for concrete- Specifications.” *Bureau of Indian Standards*, New Delhi.IS: 456. (2000).

IS: 516:2014. (2004). “Methods of Tests for Strength of Concrete.” *Bureau of Indian Standards*, New Delhi, India.

IS: 12089. (1987). “Specification for Granulated Slag for the Manufacture of Portland Slag cement.” *Bureau of Indian Standards*, New Delhi, India.

IS: 2386. (1963). “Methods of test for aggregates for concrete.” *Bureau of Indian Standards*, New Delhi, India.

IS: 5816. (1999). “Indian Standard Splitting tensile strength of concrete- method of test.” *Bureau of Indian Standards, New Delhi*, 5816, 1–14.

Issa, M. A., Chudnosky, A., Issa, M. A., and Islam, M. (2003). “Effect of Notch/Depth Ratio on Fracture Behaviour of Plain Concrete.” *Role of Concrete In Sustainable Development*, Thomas Telford Publishing, 27–36.

Jalal, M., Grasley, Z., Gurganus, C., and Bullard, J. W. (2020). “A new nonlinear formulation-based prediction approach using artificial neural network (ANN) model for rubberized cement composite.” *Engineering with Computers*, Springer London, (0123456789).

Jayakesh, K., and Suresha, S. N. (2018). “Experimental investigation of interface treatment technique on interface shear bond fatigue behavior of Ultra-Thin Whitetopping.” *Construction and Building Materials*, Elsevier Ltd, 161, 489–500.

Jensen, E. A., and Hansen, W. (2000). “Fracture Energy Test for Highway Concrete: Determining the Effect of Coarse Aggregate on Crack Propagation Resistance.” *Transportation Research Record: Journal of the Transportation Research Board*, 1730(1), 10–17.

Jensen, E. A., and Hansen, W. (2001). “Mechanism of Load Transfer-Crack width Relation in JPCP: Influence of Coarse Aggregate Properties.” *7th International Conference on Concrete Pavements - Orlando, Florida*.

Jensen, E. A., and Hansen, W. (2006). “Nonlinear aggregate interlock model for concrete pavements.” *International Journal of Pavement Engineering*, 7(4), 261–273.

Kallannavar, V., Kattimani, S., Soudagar, M. E. M., Mujtaba, M. A., Alshahrani, S., and Imran, M. (2021). “Neural network-based prediction model to investigate the influence of temperature and moisture on vibration characteristics of skew laminated composite sandwich plates.” *Materials*, 14(12).

Kaloop, M. R., El-Badawy, S. M., Ahn, J., Sim, H. B., Hu, J. W., and Abd El-Hakim, R. T. (2020). “A hybrid wavelet-optimally-pruned extreme learning machine model for the estimation of international roughness index of rigid pavements.” *International Journal of Pavement Engineering*, Taylor & Francis, 0(0), 1–15.

Kapiri, M., Tutumluer, E., and Barenberg, E. J. (2000). “Analysis of Temperature Effects on Pavement Response at Denver International Airport.” *The 2020 Vision of Air Transportation*, American Society of Civil Engineers, Reston, VA, 125–143.

Kappenman, R. F. (1985). “Estimation for the three-parameter Weibull, lognormal, and gamma distributions.” *Computational Statistics & Data Analysis*, 3(C), 11–23.

Karimipour, A. (2022). “Influence of micro polypropylene fibres on the fracture energy and mechanical characteristics of recycled coarse brick aggregate concrete.” *Construction and Building Materials*, Elsevier Ltd, 314(PA), 125667.

Karimipour, A., and de Brito, J. (2021). “Influence of polypropylene fibres and silica fume on the mechanical and fracture properties of ultra-high-performance geopolymer concrete.” *Construction and Building Materials*, Elsevier Ltd, 283, 122753.

Kasu, S. R., Deb, S., Mitra, N., Muppireddy, A. R., and Kusam, S. R. (2019). “Influence of aggregate size on flexural fatigue response of concrete.” *Construction and Building Materials*, Elsevier Ltd, 229(September), 116922.

Kasu, S. R., Mitra, N., and Muppireddy, A. R. (2020). “Influence of polyester microfiber reinforcement on flexural fatigue characteristics of concrete.” *Road Materials and Pavement Design*, Taylor & Francis, 0(0), 1–17.

Kazi, A., and Al-Mansour, Z. R. (1980). “Influence of geological factors on abrasion and soundness characteristics of aggregates.” *Engineering Geology*, 15(3–4), 195–203.

Khalilpour, S., BaniAsad, E., and Dehestani, M. (2019). “A review on concrete fracture energy and effective parameters.” *Cement and Concrete Research*, Elsevier, 120(March), 294–321.

Khasawneh, M. A., Taamneh, M. M., and Albatayneh, O. (2019). “Evaluation of static creep of FORTA-FI strengthened asphalt mixtures using experimental, statistical and feed-forward back-propagation ANN techniques.” *International Journal of Pavement Research and Technology*, 12(1), 43–53.

Khazanovich, L., and Gotlif, A. (2003). *Evaluation of Joint and Crack Load Transfer Final Report (Archieved)*. Federal Highway Administration, Report, FHWA-RD-02-088, McLean.

King, D., and Roesler, J. (2014). “Backcalculation Procedure for Bonded Concrete Overlays of Asphalt Pavement.” *Transportation Research Record*, 2457(2), 72–79.

Kumar, C. N. S., and Rao, T. D. G. (2010). “Fracture parameters of high-strength concrete – mode II testing.” *Magazine of Concrete Research*, 62(3), 157–162.

Kuo, C.-M. (1998). “Study of Load Transfer Parameter in AASHTO Design Guide for Concrete Pavement.” *Transportation Research Record*, 1629(1), 1–5.

Lakavath, C., Suriya Prakash, S., and Dirar, S. (2021). “Experimental and numerical studies on shear behaviour of macro-synthetic fibre reinforced prestressed concrete beams.” *Construction and Building Materials*, Elsevier Ltd, 291, 123313.

Lee, S.-W., Jeong, J.-H., and Chon, B.-J. (2010). “Probabilistic modelling of pavement joint opening.” *Proceedings of the ICE - Transport*, 163(1), 9–17.

Lekshmipathy, J., Samuel, N. M., and Velayudhan, S. (2020). “Vibration vs. vision: best approach for automated pavement distress detection.” *International Journal of Pavement Research and Technology*, 13(4), 402–410.

Leong, G. W., Mo, K. H., Loh, Z. P., and Ibrahim, Z. (2020). “Mechanical properties and drying shrinkage of lightweight cementitious composite incorporating perlite microspheres and polypropylene fibers.” *Construction and Building Materials*, Elsevier Ltd, 246, 118410.

Madasamy, C., Harik, I. E., Allen, D. L., and Fleckenstein, L. J. (1999). “Laboratory Testing and Analysis of Joints for Rigid Pavements.” Report, University of Kentucky.

Maitra, S. R., Reddy, K. S., and Ramachandra, L. S. (2009). “Load Transfer Characteristics of Dowel Bar System in Jointed Concrete Pavement.” *Journal of Transportation Engineering*, 135(11), 813–821.

Maitra, S. R., Reddy, K. S., and Ramachandra, L. S. (2010). “Load Transfer Characteristics of Aggregate Interlocking in Concrete Pavement.” *Journal of Transportation Engineering*, 136(3), 190–195.

Maitra, S. R., Reddy, K. S., and Ramachandra, L. S. (2014). “Numerical investigation of fatigue characteristics of concrete pavement.” *International Journal of Fracture*, 189(2), 181–193.

Mansur, M. A., Vinayagam, T., and Tan, K.-H. (2008). “Shear Transfer across a Crack in Reinforced High-Strength Concrete.” *Journal of Materials in Civil Engineering*, 20(4), 294–302.

Marecos, V., Fontul, S., de Lurdes Antunes, M., and Solla, M. (2017). “Evaluation of a highway pavement using non-destructive tests: Falling Weight Deflectometer and Ground Penetrating Radar.” *Construction and Building Materials*, 154, 1164–1172.

Mattock, A. H., Li, W. K., and Wang, T. C. (1976). “Shear transfer in lightweight reinforced concrete.” *PCI Journal*, 21(1), 20–39.

Mehta, P. K., and Monteiro, P. J. M. (2014). *Concrete: Microstructure, Properties, and Materials, Fourth Edition*. McGraw-Hill Education, New York.

Millard, S. G., and Johnson, R. P. (1984). “Shear transfer across cracks in reinforced concrete due to aggregate interlock and to dowel action.” *Magazine of concrete research*, *36*(126), 9-21.

Ministry of Road Transport and Highway. (2013). “Specifications for road and bridge works.” 5th Revision, Indian Road Congress, New Delhi, India.

Motamedi, S., Song, K.-I., and Hashim, R. (2015). "Prediction of unconfined compressive strength of pulverized fuel ash–cement–sand mixture." *Materials and Structures*, 48(4), 1061–1073.

N. Dudley, W., Wickham, AOCN, R., and Coombs, N. (2016). "An Introduction to Survival Statistics: Kaplan-Meier Analysis." *Journal of the Advanced Practitioner in Oncology*, 7(1), 91–100.

Nallathambi, P., Karihaloo, B. L., and Heaton, B. S. (1984). "Effect of specimen and crack sizes, water/cement ratio and coarse aggregate texture upon fracture toughness of concrete." *Magazine of Concrete Research*, 36(129), 227–236.

Nam, B. H., Yeon, J. H., and Behring, Z. (2014). "Effect of daily temperature variations on the continuous deflection profiles of airfield jointed concrete pavements". *Construction and Building Materials, 73*, 261-270.

Nazari, A., and Sanjayan, J. G. (2015). "Modeling of compressive strength of geopolymers by a hybrid ANFIS-ICA approach." *Journal of Materials in Civil Engineering*, 27(5), 1–8.

Nikbin, I. M., Beygi, M. H. A., Kazemi, M. T., Vaseghi Amiri, J., Rahmani, E., Rabbanifar, S., and Eslami, M. (2014). "Effect of coarse aggregate volume on fracture behavior of self compacting concrete." *Construction and Building Materials*, Elsevier Ltd, 52, 137–145.

Nivedya, M. K., and Mallick, R. B. (2020). "Artificial neural network-based prediction of field permeability of hot mix asphalt pavement layers." *International Journal of Pavement Engineering*, Taylor & Francis, 21(9), 1057–1068.

Noushini, A., Samali, B., and Vessalas, K. (2013). "Effect of polyvinyl alcohol (PVA) fibre on dynamic and material properties of fibre reinforced concrete." *Construction and Building Materials*, Elsevier Ltd, 49, 374–383.

Noushini, A., Vessalas, K., and Samali, B. (2014). "Static mechanical properties of polyvinyl alcohol fibre reinforced concrete (PVA-FRC)." *Magazine of Concrete Research*, 66(9), 465–483.

Nowlen, W. J. 1(968). "Influence of aggregate properties on effectiveness of interlock joints in concrete pavements." *Journal of Portland Cement Association*, 10 (2), 2–8.

Ongel, A., and Harvey, J. (2004). "Analysis of 30 Years of Pavement Temperatures using the Enhanced Integrated Climate Model (EICM)." *California Department of Transportation*.

Ostadi, N. K. (2013). "Enhancing analytical toolboxes of pavement management systems via integration of computational inteliggence."

Owusu-antwi, E. B., Meyer, A. H., and Hudson, W. R. (1990). A*ssessing Load Transfer Across Joints and Cracks in Rigid Pavements using the Falling Weight Deflectometer*. Report No. 460-2, Centre for Transportation Research, The University of Texas at Austin, 1990.

Pane, I., Hansen, W., and Mohamed, A. R. (1998). "Three-dimensional finite element study on effects of nonlinear temperature gradients in concrete pavements." *Transportation Research Record*, (1629).

Paulay, T. and Loeber, P. J. (1974). "Shear Transfer by Aggregate Interlock." Special Publication SP42, American Concrete Institute.

Perera, R. W., Kohn, S. D., and Tayabji, S. (2005). "Achieving a High Level of Smoothness in Concrete Pavements Without Sacrificing Long-Term Performance." *FHWA-HRT-05-068*, (October).

Peter Taylor, Kosmatka, S. H., Gerald, and Voigt. (2007). *Integrated Materials and Construction Practices for Concrete Pavement: A State of the Practice Manual*.

Poblete, M., R. Valenzuela, and Salsilli, R. (1998). "Load Transfer in Undoweled Transverse Joints of PCC Pavements." *Transportation Research Record*, 1207.

Pradena, M., Houben, L., and Prof, A. (2017). "Influence of early-age behaviour on structural performance of concrete pavements." *Journal of the Croatian Association of Civil Engineers*, 69(9), 875–883.

Pruijssers, A. F., and Lung, G. (1985). "Shear transfer across a crack in concrete subjected to repeated loading. Experimental results: Part I." *Report Stevin Laboratory, Concrete Structures 5-85-12*.

Ramírez, L. C. (2010). "Concrete Mixture Properties affecting the Aggregate Interlock Mechanism of Joints and Cracks for Rigid Pavement Systems." Masters Thesis, University of Pittsburgh, Pittsburgh

Ramsamooj, D. V. (1999). "Stresses in Jointed Rigid Pavements." *Journal of Transportation Engineering*, 1(April), 101–107.

Rao, C., Tutumluer, E., and Kim, I. T. (2002). "Quantification of Coarse Aggregate Angularity Based on Image Analysis." *Transportation Research Record: Journal of the Transportation Research Board*, 1787(02), 117–124.

Rao, G. A., and Prasad, B. K. R. (2002). "Fracture energy and softening behavior of high-strength concrete." *Cement and Concrete Research*, 32(2), 247–252.

Rao, K. B., Desai, V. B., and Mohan, D. J. (2011). "Experimental investigations on mode II fracture of concrete with crushed granite stone fine aggregate replacing sand." *Materials Research*, 15(1), 41–50.

Rasmussen, R. O., and Rozycki, D. K. (2004). *Thin and ultra-thin whitetopping: A synthesis of highway practice* (Vol. 338). Transportation Research Board.

Reis, J. M. L., and Ferreira, A. J. M. (2004). "A contribution to the study of the fracture energy of polymer concrete and fibre reinforced polymer concrete." *Polymer Testing*, 23(4), 437–440.

Reinhardt, H.W., Ošbolt, J., Shilang, X., and Dinku, A. (1997). "Shear of structural concrete members and pure mode II testing." *Advanced Cement Based Materials*, 5 (3–4), 75–15 85.

Reinhardt, H.W. and Xu, S. (2000). "A practical testing approach to determine mode fracture energy $G_{(IIF)}$ for concrete." *International Journal of Fracture*, 105 (2), 107–18 125.

Rezaali, M., Quilty, J., and Karimi, A. (2021). "Probabilistic urban water demand forecasting using wavelet-based machine learning models." *Journal of Hydrology*, Elsevier B.V., 600(April), 126358.

Roesler, J., and Chupanit, P. (2005). "Effect of Coarse Aggregate on Concrete Fracture Energy and Joint Stiffness." *Workshop on Fracture Mechanics for Concrete Pavements*, 117–121.

Roesler, J. R., Altoubat, S. A., Lange, D. A., Rieder, K. A., and Ulreich, G. R. (2006). "Effect of synthetic fibers on structural behavior of concrete slabs-on-ground." *ACI Materials Journal*, 103(1), 3–10.

Roesler, J. R., and Barenberg, E. J. (1999). "Fatigue and Static Testing of Concrete Slabs." *Transportation Research Record: Journal of the Transportation Research Board*, 1684(1), 71–80.

Roesler, J. R., Cervantes, V. G., and Amirkhanian, A. N. (2012). "Accelerated performance testing of concrete pavement with short slabs." *International Journal of Pavement Engineering*, 13(6), 494–507.

Roesler, J. R., Hiller, J. E., and Littleton, P. C. (2005). "Large-scale airfield concrete slab fatigue tests." *Proceedings - 8th International Conference on Concrete Pavements: Innovations for Concrete Pavement: Technology Transfer for the Next Generation*, 3, 1247–1268.

Rufino, D., and Roesler, J. (2004). "Effect of Pavement Temperature on Concrete Joint Responses." *2004 FAA worldwide Airport Technology Transfer Conference*, Atlantic City, New Jersey, USA, 1–15.

Ryu, S., Lin, W., and Cho, Y. (2018). "Experimental and Numerical Evaluations on the Shape Factor of Silicone Sealant for Concrete Pavements under Vertical Loading." *Journal of Performance of Constructed Facilities*, 32(4), 04018032.

Sadeghi, V., and Hesami, S. (2018). “Investigation of load transfer efficiency in jointed plain concrete pavements (JPCP) using FEM.” *International Journal of Pavement Research and Technology*, Chinese Society of Pavement Engineering, 11(3), 245–252.

Saouma, V. E., Broz, J. J., Brühwiler, E., and Boggs, H. L. (1991). “Effect of Aggregate and Specimen Size on Fracture Properties of Dam Concrete.” *Journal of Materials in Civil Engineering*, 3(3), 204–218.

Siamardi, K., and Shabani, S. (2021). “Evaluation the effect of micro-synthetic fiber on mechanical and freeze-thaw behavior of non-air-entrained roller compacted concrete pavement using response surface methodology.” *Construction and Building Materials*, Elsevier Ltd, 295, 123628.

Siregar, A. P. N., Rafiq, M. I., and Mulheron, M. (2017). “Experimental investigation of the effects of aggregate size distribution on the fracture behaviour of high strength concrete.” *Construction and Building Materials*, 150, 252–259.

Snyder, M. B., and Raja, Z. I. (1991). “Factors Affecting Deterioration of Transverse Cracks in Jointed Reinforced Concrete Pavements.” *Transportation Research Record*, 1307, 162–168.

Swarna, S. T., Reddy, K. S., Reddy, M. A., and Pandey, B. B. (2018). “Analysis of Stresses Due to Traffic and Thermal Loads in Two-Lift Bonded Concrete Pavements by Finite Element Method.” *Advances in Civil Engineering Materials*, 7(2), 20170028.

Tabatabaie, A. M., and Barenberg, E. J. (1978). “Finite-element analysis of jointed or cracked concrete pavements.” *Transportation Research Record*, (671), 11–19.

Tabatabaie, A.M., Barenberg, E.J. and Smith, R.E., (1979). “Longitudinal Joint Systems in Slip-Formed Rigid Pavements. Volume II. Analysis of Load Transfer Systems for Concrete Pavements.” Illinois University at Urbana-Champaign.

Tassios, T. P., & Vintzēleou, E. N. (1987). “Concrete-to-concrete friction.” *Journal of Structural Engineering*, *113*(4), 832-849.

Theodorsson, E. (1988). “BASIC computer program to summarize data using nonparametric and parametric statistics including Anderson-Darling test for normality.” *Computer Methods and Programs in Biomedicine*, 26(2), 207–213.

Tia, M., Armaghani, J. M., Chung-Lung Wu, Shau Lei, and Toye, K. L. (1987). “FEACONS III Computer Program for Analysis of Jointed Concrete Pavements.” *Transportation Research Record*, 12–22.

Uddin, W., Hackett, R. M., Joseph, A., Pan, Z., and Crawley, A. B. (1995). “Three-Dimensional Finite-Element Analysis of Jointed Concrete Pavement with Discontinuities.” *Transportation Research Record*, (1482), 26–32.

Vandenbossche, J. (1999). “Estimating potential aggregate interlock load transfer based on measurements of volumetric surface texture of fracture plane.” *Transportation Research Record*, (99), 59–63.

Velazco, G., Visalvanich, K., and Shah, S. P. (1980). “Fracture behavior and analysis of fiber reinforced concrete beams.” *Cement and Concrete Research*, 10(1), 41–51.

Vepa, T. S., and George, K. P. (1997). “Deflection Response Models for Cracked Rigid Pavements.” *Journal of Transportation Engineering*, 123(5), 377–384.

Wadkar, A., Mehta, Y., Cleary, D., Guo, E., Musumeci, L., Zapata, A., and Kettleson, W. (2011). “Load-transfer efficiencies of rigid airfield pavement joints based on stresses and deflections.” *Journal of Materials in Civil Engineering*, *23*(8), 1171-1180.

Walraven, J. C. (1980). “Aggregate Interlock: a Theoretical and Experimental Analysis.” Doctoral Dissertation, *Delft University Press*.

Wang, H., Xie, P., Ji, R., and Gagnon, J. (2021). “Prediction of airfield pavement responses from surface deflections: comparison between the traditional backcalculation approach and the ANN model.” *Road Materials and Pavement Design*, Taylor & Francis, 22(9), 1930–1945.

Wattar, S. W. (2001). “Aggregate interlock behavior of large crack width concrete joints in pcc airport pavements.” Doctoral dissertation, University of Illinois, Urbana-Champaign.

W.G. Westall. (1965). “Methods of Forming Joints in Portland Cement Concrete Pavement.” HRB, Highway Research Record 80, pp. 1-9.

Wu, C.-P., and Shen, P.-A. (1996). “Dynamic Analysis of Concrete Pavements Subjected to Moving Loads.” *Journal of Transportation Engineering*, 122(5), 367–373.

Xu, H., Shao, Z., Wang, Z., Cai, L., Li, Z., Jin, H., and Chen, T. (2020). “Experimental study on mechanical properties of fiber reinforced concrete: Effect of cellulose fiber, polyvinyl alcohol fiber and polyolefin fiber.” *Construction and Building Materials*, Elsevier Ltd, 261, 120610.

Xu, H., Wang, Z., Shao, Z., Cai, L., Jin, H., Zhang, Z., Qiu, Z., Rui, X., and Chen, T. (2021). “Experimental study on durability of fiber reinforced concrete: Effect of cellulose fiber, polyvinyl alcohol fiber and polyolefin fiber.” *Construction and Building Materials*, Elsevier Ltd, 306(June), 124867.

Yang, K.-H., Sim, J.-I., Kang, J.-H., and Ashour, A. F. (2012). “Shear capacity of monolithic concrete joints without transverse reinforcement.” *Magazine of Concrete Research*, 64(9), 767–779.

Yazdanbakhsh, A., Altoubat, S., and Rieder, K. A. (2015). “Analytical study on shear strength of macro synthetic fiber reinforced concrete beams.” *Engineering Structures*, Elsevier Ltd, 100, 622–632.

Yazici, Ş., Mardani-Aghabaglou, A., Tuyan, M., and Üte, A. A. (2015). “Mechanical properties and impact resistance of roller-compacted concrete containing polypropylene fibre.” *Magazine of Concrete Research*, 67(16), 867–875.

Yew, M. K., Mahmud, H. Bin, Shafigh, P., Ang, B. C., and Yew, M. C. (2016). “Effects of polypropylene twisted bundle fibers on the mechanical properties of high-strength oil palm shell lightweight concrete.” *Materials and Structures/Materiaux et Constructions*, Springer Netherlands, 49(4), 1221–1233.

Yi, W.-J., Deng, Q., and Tang, F. (2017). “Effect of Coarse Aggregate Size on the Shear Behavior of Beams without Shear Reinforcement.” *ACI Structural Journal*, 114(5), 1131–1142.

Yoder, E. J., and Witczak, M. W. (1991). *Principles of pavement design*. John Wiley & Sons.

Zaman, M., and Alvappilai, A. (1995). “Contact-element model for dynamic analysis of jointed concrete pavements.” *Journal of Transportation Engineering*, 121(5), 425–433.

Zhang, P., and Li, Q. (2013). “Effect of polypropylene fiber on durability of concrete composite containing fly ash and silica fume.” *Composites Part B: Engineering*, Elsevier Ltd, 45(1), 1587–1594.

Zimmermann, T., Strauss, A., and Bergmeister, K. (2012). “Structural behavior of low- and normal-strength interface mortar of masonry.” *Materials and Structures/Materiaux et Constructions*, 45(6), 829–839.

APPENDIX A

The shear stress Vs shear displacement plots used to determine the joint shear stiffness and fracture energy in Chapter 4 are shown below.

A.1 The shear stress Vs shear displacement plots of the plain PQC cylindrical specimens A19, A26.5 and A31.5 with a GD of 1/4th of diameter are shown in Figure A.1, A.2 and A.3, respectively.

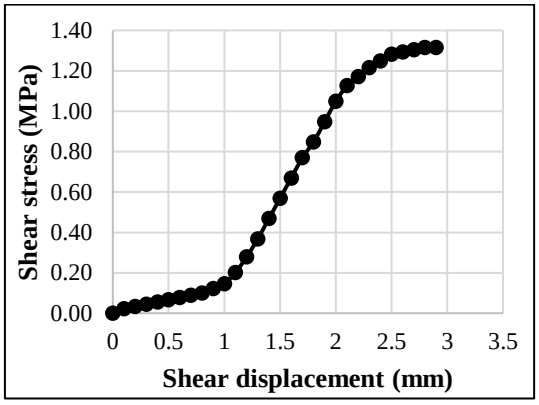

Figure A.1 Shear stress Vs shear displacement plot of A19 plain PQC mix

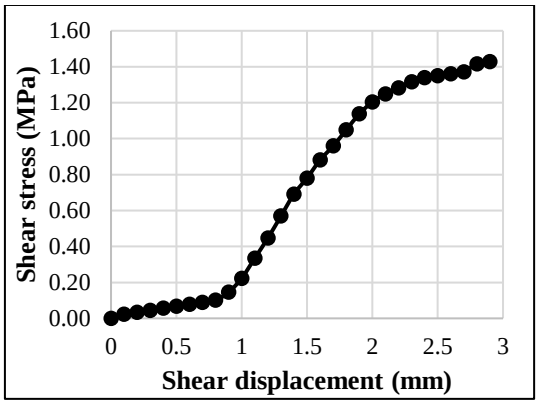

Figure A.2 Shear stress Vs shear displacement plot of A26.5 plain PQC mix

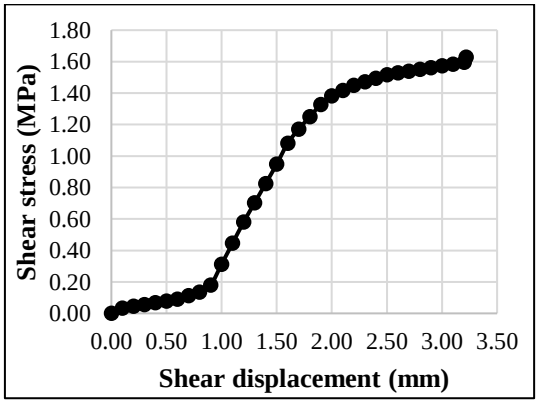

Figure A.3 Shear stress Vs shear displacement plot of A31.5 plain PQC mix

A.2 The shear stress Vs shear displacement plots of the plain PQC cylindrical specimens A19, A26.5 and A31.5 with a GD of 1/3rd of diameter are shown in Figure A.4, A.5 and A.6, respectively.

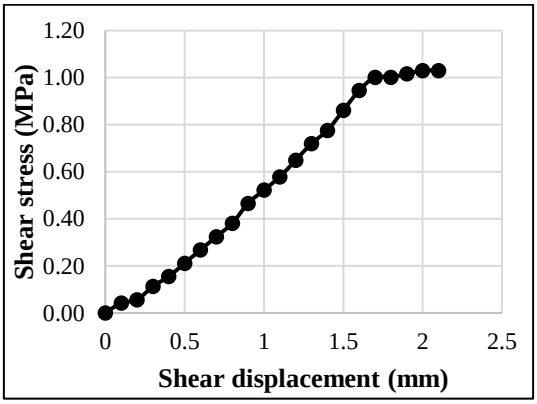

Figure A.4 Shear stress Vs shear displacement plot of A19 plain PQC mix

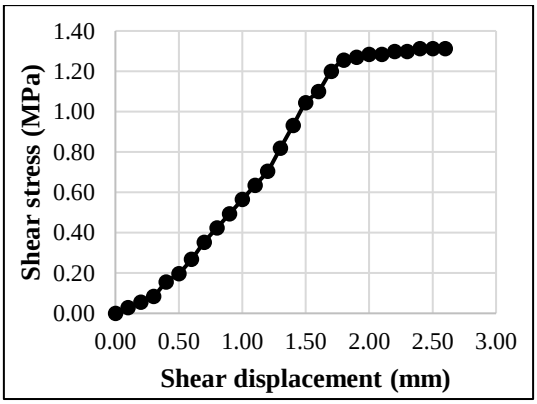

Figure A.5 Shear stress Vs shear displacement plot of A26.5 plain PQC mix

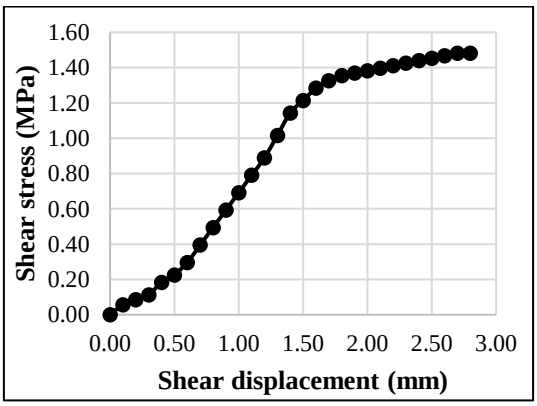

Figure A.6 Shear stress Vs shear displacement plot of A31.5 plain PQC mix

A.3 The shear stress Vs shear displacement plots of the micro-fiber reinforced PQC cylindrical specimens F0.9, F2.1 and F3.0 with a GD of 1/4th of diameter are shown in Figure A.7, A.8 and A.9, respectively.

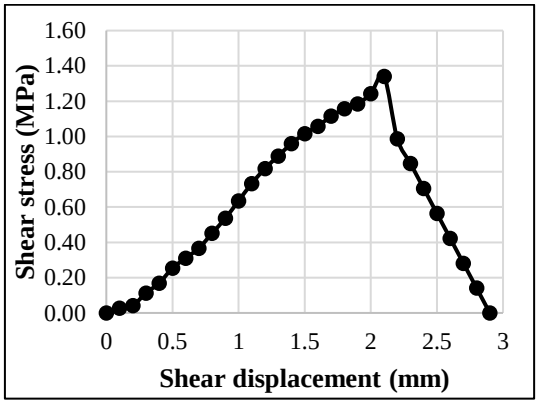

Figure A.7 Shear stress Vs shear displacement plot of F0.9 fiber reinforced PQC mix

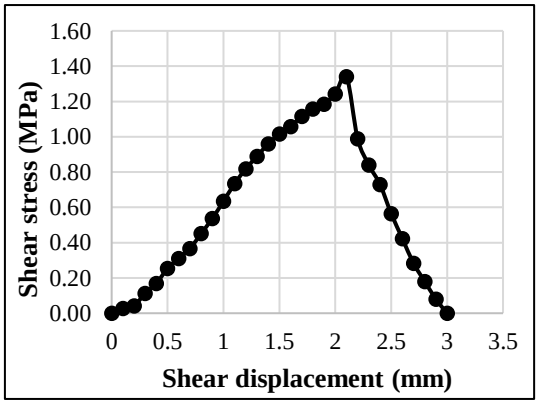

Figure A.8 Shear stress Vs shear displacement plot of F2.1 fiber reinforced PQC mix

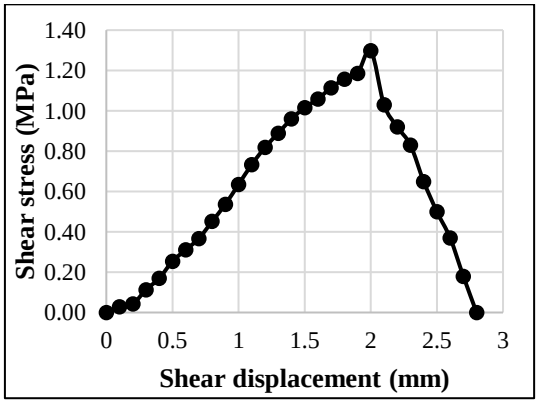

Figure A.9 Shear stress Vs shear displacement plot of F3.0 fiber reinforced PQC mix

A.4 The shear stress Vs shear displacement plots of the micro-fiber reinforced PQC cylindrical specimens F0.9, F2.1 and F3.0 with a GD of 1/3rd of diameter are shown in Figure A.10, A.11 and A.12, respectively.

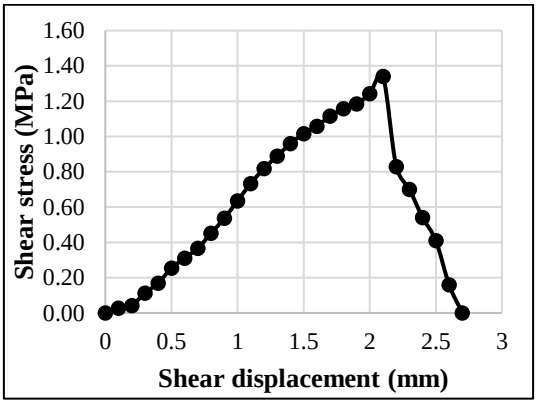

Figure A.10 Shear stress Vs shear displacement plot of F0.9 fiber reinforced PQC mix

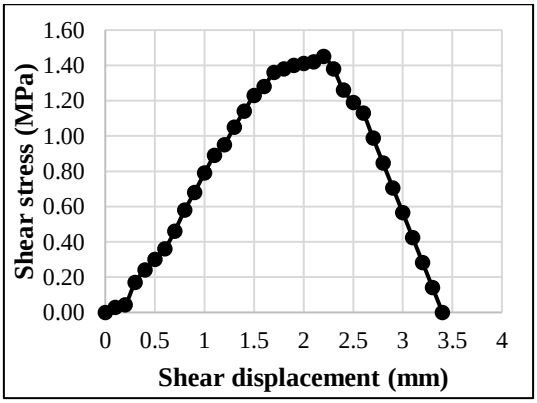

Figure A.11 Shear stress Vs shear displacement plot of F2.1 fiber reinforced PQC mix

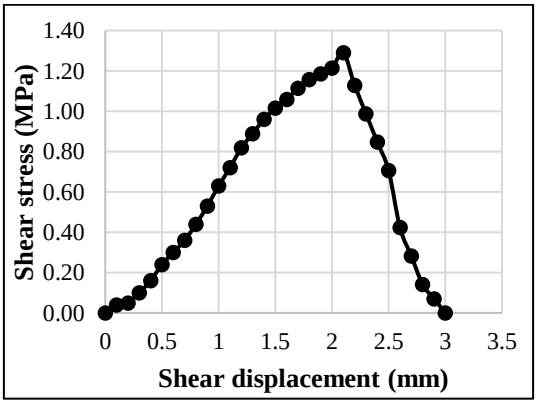

Figure A.12 Shear stress Vs shear displacement plot of F0.9 fiber reinforced PQC mix

A.5 The shear stress Vs shear displacement plots of the macro-fiber reinforced PQC cylindrical specimens PF0.25, PF.50 and PF0.75 with a GD of 1/4th of diameter are shown in Figure A.13, A.14, and A.15, respectively.

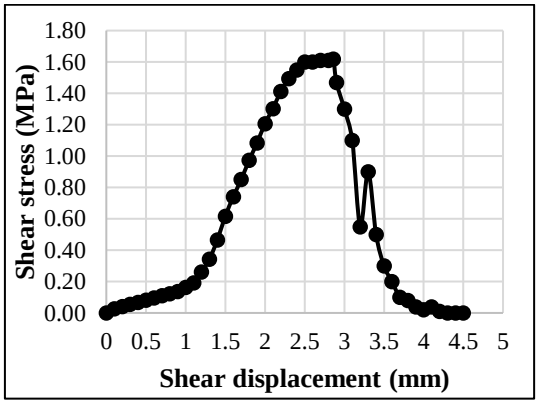

Figure A.13 Shear stress Vs shear displacement plot of PF0.25 macro-fiber reinforced PQC mix

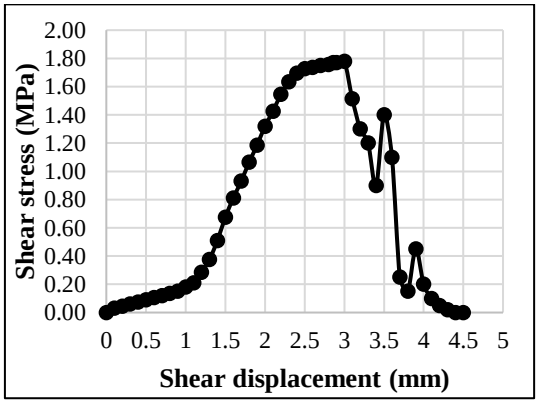

Figure A.14 Shear stress Vs shear displacement plot of PF0.5 macro-fiber reinforced PQC mix

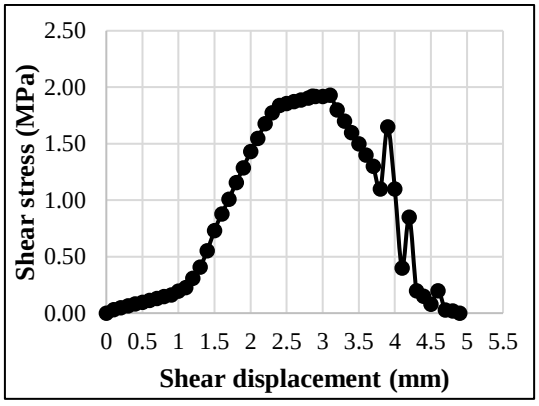

Figure A.15 Shear stress Vs shear displacement plot of PF0.75 macro-fiber reinforced PQC mix

A.6 The shear stress Vs shear displacement plots of the macro-fiber reinforced PQC cylindrical specimens PF0.25, PF.50 and PF0.75 with a GD of 1/3rd of diameter are shown in Figure A.16, A.17, and A.18, respectively.

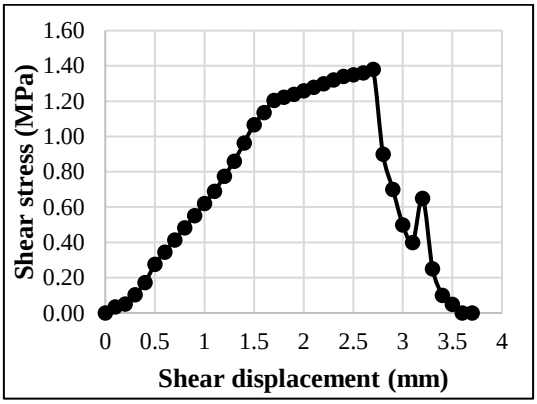

Figure A.16 Shear stress Vs shear displacement plot of PF0.25 macro-fiber reinforced PQC mix

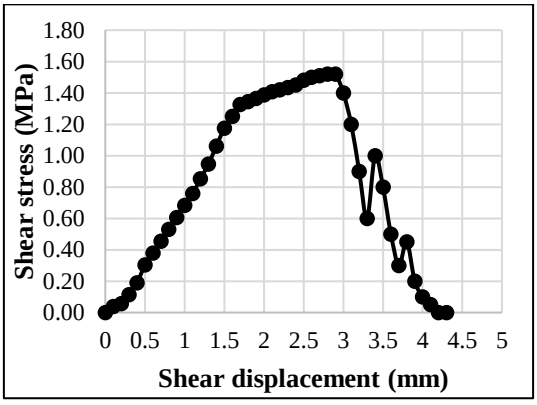

Figure A.17 Shear stress Vs shear displacement plot of PF0.5 macro-fiber reinforced PQC mix

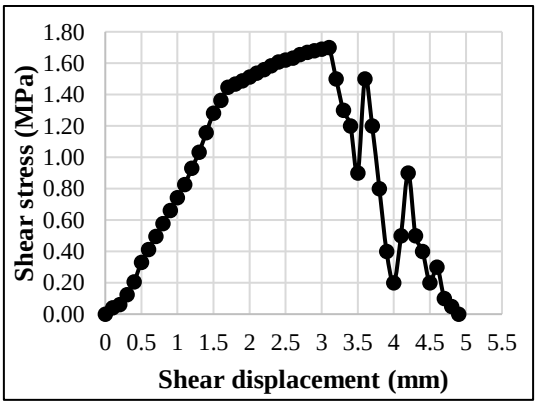

Figure A.18 Shear stress Vs shear displacement plot of PF0.75 macro-fiber reinforced PQC mix

APPENDIX B

B.1 Material input data for the 3-D finite element (FE) model in ANSYS for static shear test on preformed cylindrical specimens is shown in Table B.1.

Table B.1 Material input data for 3-D finite element (FE) model in ANSYS

Mix ID	Material Property			Joint stiffness (K), MPa/mm	
	Compressive strength, MPa	Flexural strength, MPa	Modulus of Elasticity, MPa	GD =1/4th of diameter	GD =1/3rd of diameter
A19	50.7	5.07	34471	1.31	1.06
A26.5	45.33	4.73	32654	1.43	1.29
A31.5	43.11	4.53	31800	1.61	1.45
F0.9	50.67	5.27	35170	1.29	1.34
F2.1	52.44	5.67	35976	1.35	1.42
F3.0	44.89	5.00	34075	1.26	1.30
PF0.25	52.81	5.33	35974	1.62	1.38
PF0.50	56.33	5.80	36867	1.78	1.52
PF0.75	45.00	6.00	37433	1.93	1.70

The spring stiffness is calculated by multiplying the contact area at the grooved cross-section with joint stiffness. For example, the spring stiffness of A19 plain PQC mix with a GD of 1/3rd diameter is calculated by:

Spring stiffness = joint stiffness × area of contact at the grooved cross-section

$= 0.64 \times \pi \times 100^2 \times 0.25$

$= 5027.2$ N/mm

Similarly, the spring stiffness values for all the mixes were obtained.

B.2 Material input data for 3-D finite element (FE) model in ANSYS for simulated small-scale test setup beam specimens subjected flexural loading at the joint.

The material properties shown in Table B.1 were used to model the concrete beam. The spring stiffness is calculation sample from the relationship between non-dimensional joint stiffness AGG* and LTE (Ioannides and Korovesis 1990) is shown below:
The AGG* corresponding to LTE of 20.28% of A31.5 plain PQC beam with 1/3rd of GD is 0.2 (From Figure 2.1)

AGG = AGG* × k*l*

l of concrete beam = $\left(\sqrt{\frac{Eh^3}{12k\,(1-\mu^2)}}\right)^{1/4}$

$= \left(\sqrt{\frac{31800 \times 100^3}{12 \times 0.09\,(1-0.15^2)}}\right)^{1/4}$

= 736.67 mm

AGG = 0.2 × 0.09 × 736.67

= 13.26 MPa

Spring stiffness = AGG × contact area/ width of beam

= 13.26 × 6666.67/100

= 884 N/mm

Similarly, the spring stiffness values for all the mixes with different GD were obtained.

APPENDIX C

The ANN script used in the present study in MATLAB software is given below:

```
% Solve an Input-Output Fitting problem with a Neural Network
% Created 26-Aug-2020 12:25:16
%
% This script assumes these variables are defined:
%
%   input - input data: Seven deflection values, and Temperature of pavement and  load
    applied generated from Latin Hypercube Sampling (LHS) matrix of size (5000 × 9).
%   output - target data: Joint stiffness calculated from the analytical models matrix of
    size (5000 × 1).

x = input;
t = output;

% Choose a Training Function
% For a list of all training functions type: help nntrain
% 'trainlm' is usually fastest.
% 'trainbr' takes longer but may be better for challenging problems.
% 'trainscg' uses less memory. Suitable in low memory situations.
trainFcn = 'trainbr';  % BR.

% Create a Fitting Network
hiddenLayerSize = 10;
net = fitnet(hiddenLayerSize,trainFcn);

% Setup Division of Data for Training, Validation, Testing
net.divideParam.trainRatio = 60/100;
net.divideParam.valRatio = 20/100;
net.divideParam.testRatio = 20/100;

% Train the Network
[net,tr] = train(net,x,t);

% Test the Network
y = net(x);
e = gsubtract(t,y);
performance = perform(net,t,y)

% View the Network
view(net)

% Plots
```

% Uncomment these lines to enable various plots.
%figure, plotperform(tr)
%figure, plottrainstate(tr)
%figure, ploterrhist(e)
%figure, plotregression(t,y)
%figure, plotfit(net,x,t)
%

****

LIST OF PUBLICATIONS

International Journals

- Bellary, A., and Suresha, S. N. (2021). "Influence of NMAS and groove depths on the static and fatigue shear performance of aggregate interlocking in PQC mixes." *Int. J. Pavement Eng.*, 0(0), 1–13. https://doi.org/10.1080/10298436.2021.19683923
- Bellary, A., and Suresha, S. N. (2022). "ANN Model to Predict Joint Stiffness of White-topped Pavements Using Falling Weight Deflectometer (FWD) Data." Int. J. Pavement Res. Technol. https://doi.org/10.1007/s42947-021-00137-8.

International Conference

- Bellary, A., and Suresha, S. N. (2022). "Influence of Coarse Aggregate Size and Type on the Design Thickness of Rigid Pavements for Indian Conditions." In Road and Airfield Pavement Technology, Springer, ICPT 2021 Sri Lanka. https://doi.org/10.1007/978-3-030-87379-0_31.

National Conference

- Bellary, A., and Suresha, S. N. (2020). "Influence of Aggregate size and type on mechanical properties of pavement quality concrete (PQC)." 7th Conference on Transportation Systems Engineering and Management (CTSEM 2020) held on 29-30 December 2020.

BIO-DATA

Name : Mr. Ashik Bellary

E-mail : ashik.bellary@gmail.com

ORCiD : 0000-0001-8462-7692

Mobile No. : 9738255856

Postal Address : #22 Raja Ratna Saptapur,
Sadashiv Nagar, Dharwad - 580001
Karnataka, India.

Academic and Professional Achievements:

- Selected in the Campus Interview of **Larsen & Toubro Limited (Geo-structure IC)** in 2013 held in KLE Technological University, Hubli.
- Qualified **GATE - 2014** in Civil Engineering paper (score = **359** and percentile = **86.97 %**).
- Received **Prof. C E G Justo Gold Medal** in 53rd Bangalore University convocation for scoring highest marks in ME - Highway Engineering.
- Received the **Best Project of the Year – 2017 (For Guiding the Undergraduate Project)** award in KSCST's SPP exhibition held at NMAM Institute of Technology, Nitte.

Educational Qualifications:

Name of the course	**School/College**	**Month-Year of passing**	**Percentage of marks obtained**
PhD	NITK, Surathkal - 575025	Pursuing	CGPA = 8.5
Master of Engineering (M.E) in Highway Engineering	UVCE Bangalore -56	December 2016	84.33 %
Bachelor of Engineering (B.E) in Civil Engineering	B V Bhoomareddi College of Engineering and Technology Hubli -31	June 2014	CGPA = 9.16
PUC	Karnataka Science College Dharwad - 01	March 2010	75.67 %
SSLC	K E Board's High School, Malamaddi Dharwad - 07	March 2008	89.76 %

BIO-DATA

Experience:

Name of the Institution	Areas of experience	Duration
Karnataka Law Society's Vishwanath Rao Deshpande Institute of Technology, Haliyal-581329	Teaching	One year (18/07/2016 to 18/07/2017)

Technical Skills:

Operating System	:	Windows XP/Vista/7/8/10
Application Software	:	ANSYS (APDL and workbench), Auto CAD, KENPAVE, EverFE, MS Office, Solid EDGE, Staad Pro, 3DSMAX, Sidra and Vissim.
Languages	:	C programming, MATLAB

Academic Projects: (Guided)

- Soil stabilization using Geosynthetic Material (Bamboo Fibers) KSCST sponsored Project (Jan 2017-June 2017).
- Marshall mix design for warm mix using GGBS (January 2017 - June 2017).

Academic Projects:

- Experimental and Numerical Study on Performance of Undowelled Joints in Concrete Pavements (August 2017 – till date) **PhD research work**.
- Laboratory studies on Stone Matrix Asphalt using Cement, Stone Dust as filler materials and Bagasse as a stabilizing additive (August 2015 - June 2016) Final year **ME project**.
- Upgradation of Road stretch of SH-34 connecting Inamhongal to Hire-Ulligere: A detailed project report (DPR) submitted in partial fulfillment of ME degree (August 2015 – January 2016).
- Congestion Reducing Measures in Dharwad CBD Area (August 2013 - June 2014). Major Project in the Final year **BE project** related to transportation engineering.
- Planning, analyzing and Designing of Hospital building (August 2012 - December 2012).
- Extensive Survey Project (January 2013 - May 2013) Involving Irrigation, Highway, Water supply and Sanitary Projects.

BIO-DATA

Details of Research Papers Published/Accepted in Journal:

i. **Bellary, A.**, and Suresha, S. N. (2021). "Influence of NMAS and groove depths on the static and fatigue shear performance of aggregate interlocking in PQC mixes." *Int. J. Pavement Eng*., 0(0), 1–13. https://doi.org/10.1080/10298436.2021.19683923

ii. **Bellary, A.**, and Suresha, S. N. (2022). "ANN Model to Predict Joint Stiffness of White-topped Pavements Using Falling Weight Deflectometer (FWD) Data." *Int. J. Pavement Res. Technol*. https://doi.org/10.1007/s42947-021-00137-8

Details of Research Papers Presented in National/International Conferences:

i. **Bellary, A.**, and Suresha, S. N. (2022). "Influence of Coarse Aggregate Size and Type on the Design Thickness of Rigid Pavements for Indian Conditions." In Road and Airfield Pavement Technology, Springer, ICPT 2021 Sri Lanka. https://doi.org/10.1007/978-3-030-87379-0_31 **(Book Chapter)**

ii. **Bellary, A.**, and Suresha, S. N. (2021). "Sensitivity Analysis of Variation in Modulus of Elasticity of Concrete on Thickness of Rigid Pavement as per IRC:58-2015." Paper presented in 8th Conference on Transportation Systems Engineering and Management, NIT Calicut.

iii. **Bellary, A.**, and Suresha, S. N. (2020), "Influence of Aggregate Size and Type on Mechanical Properties of Pavement Quality Concrete (PQC)." Paper presented in 7th Conference on Transportation Systems Engineering and Management, KSCSTE-NATPAC & CET, Kerala, India, December 29-30, 2020.

iv. **Bellary, A.**, and Suresha, S. N. (2019), "Influence of Coefficient of Thermal Expansion of Concrete on Curling Stresses in Rigid Pavements." Paper presented in sixth edition of the colloquium on Transportation Systems Engineering and Management (CTSEM, 2019) held at SVNIT, Surat.

v. Gupta, L., **Bellary, A.** (2018). "Comparative study on the behavior of bituminous concrete mix and warm mix asphalt prepared using lime and Zycotherm as additive." Mater. Today Proc. 5(1), 2074–2081 https://doi.org/10.1016/j.matpr.2017.09.203 **(Conference Paper)**

vi. **Bellary, A.**, Gupta, L. "Laboratory studies on Warm Bituminous Concrete mix prepared using GGBS as filler material and Zycotherm as additive." Presented in International conference on Recent research development in science, engineering and management. (ISBN: 978-81-931039-0-6)